NOTICE

AVIS

The quality of this microform is heavily dependent upon the quality of the original thesis submitted for microfilming. Every effort has been made to ensure the highest quality of reproduction possible.

If pages are missing, contact the university which granted the degree.

Some pages may have indistinct print especially if the original pages were typed with a poor typewriter ribbon or if the university sent us an inferior photocopy.

Reproduction in full or in part of this microform is governed by the Canadian Copyright Act, R.S.C. 1970, c. C-30, and subsequent amendments.

La qualité de cette microforme dépend grandement de la qualité de la thèse soumise au microfilmage. Nous avons tout fait pour assurer une qualité supérieure de reproduction.

S'il manque des pages, veuillez communiquer avec l'université qui a conféré le grade.

La qualité d'impression de certaines pages peut laisser à désirer, surtout si les pages originales ont été dactylographiées à l'aide d'un ruban usé ou si l'université nous a fait parvenir une photocopie de qualité inférieure.

La reproduction, même partielle, de cette microforme est soumise à la Loi canadienne sur le droit d'auteur, SRC 1970, c. C-30, et ses amendements subséquents.

Canada

UNIVERSITY OF ALBERTA

Thin Film Iron Silicides

BY

David Snell   (C)

A thesis submitted to the Faculty of Graduate Studies and Research in partial fulfillment
of the requirements for the degree of Master of Science

DEPARTMENT OF ELECTRICAL ENGINEERING

Edmonton, Alberta
Spring, 1992

Canada

UNIVERSITY OF ALBERTA

RELEASE FORM

NAME OF AUTHOR: **David Snell**

TITLE OF THESIS: **Thin Film Iron Silicides**

DEGREE: **Master of Science**

YEAR THIS DEGREE GRANTED: **1992**

Permission is hereby granted to the University of Alberta Library to reproduce single copies of this thesis and to lend or sell such copies for private, scholarly or scientific research purposes only.

The author reserves all other publication and orther rights in association with the copyyright in the thesis, and except as hereinbefore provided neither the thesis nor any substantial portion thereof may be printed or otherwise reproduced in any material form whatever without the author's prior written permission.
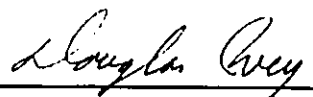
112 Varsity Estates Place, N.W.
Calgary, Alberta
Canada T3B 3B6

Dated: Jan 28/92

UNIVERSITY OF ALBERTA

FACULTY OF GRADUATE STUDIES AND RESEARCH

The undersigned certify that they have read, and recommend to the Faculty of Graduate Studies and Research for acceptance, a thesis entitled **Thin Film Iron Silicides** submitted by **David Snell** in partial fulfillment of the requirements for the degree of **Master of Science.**

_____

Dr. D. G. Ivey – Co-supervisor

_____

Dr. M. J. Brett – Co-supervisor

_____

Dr. R. Fedosejevs

_____

Dr. A. Pierre

Date   Jan 28/72

Abstract

In recent years metal silicides have attracted attention with their potential for application in microelectronics. Low resistivities and hig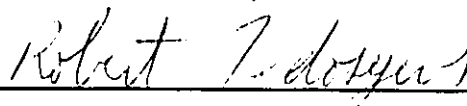h stabilities couple well with the potential for epitaxial growth to make silicides an excellent choice for silicon based devices. Applications for the material include electronic gates, interconnects, and ohmic and Schottky barrier contacts to silicon. Select silicides possess phases displaying semiconducting properties, allowing for the simple integration of semiconducting heterostructures with standard silicon circuits. The band gaps of many of these materials allow them to be used in optical devices operating in the near infrared range.

The research outlined in this thesis involves the formation of continuous layers of one such material: iron disilicide. With a band gap of $0.9 \pm .1$ eV, iron disilicide is a semiconducting material possessing optical possibilities. Difficulty has persisted in the formation of continuous layers of this material; a difficulty which limits the usefulness of the silicide for electronic purposes. Experimentally, this work examines the problems of silicide formation, and succeeds in forming continuous layers of iron disilicide with a methodology well within reach of circuit processing techniques. The work also verifies the band gap quoted in the literature.

Included in this thesis is a review of general silicide properties, and how these properties relate to the microelectronic industry. Semiconducting and conducting iron disilicide are reviewed in detail.

Acknowledgements

Table of Contents

CHAPTER 5
Thin Film Failure

55

CHAPTER 6
Characterization

62

CHAPTER 7
Thin Film Deposition

71

CHAPTER 8   81
Formation of β FeSi$_2$

CHAPTER 9   99
Conclusions

List of Tables

List of Figures

Symbols

Symbols listed here are used commonly throughout the text. Other symbols appear and are defined locally, as are any alterations to the symbols in this list.

a	Acceleration
A	Cross sectional area
A^{**}	Richardson's Constant
b	μ_n/μ_p
B	Magnetic field strength (scalar)
$\overline{B}$	Magnetic field vector (strength and direction)
c	Speed of light, 2.998×10^8 m/s
C	Concentration
d	Depth of a conductor
D	Diffusivity
e	Absolute value of electronic charge
E_a	Activation energy
E_g	Band gap
F	Diffusional flux
$\overline{F}$	Force (vector)
ΔG	Change in free energy
ΔG_v	Change in volume free energy (excludes surface free energy)
h	Planck's Constant, 4.136×10^{-15} eV·s
ΔH_R	Heat of reaction
I	Current
I_0	Saturation current of a p/n junction
J	Current Density or Atomic flux
k	Boltzmann's Constant
k_s	Chemical reaction rate constant at a reaction interface
k^o	Frequency with which an atom moves between two sites
K	Cliff-Lorimer Factor
L	Length of a conductor
m^*	Effective mass of a charge carrier
n	Concentration of n type charge carriers (charge/cm^3)
N	Number of charge carriers (n and p type) or number of atoms
N_D	Number of charge donors
p	Concentration of p type charge carriers (charge/cm^3)

q	Value of electronic charge, e for positive charge, -e for negative charge
r	Radius
r_c	Contact resistance
R_c	Specific contact resistance (independent of area)
R_h	Hall coefficient
ΔS	Change in entropy
t	Time (seconds)
T	Temperature (Kelvin)
$\bar{v}$	Velocity of an electron in an electric or magnetic field
V	Voltage
V_h	Hall voltage
w	Width of a conductor
x	Distance or thickness
x^c	Critical Thickness

Greek Letters

α	Optical absorption coefficient
ε	Electric field (vector)
ε	Electric field (magnitude)
ε_h	Hall field
ϕ_B	Schottky barrier height (volts)
γ	Surface Energy
λ	Wavelength or length of an atomic jump
μ	Chemical potential
μ	Mobility of a charge carrier
ν	Drift velocity diffusional atoms
θ_μ	Driving force for silicide formation
ρ	Resistivity
σ	Conductivity
$\Delta\sigma$	Change in surface energy
τ	Time between collisions or scattering events
υ_d	Average drift velocity of charge carriers

Abbreviations

BOE   Buffered Oxide Etch
CVD   Chemical Vapor Deposition
EDX   Energy Dispersive X-ray analysis
HF   Hydrofluoric acid
LPE   Liquid Phase Epitaxy
MBE   Molecular Beam Epitaxy
MOCVD   Metal-Organic Chemical Vapor Deposition
MOVPE   Metal-Organic Vapor Phase Epitaxy
SEM   Scanning Electron Microscopy
SPE   Solid Phase Epitaxy
TEM   Transmission Electron Microscopy
XRD   X-Ray Diffraction

Chapter 1

Introduction

As the current microelectronics industry continues to press against the limits of semiconductor technology, new materials are being demanded to satisfy a number of needs. The ambition of VLSI and ULSI technology is to increase the density and speed of devices on an integrated chip, an endeavor that requires these devices to be made with increasingly smaller line widths. As devices decrease in size, the materials from which they are produced show not only an increased resistance, but a decreased stability to effects such as electromigration, thermomigration, interdiffusion and agglomeration. Stability is becoming increasingly difficult to maintain with the use of metals, and more stable materials such as polysilicon are showing the effects of their high resistivities. Table 1-1 displays some of the difficulties in using metals in semiconductor technologies. Polysilicon, while immune to these effects, possesses a resistivity orders of magnitude greater than metals, and is becoming unsuitable for use in low resistivity metallizations.

Property	Difficultly in VLSI process
Low (<800°C) to medium (<1100°C) eutectic temperature when mixed with silicon	Instability at high temperatures required for many semiconductor processing steps, such as diffusion of dopants.
High diffusivity and interaction with silicon	Metallizations and structures may react with silicon at low temperatures(<450°C)
High oxidation rate, poor oxidation stability	Materials oxidize easily during processing
Interaction with SiO_2	Reaction with passivating layer
Poor etchability	Difficult to pattern devices
Electromigration	High instability over time

Table 1-1   Unsuitable properties of metals for use in VLSI applications[1]

One class of material which promises to alleviate many problems facing silicon technology is that of silicon and metal compounds known as silicides. Silicides possess a resistivity substantially less than polysilicon, while maintaining stability with respect to temperature and silicon substrates. A number of silicides exist, as more than half the elements in the periodic table react with silicon to form one or more silicides, but not all are suitable for use in integrated circuit technology. Table 1-2 outlines the desired properties of a silicide destined for such use. Of the possible elements, silicides of the refractory through near noble metals are of the most interest[1] (Groups IVB, VB, VIB, VIIB and VIIIB in the periodic table). The most useful of these are the silicides which form through the solid state reaction of metal and silicon to form a silicide stable with respect to silicon[1]. These silicides are listed in Table 1-3. Although each silicide possesses properties unique unto itself, the silicides of Table 1-3 can be grouped according to the metal from which they were formed: refractory metal silicides and near noble metal silicides. The properties of these general groups are compared in Table 1-4. Group VIIB silicides, which lie between the refractory and near noble metal silicides, are less understood and are not included. From the comparison it can be seen that the refractory metals are particularly suitable for use in electronic interconnects.

Although silicides originally attracted attention because of their low resistivity and high temperature stability[1], electronic interconnections are not their only

Property
Low resistivity
Easy to form
Easy to etch
Stability in oxidizing ambients, yet should be possible to oxidize
Mechanical stability; good adherence to silicon with low stress
Should possess a smooth surface to allow for multiple layer circuits.
Stability throughout processing, regardless of the temperatures or conditions
Should not react with final metal or silicon.
Should not contaminate devices, wafers, or working apparatus
Good device characteristics and lifetimes[†]
Low contact resistance, minimal junction penetration[†]

[†] Not important for use as interconnect material

Table 1-2   Desired properties of metal silicides[1]

Refractory Silicides		Near Noble Silicides	
$TiSi_2$	$CrSi_2$	$FeSi_2$	$OsSi_2$
$ZrSi_2$	$MoSi_2$	$CoSi_2$	$IrSi_3$
$HFSi_2$	WSi_2	$NiSi_2$	$PtSi$
VSI_2		Ru_2Si_3	
$NbSi_2$	$MnSi_{1.73}$	$RhSi_2$	
$TaSi_2$	$ReSi_2$	Pd_2Si	

Table 1-3   Important silicides of groups IVB - VIIIB (adapted from Murarka[1])

application. Silicides, because of their high stability with respect to silicon, are also suitable for use as low resistance contacts between metal lines and a silicon substrate. Silicides deposited directly in the contact window between metal and silicon do not diffuse into the substrate, preserving the shallow junctions initially formed[2]. Silicides formed by reacting metal deposited into these windows offer the possibility of reliable and reproducible formation of Schottky barrier contacts, as the solid state interaction of metal and silicon leads to relatively imperfection free and pure silicon–silicide interfaces (chapters 2,4).

Property	Near Noble Silicides	Refractory silicides
Resistivity of the metal	Nearly the same for all metals: 7.5 ± 2.5 $\mu\Omega{\cdot}cm$	Decreases with atomic number in a period and in a group
Resistivity of the silicide	Nearly the same: 25 ± 10 $\mu\Omega{\cdot}cm$. No correlation with atomic number	Increases with atomic number in a period, and in a group
Schottky barrier height (n type silicon)	Greater than half the silicon band gap energy; increases with atomic number	All have similar value, 0.55 ± 0.05 eV
Formation temperature	200 - 600°C	>600°C
Dominant diffuser	Metal	Silicon
High temperature stability	Poor	Good

Table 1-4   Comparative properties of Near Noble and Refractory Silicides[1]
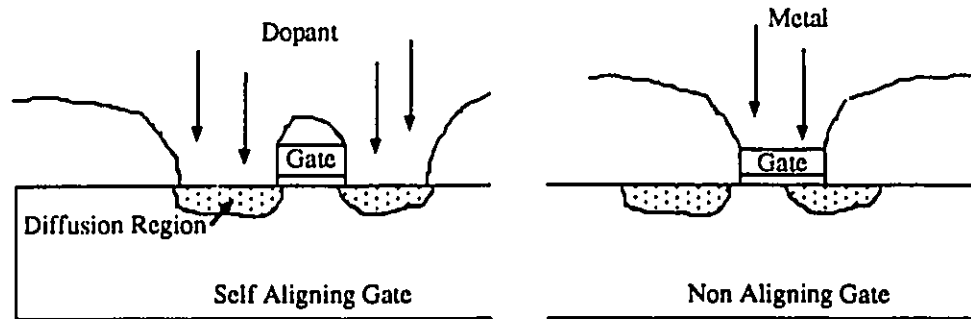
Figure 1-1 Self alignment procedure

In a self aligning process a transistor gate is formed prior to the formation of the doped regions, and acts as a mask to protect the region beneath the gate from the dopant. In a non aligning process, doped regions are formed first, and the gate is formed in the gap between the regions afterwards. This process is susceptible to error in mask alignment.

The high temperature stability of silicides makes them useful for self aligned structures such as electronic gates. Self aligning involves the deposition of material on a silicon substrate just prior to the doping of n^+ or p^+ diffusion regions. The self aligning material prevents doping of the silicon beneath it while allowing the regions around it to be doped. (Figure 1-1). This prevents the need to precisely align diffusion and gate masks during circuit fabrication, and eliminates the need for device gates to be made larger to accommodate a margin of error. Metals cannot survive the high temperature diffusion of dopants, eliminating m from use as a self aligning material. This has necessitated the use of polysilicon for gate metallization, even though the material possesses a high resistivity. This in turn has resulted in a severe increase in the RC delay of VLSI circuits, which has served to limit the size and speed of their devices.

Semiconducting Silicides

Since the late 1950's an increased focus has been placed on the semiconducting properties of many silicides. Semiconducting silicides have been investigated for use in opto-electronic as well as thermoelectric devices[3-7]. Some of the foreseen uses include photodetectors, semi-conductor lasers, power production, cooling, thin film resistors and electro-optic interconnects to microelectronic circuits. Metal silicon bilayers are also being investigated for use as substrates in optical storage[8].

Semiconducting silicides offer many advantages over materials currently used for advanced technologies such as optoelectronics. Silicides are considerably cheaper and easier to produce than materials such as GaAs and InP, and there is the possibility of growing silicides directly upon a silicon wafer with little processing required, allowing silicides to assist with the integration of optical and electronic devices.

Silicide		
$CrSi_2$	$BaSi_2$	$IrSi_{1.75}$
$FeSi_2$	$OsSi_2$	Ru_2Si_3
$LaSi_2$	Ca_2Si	$MnSi_{1.73}$
$ReSi_2$	Mg_2Si	

Table 1-5   Selected semiconducting silicides

A number of silicides display semiconducting properties (Table 1-5). With few exceptions, these silicides are the most silicon rich to form from their parent metal. One of these silicides, $FeSi_2$, is of particular interest as it possesses a dual semiconducting, conducting character. A low temperature, semiconducting phase (labeled as the β phase) exists in addition to a high temperature, metallic phase (labeled as the α phase). With a band gap in the near infrared, iron silicide presents an intriguing possibility for use in microelectronic technology for the integration of optical and electronic structures, as both semiconducting devices and electronic interconnect could be fabricated from the source material.

Chapters 2 through 5 of this work present a detailed literature review of material relevant to the use of silicides. The formation of silicides as a whole, and iron silicide in particular, is discussed in detail in chapters 2 and 4. The semiconducting and conducting properties of silicides are discussed as a group in chapter 3, with extra emphasis again falling on iron silicide. Chapters 6 through 9 describe the experimental aspects of this work, the main objective of which has been to develop a method for the formation of stable, continuous layers of semiconducting iron silicide on silicon substrates. Thin layers, less than 0.5 μm in thickness, have been studied for effects such as agglomeration and oxidation during formation, and a method to form good silicide thin films has been developed. The quality and composition of the silicide films has been characterized, and is discussed in Chapter 8. The energy gap of the semiconducting phase has also been determined, and is likewise discussed in Chapter 8.

Formation of Silicides

2.1 Silicide Growth

Silicide layers are most commonly formed by depositing and reacting thin metal layers on bulk silicon substrates. Formation may also be accomplished by codeposition of metal and silicon on any substrate. Metal and silicon are deposited in stoichiometric proportion to form the silicide as deposition transpires. Several advantages for such deposition exist, such as the ability to form silicides on non-silicon substrates, the formation of epitaxial layers (q.v.), and the formation of silicides at lower temperatures (q.v.). However, these processes, being difficult and expensive, are less widely used.

Reaction of metal and silicon requires interdiffusion between the materials; this in turn requires elevated temperatures. Conventional furnace annealing, or annealing in pure flowing gas, are simple methods for which diffusion may be stimulated. Once the possibility of interdiffusion is present, silicide formation proceeds with a dependence on kinetic and thermodynamic considerations.

2.1.1 Nucleation

The premier occurrence in silicide formation is the nucleation of silicide at or near the interface between metal and silicon[9]. Driven by a reduction in free energy, ΔG, metal (A) and silicon (B) react to form the silicide phase ($A_x B_y$). The reduction in free energy is proportional to the volume of the new phase formed. Assuming this phase initially forms spherical nuclei, ΔG is proportional to $(4/3)\pi r^3$, where r is the radius of a newly formed nucleus. The antithesis to this is the increase in surface energy accompanying the creation of a second interface; an effect synonymous with nuclei formation. Surface energy is dependent on surface area—$4\pi r^2$ for spherical nuclei—and the change in free energy, dependent now on competing effects, becomes

$$\Delta G = (4/3)\pi r^3 \Delta G_v + 4\pi r^2 \Delta\sigma \qquad (2.1)$$
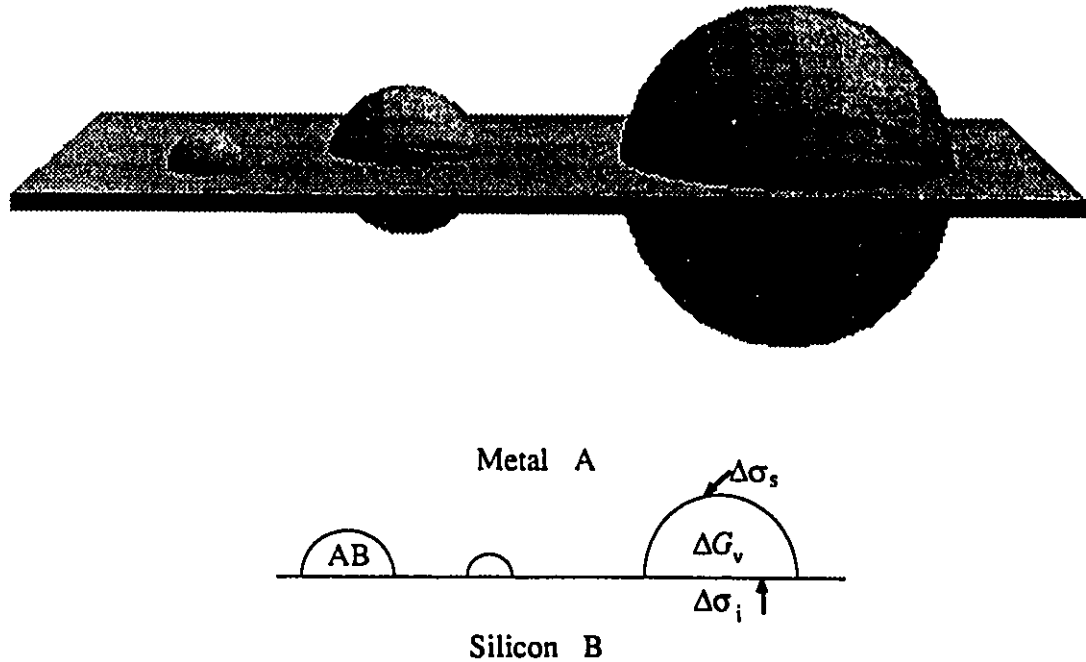
Figure 2-1   Formation of nuclei in silicide metal system. Smaller nuclei tend to shrink and disappear, while larger nuclei grow to form a silicide phase.

where ΔG_v is the change in free energy per unit volume and $\Delta\sigma$ is the change in surface energy per unit area. This is true for homogeneous nucleation, where nucleation occurs within the metal or silicon layer. If a nucleus forms at the metal–silicon interface (heterogeneous nucleation), a section of this interface is disposed during formation. The metal – silicon interface itself possesses surface energy, and its elimination reduces the free energy of the nucleus (Figure 2-1). Destruction of the interface serves as a driving force for nucleation. Surface energy becomes

$$\text{Surface energy} \propto \Delta\sigma_s - \Delta\sigma_i$$

$$= 2\pi r^2 \, \Delta\sigma_{ss} + 2\pi r^2 \, \Delta\sigma_{sm} - \pi r^2 \, \Delta\sigma_i$$

$$= 4\pi r^2 \, (\Delta\sigma_{ss}/2 + \Delta\sigma_{sm}/2 - \Delta\sigma_i/4)$$

$$= 4\pi r^2 \, \Delta\sigma'$$

where $\Delta\sigma'$ is equal to $\Delta\sigma_{ss}/2 + \Delta\sigma_{sm}/2 - \Delta\sigma_i/4$. $\Delta\sigma_s$ is the total energy contribution of the silicide interface, $\Delta\sigma_{ss}$ is the energy contribution of the silicide–silicon interface, $\Delta\sigma_{sm}$ is the energy contribution of the silicide–metal interface and $\Delta\sigma_i$ is the energy contribution
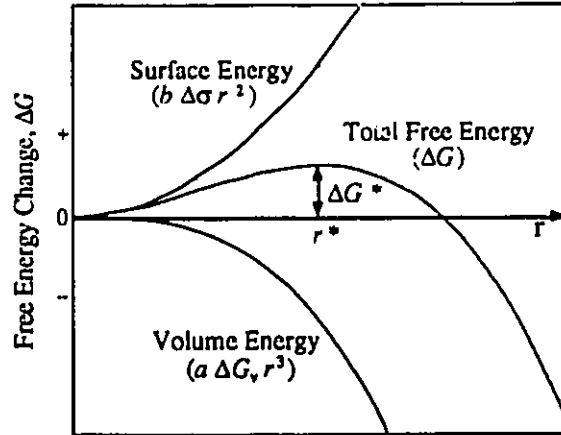
Figure 2-2   Free energy change during nucleation, as a function of nuclei radius. Shown is the surface energy, volume free energy and total free energy change of the system.

of the metal–silicon interface. By setting $\Delta\sigma = \Delta\sigma'$ for the heterogeneous case, equation 2.1 maintains its validity. Due to the negative effect (on the surface energy) of destroying the silicon–metal interface, the surface energy for heterogeneous nucleation is always less than that for homogeneous nucleation, making nucleation more likely to occur at the interface. An exception exists when nucleation occurs at a defect buried within the metal or silicon layer, as defects reduce the energy of nucleation by a value equivalent to the energy associated with the defect.

ΔG varies as a function of r, attaining a maximum when the nuclei possess a critical size $r=r^*$ (Figure 2-2). By maximizing ΔG with respect to r, the *critical radius* is given by

$$r^* = \frac{-2b\,\Delta\sigma}{3a\,\Delta G_v} \tag{2.2}$$

where a and b are the geometric factors $4/3\pi$ and 4π respectively. The change in free energy ΔG^*, at r^*, is

$$\Delta G^* = \frac{4b^3\,\Delta\sigma^3}{27a^2\,\Delta G_v^2} \tag{2.3}$$

Equation 2.3 holds true for a nucleus of any shape, differing only in the values of a and b. For spherical nuclei equation 2.3 becomes

$$\Delta G^* = \frac{16\pi\,\Delta\sigma^3}{3\,\Delta G_v^2}$$

(2.4)

The radius r^* is the point at which the rate of change of free energy is equal to zero. If an "embryo" possess a radius smaller than r^*, ΔG must increase for it to grow. This requires energy from other sources, and the preference is for embryos to disappear. For a radius greater than r^*, ΔG decreases with increasing radius size and embryos tend to grow. These embryos are called nuclei.

The rate of nucleation, $\partial n/\partial t$ (nuclei formed per unit volume per unit time), is proportional to the density of the nuclei and to the rate at which nuclei can form. Respectively, these factors are proportional to

$$\exp\left(-\frac{\Delta G^*}{kT}\right)$$

and

$$\exp\left(-\frac{E_a}{kT}\right)$$

where E_a is the activation energy for an atom to move from one position to another. Combining these factors leads to an equation for the rate of nucleation:

$$\frac{\partial n}{\partial t} = K \, \exp\left(-\frac{\Delta G^*}{kT}\right)\exp\left(-\frac{E_a}{kT}\right)$$

(2.5)

Competition between the gain in free energy ΔG and the loss of surface energy $\Delta\sigma$ gives rise to nucleation with an activation energy ΔG^* proportional to $\Delta\sigma^3/\Delta G_v^2$. For silicide formation $|\Delta G_v|$ is normally large, resulting in a small ΔG^* and rapid nucleation[10]. However, when a new phase nucleates it customarily necessitates a volume change resulting in a deformation energy contribution ΔH_d[10]. The activation energy becomes proportional to $\Delta\sigma^3/(\Delta G_v + \Delta H_d)^2$ [10], with ΔH_d playing a significant role in the formation of many silicides. The ΔH_d term reduces the magnitude of the denominator, increasing ΔG^*. For silicides of many rare earth metals deformation has been linked to a structure possessing significant amounts of silicon interstitial atoms, creating a silicon sublattice containing upwards of 15% vacancies[10]. This expedites the diffusion of silicon, facilitating silicide growth at temperatures as low as 400 °C. However, metal atoms in these silicides may not be mobile below temperatures of ~1000 °C[10]. Silicides forming at low temperatures possess no mechanism to accommodate deformation stress. ΔH_d is high, $|\Delta G_v + \Delta H_d|$ is small and ΔG^* is high[10]. When ΔG^* is high, silicide formation is nucleation controlled. Silicide phases that are nucleation controlled often exhibit lateral nonuniformity, while growth controlled phases are laterally uniform. An example of a nucleation controlled process is the formation of $MnSi_{1.73}$ from $MnSi$[11].
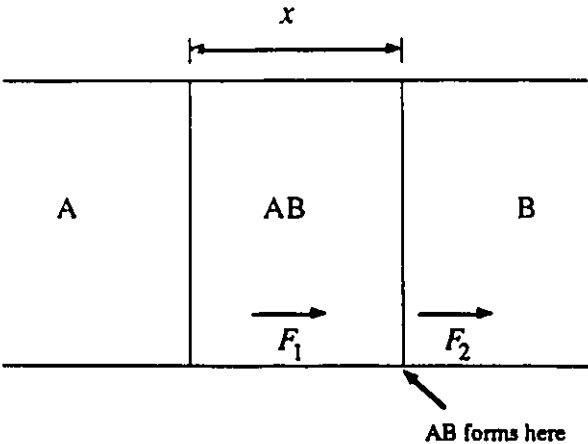
Figure 2-3 Typical Diffusion Couple

2.1.2 Growth

A typical diffusion couple, representative of metal - silicon systems, is shown in Figure 2-3. Figure 2-4 is the concentration profile for the couple. Numerous analyses exist for the formation of compound phases in such a system. A typical analysis–originally proposed by Deal and Grove (1965) for the oxidation of silicon, and repeated by Mayer and Lau (1990)[9]–is shown below. It is assumed for simplicity that A is the primary diffusing species. As is common in such analyses[9,12], silicide formation is assumed to occur at one interface.

Two steps are involved in the initial formation of metal silicide from a diffusion couple. The first is diffusion of material across the silicide layer. The diffusion flux F_1 is written as
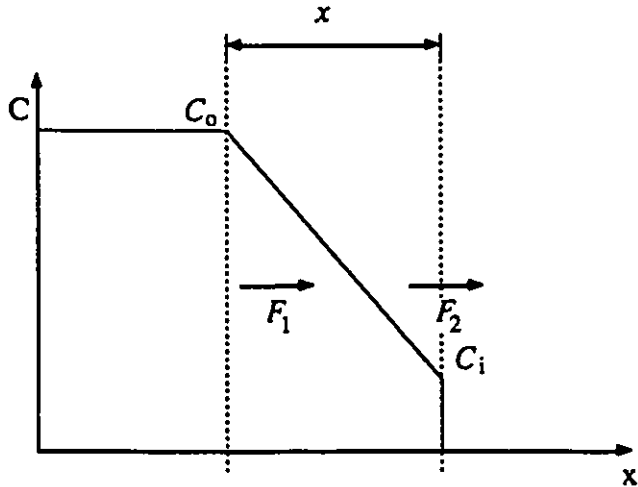
Figure 2-4 Concentration profile of diffusion couple of Figure 2-1

$$F_1 = D \frac{C_o - C_i}{x}$$

(2.6)

where D is the diffusivity, C_o and C_i are the concentrations of A on either side of the silicide phase, and x is the thickness of the phase at a given time t.

The second step requires the reaction of metal and silicon at the interface. The flux F_2 into the interface, as required for reaction, is

$$F_2 = k_s C_i$$

(2.7)

where k_s is the chemical reaction rate constant at the reaction interface. Silicide formation occurs only at the interface, and assuming that A does not dissolve in B, a steady state condition exists in which $F_1 = F_2$. Equating the two fluxes leads to

$$D \frac{C_o - C_i}{x} = k_s C_i$$

$$C_o = C_i \left(1 + \frac{k_s x}{D}\right)$$

(2.8)

$$C_i = \frac{C_o}{1 + k_s x / D}$$

(2.9)

An equation for the steady state flux F is obtained by substituting the concentrations C_o and C_i back into the original equations for flux. This is most easily accomplished by substituting equation 2.9 into equation 2.7 to obtain

$$F = \frac{k_s C_o}{1 + k_s x / D}$$

$$= \frac{D k_s C_o}{D + k_s x}$$

(2.10)

The rate at which a silicide layer grows is equal to the flux of atoms into the layer divided by the number of diffusing atoms N incorporated per unit volume of the silicide, leading to

$$\frac{\partial x}{\partial t} = \frac{F}{N} = \frac{D k_s C_o}{N (D + k_s x)}$$

or

$$\frac{\partial x}{\partial t} = \frac{k_s C_o}{N} \frac{D/x}{D/x + k_s}$$

(2.11)

For very narrow phases, where $\frac{D}{x} \gg k$, equation 2.11 reduces to

$$\frac{\partial x}{\partial t} = \frac{C_o k_s}{N}$$

showing that silicide formation is dominated by the interfacial reaction. Integrating yields

$$x = \left(\frac{C_o k_s}{N}\right) t \qquad (2.12)$$

Thus for interface controlled reactions growth occurs linearly with time.
If the silicide phase is thicker, such that $\frac{D}{x} \ll k$, equation 2.11 becomes

$$\frac{\partial x}{\partial t} = \frac{DC_o}{N} \frac{1}{x}$$

and integrating yields

$$x = \left(\frac{2DC_o t}{N}\right)^{1/2} \qquad (2.13)$$

Growth is dominated by diffusion, and is dependent on the square root of time. Equations 2.12 and 2.13 show that silicide formation is initially controlled by the interfacial reaction, switching to diffusion controlled as the phase thickens. When the phase thickness is approximately D/k a combination of diffusion and interfacial control exists.

Growth of Subsequent Phases

After metal and silicon react to form a silicide phase, it is possible for subsequent phases to form at the interface of this silicide and any unreacted material. The formation of latter phases may require the initial phase to dissociate into a more basic composition, as shown in Figure 2-5. If silicide AB_2 is the first phase to form, and silicide AB is the second, there must be a dissociation of AB_2 into the components AB and B. If B is the diffusion species, its atoms are then free to diffuse across the AB layer to react with A atoms and form AB. In this scenario, growth of AB occurs at both interfaces. This dissociation is not a necessity, as many phases may form from the simple addition of one element to an existing phase; for example, $A + AB \rightarrow A_2B$. The dissociation of a phase may be a necessary step for growth, but it will not affect the preceding analysis of growth kinetics. Dissociation is accounted for by k_s, the chemical reaction rate constant at the interface.

Silicide Formation: A+B → AB   Disociation: AB$_2$ → AB + B
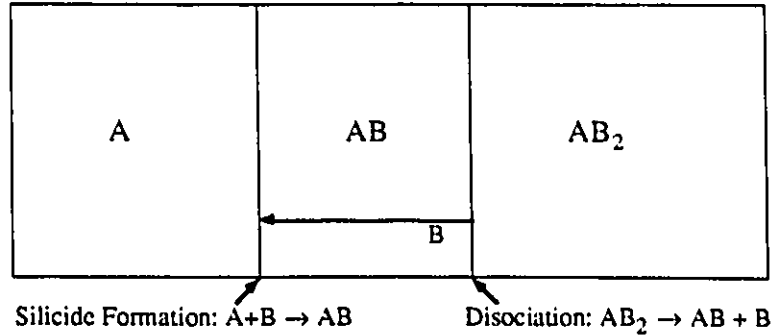
Figure 2-5   Dissociation of a silicide phase.

2.1.3 Thin Film vs Bulk Diffusion

For the purpose of silicide growth, a bulk diffusion couple of metal and silicon possesses an infinite amount of each material. Initial silicide growth is interface limited, but the availability of material means growth eventually becomes diffusion controlled as the phase thickens. Assuming formation is diffusion limited, the growth of multiple phases may be examined from a consideration of their free energies of formation.

The driving force promoting silicide formation is the exothermic reaction of silicon and metal to decrease the free energy of the system[9]. This driving force θ_μ is

$$\theta_\mu = -\frac{\partial \bar{\mu}}{\partial x} \approx -\frac{\Delta H_R}{x}$$

where $\bar{\mu}$ is the chemical potential, ΔH_R is the heat of reaction, and x is the thickness of the growing phase. $\Delta G = \Delta H_R - T\Delta S$, but it is assumed that $\Delta H_R \equiv \Delta G$ as the temperature at which silicide formation occurs is usually low with respect to the melting point of the reactants. The diffusional flux is

$$F = vC$$

$$= \frac{k^o\lambda^2 C}{kT}\left(-\frac{\partial \bar{\mu}}{\partial x}\right)$$

where v is the average velocity of diffusing atoms, C is their concentration, k^o is the frequency that an atom moves between sites when diffusing, and λ is the length of the jump. The flux dependence on the heat of reaction is then

$$F = vC = \frac{k^o\lambda^2 C}{kT}\left(\frac{-\Delta H_R}{x}\right)$$
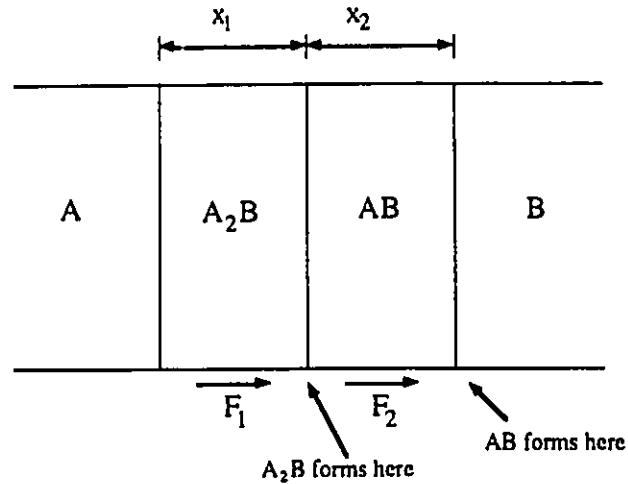
Figure 2-6   Formation of compound phases in a binary diffusion couple

and

$$F = \frac{DC}{kT}\left(\frac{-\Delta H_R}{x}\right)$$

(2.14)

The velocity of diffusing atoms can be obtained from these equations,

$$v = \frac{D}{kT}\left(\frac{-\Delta H_R}{x}\right)$$

(2.15)

Consider the growth of two phases in a binary diffusion couple (Figure 2-6), in which A is the diffusing species. If F_1 is the flux of atoms across the A_2B phase and F_2 is the flux across the AB phase, the growth rate of the A_2B phase is

$$C\frac{\partial x_1}{\partial t} = F_1 - F_2$$

(2.16)

while the growth rate of the AB phase is

$$C\frac{\partial x_2}{\partial t} = F_2 - C\frac{\partial x_1}{\partial t}$$

$$= F_2 - (F_1 - F_2) = 2F_2 - F_1.$$

(2.17)

From equations 2.14, 2.16 and 2.17

$$F_1 = \frac{\alpha}{x_1} \quad \text{and} \quad F_2 = \frac{\beta}{x_2} \tag{2.18}$$

$$\frac{\partial x_1}{\partial t} = \frac{\alpha}{x_1} - \frac{\beta}{x_2} \quad \text{and} \quad \frac{\partial x_2}{\partial t} = \frac{2\beta}{x_2} - \frac{\alpha}{x_1} \tag{2.19}$$

where

$$\alpha = \left[\frac{DC}{kT}(-\Delta H_R)\right]_{A_2B} \quad \text{and} \quad \beta = \left[\frac{DC}{kT}(-\Delta H_R)\right]_{AB}$$

Equations 2.18 and 2.19 show that neither x_1 nor x_2 may become zero, as this results in an infinite rate of growth. The AB and A_2B phases grow simultaneously once they form. As long as growth remains diffusion limited neither phase disappears.

The previous analysis assumes diffusion limited growth; however, growth of AB is likely to be initially limited by the interfacial reaction. F_2 is approximately constant, and can be written as $F_2 = \gamma$. Rewriting equation 2.19 it follows that

$$\frac{\partial x_2}{\partial t} = 2\gamma - \frac{\alpha}{x_1} \tag{2.20}$$

For $\dfrac{\partial x_2}{\partial t} \geq 0$

$$x_1^c \geq \frac{\alpha}{2\gamma} \tag{2.21}$$

Equations 2.20 and 2.21 show that the AB phase does not grow until the A_2B phase reaches a critical thickness x_1^c. In bulk diffusion A_2B will certainly grow to the requisite thickness, and growth of multiple phases is observed coincidentally.   In thin film diffusion one material is commonly consumed before the first phase reaches critical thickness. Subsequent phases form only after the previous phase grows to completion, and growth is observed one phase at a time (Figures 2-7, 2-8). Successive phases formed from thin films occur in the same sequence in which multiple phases are found in bulk couples, although some phases formed in bulk diffusion are missing in thin film diffusion. It is believed this is a reflection of the difference in supply of reactants[14].

It is possible, though less common, to find thin film systems in which multiple phases grow together. In such cases, the critical thickness of the first phase is extremely small. Examples are the Ti-Si system[15], and the Mn-Si system[16]. TiSi and TiSi$_2$ coexist prior to the complete consumption of Ti, while a number of layers appear to grow simultaneously before the consumption of Mn.

a) Thin Film Couple   b) Bulk Diffusion Couple

Figure 2-7   Structure of Silicide Growth

Figure 2-8[13]   Formation Paths for Platinum Silicide
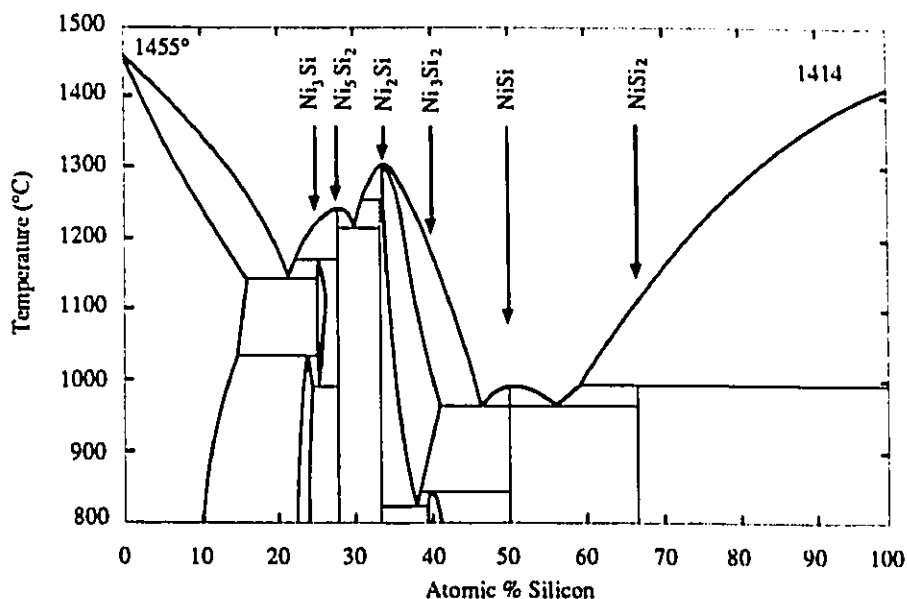
Figure 2-9   Nickel Silicon phase diagram. (Mayer and Lau, 1990)

2.1.4 Phase Formation

When exploring the phase diagram of a metal - silicon system a number of equilibrium silicide phases will generally be discovered (Figure 2-9). Numerous attempts (outlined below) have been made to reveal the nature of phase formation; seeking to explain both the order of formation as well as the presence or absence of phases in a diffusion couple. Evidence suggests that the first phase to form is invariable[14] and associated with the lowest temperature eutectic[13,17-19]. This correlation is the basis for a model by Walser and Bené, who state that "the first compound nucleated in [thin film] reaction couples is the most stable congruently melting compound adjacent to the lowest temperature eutectic in the binary phase diagram."[17] Subsequent phases are believed to be dependent on 1) the composition of the first phase formed and the stability of the phases closest to that composition (Ottaviani)[13] or 2) the compound with the smallest temperature difference between the liquidus curve and the peritectic (or peritectoid) point which lies between the first phase formed and the unreacted element (Tsaur et al.)[20]. For example if a thin nickel film is deposited on a much thicker silicon layer, the first phase to form is Ni_2Si. Subsequent phases form as $NiSi$, and $NiSi_2$. If a thick nickel layer is present on a thinner silicon layer, the first phase to form during annealing remains Ni_2Si, but subsequent phases form as Ni_5Si_2 and Ni_3Si. This correlates well with the aforementioned models, with the absence of Ni_3Si_2 favoring the model of Tsaur et al. over that of Ottaviani. It is difficult to determine from first principles whether a particular phase will form, but a dependence on the amount of metal and silicon available, as well as the temperature of formation, can generally be observed. Growth continues until either the most thermodynamically stable phase, or a phase representative of the initial amounts

of material, grows[13] (Figure 2-8). It is generally believed that phase formation is controlled by kinetics (movement of atoms), and not thermodynamics (driving force of reaction)[9].

While substantial empirical evidence exists to support the previous models of phase formation, evidence exists to contradict them as well. A notable, although not solitary, example is the manganese–silicon system, of which the phase diagram is shown in Figure 2-10. According to the rule outlined by Walser and Bené the first phase to form in a Mn/Si system should be Mn_5Si_3. Zhang and Ivey[16] report this to be untrue; that the first phase to form is actually Mn_3Si. This is in contrast to results presented by Eizenberg and Tu[22], where MnSi is the first phase to form. It should be noted that although the reports disagree, they both dispute the theory put forth by Walser and Bené. To explain this anomaly, an alternative model for silicide formation has been put forward by Zhang and Ivey. A brief description of the model follows[23]:

> In a thin film diffusion couple, the boundary between the growing phase (product) and the contracting phase is defined as the reaction region (Figure [2-11]). One of the reactants, designated as the moving reactant, diffuses through the growing phase to arrive at the reaction region. The other reactant, which may be either an element or a compound and is the contracting phase, is considered to be a nonmoving reactant due to its low diffusivity in the growing phase. If the moving reactant does not dissolve in the contracting phase (as in most silicide formation reactions), some of the nonmoving reactant has to dissolve from its own lattice into the reaction region. The two reactants are mixed together in the reaction region and
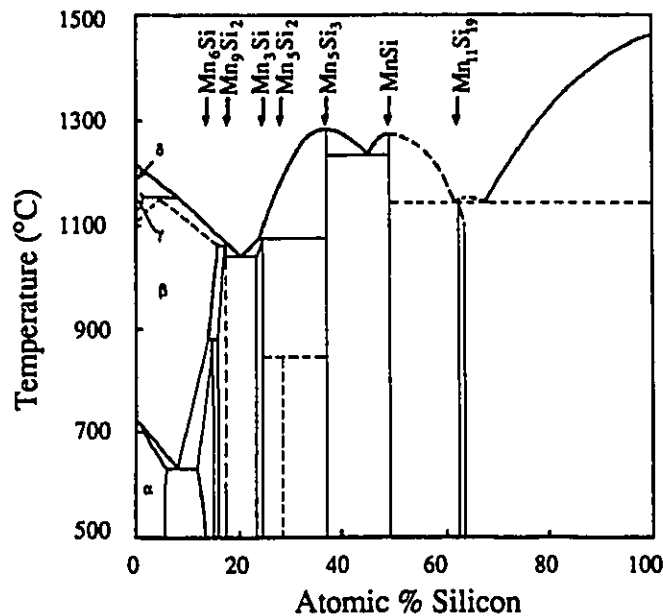
Figure 2-10   Manganese Silicon phase diagram (From Shunk[21])
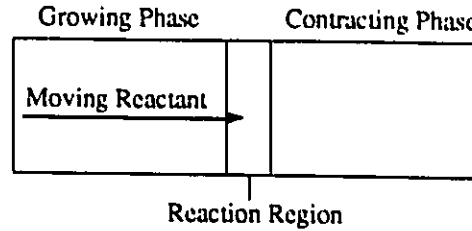
Figure 2-11   Growing and contracting phases (Zhang and Ivey)

are then rearranged on the lattice of the growing phase. The composition in the reaction region will determine which reaction is kinetically preferred. Since the number of dissolved nonmoving atoms in the reaction region is limited, the composition in this region would mainly depend on the diffusivity of the moving reactant. Thus, the faster the moving reactant diffuses, the higher the concentration of moving reactant in the reaction region. Which reaction will be kinetically preferred is mainly determined by diffusion of the moving reactant. In addition, it is reasonable to apply thermodynamic criteria for solution reactions to the reaction in the reaction region, because this region is essentially an atomic mixture.

Exact details of their model are presented by Zhang and Ivey, but some important considerations may be highlighted. 1) The composition of the reaction region determines which reaction is kinetically preferred. 2) The composition of the reaction region depends on the diffusivity of the moving reactant. The faster the reactant diffuses, the higher the concentration of the reactant in the reaction region. 3) The diffusivity and identity of the moving reactant may change with the formation of subsequent layers. 4) Because the reaction region is essentially an atomic mixture, the thermodynamic criterion $\Delta G < 0$ can be applied to the reaction. This criterion is important only insofar as determining if a reaction is thermodynamically allowed. It is unimportant which reaction is thermodynamically preferred. These points suggest that silicide formation depends on which species is the moving reactant, as well as on the diffusivity of that species. This model finds considerable support in the observation by Mayer and Lau[9] that the first phase formed is typically richer in the primary diffusing element. This tends to contradict the previous assertion of a dependence on equilibrium (phase diagram) considerations, but is consistent with observations that Ni_2Si[24], Pt_2Si[24] and Co_2Si[9] always grow when unreacted metal is present on the silicide layer. Figure 2-12 shows the silicide formation paths for several metal silicides, from which the previous connection can be established. As well, it adequately accounts for several anomalies displayed by previous formation models[16].

IIIA	IVA	VA	VIA	VIIA	VIII	VIII	VIII	IB	IIB
Sc	Ti_5Si_3 $TiSi$ $TiSi_2$	VSi_2	$CrSi_2$	$MnSi$ $MnSi_2$	$FeSi$ $FeSi_2$	Co_2 $CoSi$ $CoSi_2$	Ni_2 $NiSi$ $NiSi_2$	Cu	Zn
$YSi_{1.7}$	$ZrSi_2$	$NbSi_2$	$MoSi_2$	Tc	Ru	$RhSi$ Rh_4Si_5 Rh_3Si_4	Pd_2Si $PdSi$	Ag	Cd
La	$Hf\,Si$ $HfSi_2$	$TaSi_2$	WSi_2	Re	Os	$IrSi$ $IrSi_{1.75}$	Pt_2 $PtSi$	Au	Hg

Figure 2-12   Silicides formed by thermal annealing. Primary diffusing species is underlined, where known. Silicides are listed in order of formation. (From information in Mayer and Lau, 1990[9])

2.1.5 Diffusing Species

The diffusing species can be determined through the application of various marker techniques, two of which are commonly exploited. The first of these substitutes atoms of one or both elements with radioactive isotopes of those elements. These isotopes possess the same chemical properties as stable atoms, and their movement is easily traced through their radioactivity[9]. If such radioactive "tracer isotopes" are used to determine the diffusion coefficient, the coefficient measured is denoted as D^*, and is termed the *tracer diffusion coefficient*. D^* gives a reasonable approximation of D only when very small layers (<50 nm) of the radioactive material are used.

The second common method of studying diffusion entails the placement of a marker layer between two materials prior to interdiffusion. These layers are chemically inert with respect to the materials they separate, and do not significantly affect the overall diffusion between the two materials. The position of these layers is not coupled to the motion of a single material, but equally dependent on the motion of both elements. Under these conditions the marker serves as a plane against which the flux of material can be measured. As atoms diffuse across the plane, the marker shifts in a direction opposing the overall flux of atoms (Figure 2-13), due to a change in the amount of material on each side of the plane. Silicides form on the side to which diffusion occurs. Typical materials used for marker planes are implanted inert gases; a thin (~3nm), discontinuous tungsten film covering only a few percent of the surface; and thin, continuous oxide layers of one or both materials[1,25,26].

Interdiffusion between metal and silicon is most often dominated by the diffusion of one material. The identity of this material has direct import on the use of a silicide with integrated circuits[27,28]. When a silicide structure is grown on silicon, growth is more easily controlled if diffusion is dominated by the metal. To integrate a silicide structure on a patterned wafer, the wafer is completely covered with SiO_2 save for those areas desired for silicide growth. Metal is deposited on the wafer and reacted to form silicide
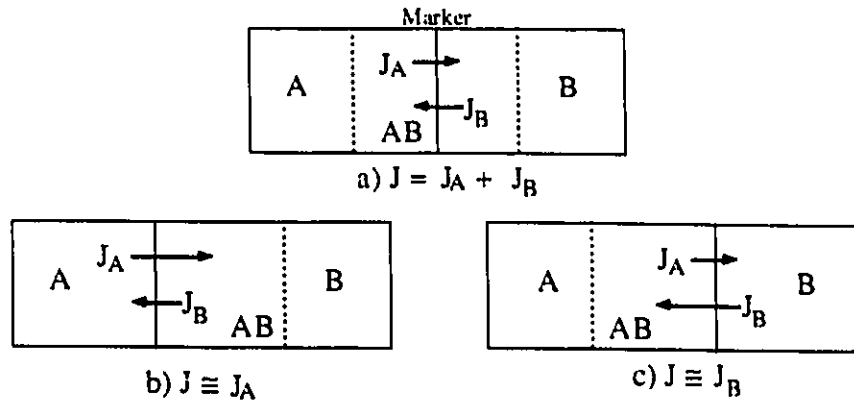
Figure 2-13   Marker plane between layers of a diffusion couple. J is the diffusion flux crossing the plane. a) Flux of A is equal to B, and the marker plane does not move. Silicide formation takes place around the marker. b) Flux J_A dominates diffusion, and the marker plane moves towards the A side. Silicide formation takes place on the B side of the marker. c) Flux J_B dominates diffusion, and the marker plane moves towards the B side. Silicide formation takes place on the A side of the marker.

wherever silicon is exposed. Selective etching removes excess metal and oxide, leaving silicide in the desired areas (Figure 2-14). A problem exists when silicon is the main diffuser as silicon diffuses into the metal around the SiO_2 covering, forming silicide around the window intended to define the area of growth. This reduces the precision with which structures can be produced.

The identity of the diffusing species is dependent on the metal involved, as well as the temperature at which diffusion occurs. It has been observed[13] that at low
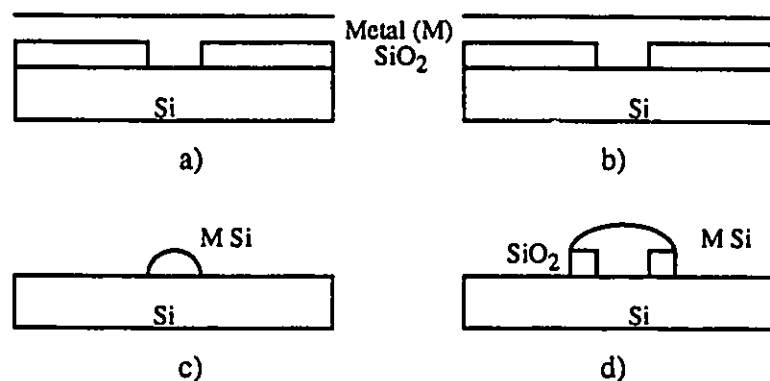
Figure 2-14 : Silicide Patterning.   a) and (b) show metal deposited on silicon before silicide growth occurs. (c) shows a device remaining after the growth and etching of a silicide in which metal is the diffuser, (d) silicon is the diffuser.

temperatures (less than ~ 600 °C) the principle moving species is generally metal, while at high temperatures (greater than ~ 700 °C) it is silicon. High temperatures are generally required to form silicides from refractory metals, while silicides of noble and rare earth metals form at low temperatures. Rare earth metals are an exception to the previous diffusion guideline, however, as silicon, not metal, is the main diffuser. A summary of the main diffusing species can be seen in Figure 2-12.

If a silicide is formed from a noble metal the first phase to form is a metal rich silicide, and as stated previously, the principle diffusing species is metal. The thickening of this phase is usually proportional to the square root of the diffusion time, suggesting a diffusion limited growth mechanism. Refractory metals, on the other hand, form an initial phase rich in silicon, but also tend towards diffusion limited growth[13]. In this case the principle diffusing species is silicon. These results tend to support the "ordered Cu_3Au effect", which says that in intermetallic compounds the dominant mobile species is usually the species with the majority of atoms[10,29]. This effect can be easily explained with the fact that the majority atoms constitute a continuous network on which a vacancy can easily migrate[10]. Motion of the minority atoms requires that a vacancy of both the majority and minority atom be present or that there is a local disruption in the crystal lattice. Both these cases result in a larger activation energy for minority atoms. Rare earth metals can be an exception to this rule because of their less closely packed structures, which allow interstitial diffusion of large atoms such as silicon. Two other notable exceptions to this rule are $NiSi_2$ and $CoSi_2$, as the minority metal atoms are more mobile than the majority silicon atoms[10]. The reason for this has not yet been determined.

In addition to possessing a large number of silicides which seem to be contradictory to established rules, the rare earth metals are also a subject of considerable controversy. It is agreed that the first phase formed is silicon rich, but growth has been reported to be limited by diffusion[13] as well by the interface reaction[10]. The true limiting factor is probably a complex combination of the two.

2.1.6 Impurity Effects

The presence of impurities in silicide systems profoundly affects the reproducibility of silicide phases. Impurities may enter the system at various stages of processing to reside in locations throughout the system. They can have direct effect on a silicide, altering by virtue of their presence such properties as resistivity, etchability, adhesion and more. Impurity effects may be indirect, altering or commuting properties by altering silicide formation. The stoichiometry of a film may be altered by impurities in a sputter gas, or the outcome may be changed when silicides are formed through reaction.

Impurities present during reaction often redistribute during silicide growth to alter the kinetics of silicide formation. The prevalent effect is a reduction of reaction kinetics. This effect depends upon whether an impurity is mobile or immobile, as well as its
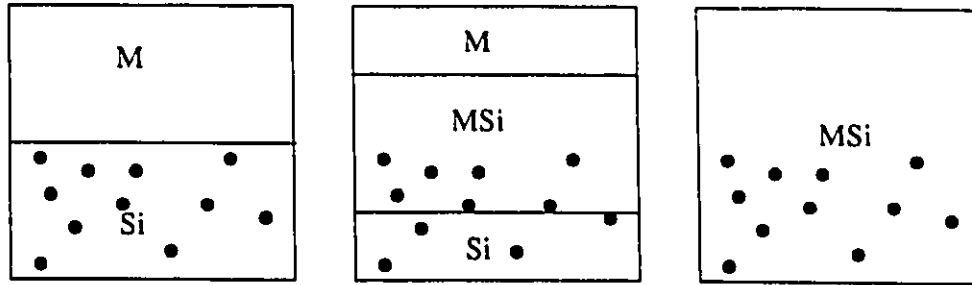
Figure 2-15   Effect of immobile impurities in the immobile species

location within the silicide system. Three locations are defined for the presence of impurities in a metal silicon system: the silicon substrate, the metal thin film, and the metal - silicon interface. The location of impurities is of tantamount importance to the effect displayed on a silicide system. A simple model, first proposed by Scott and summarized by Lien and Nicolet[30] explains the effects of impurities in a silicide. It is assumed for simplicity of illustration that metal is the mobile species, and that impurities within the system are themselves immobile. If impurities are found in the nonmobile (stationary) layer, they remain stationary with respect to this layer throughout silicide formation, and impurities will be uniformly incorporated into the silicide layer (Fig 2-15). Impurities in this situation may slow down the growth rate of silicide, but in general their influence is small. When impurities are present in the mobile layer (metal), the situation is different. Impurities accumulate at the metal - silicide interface; left behind as metal migrates through the silicide to react with silicon. Depending on the impurity concentration, three scenarios exist for this build up (Figure 2-16). The first, in which impurity levels are slight, results in the ultimate accumulation of impurity on the surface of a fully reacted silicide layer. Growth is slowed, but silicide formation is completed. The second scenario exists for higher impurity concentrations; concentrations which cause sufficient accumulation of impurity to uniformly stop silicide growth. Finally, a combination of these two effects can exist, leading to laterally non uniform layers. It is

Low Concentration   High Concentration   Nonuniform Concentration
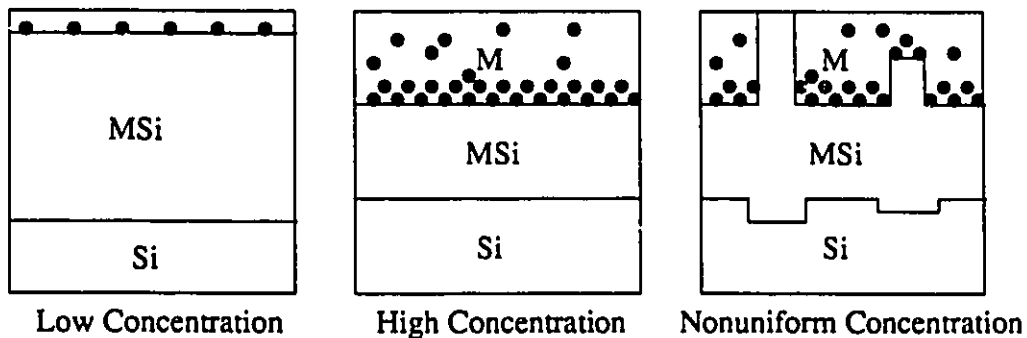
Figure 2-16   Effect of immobile impurities in the mobile species
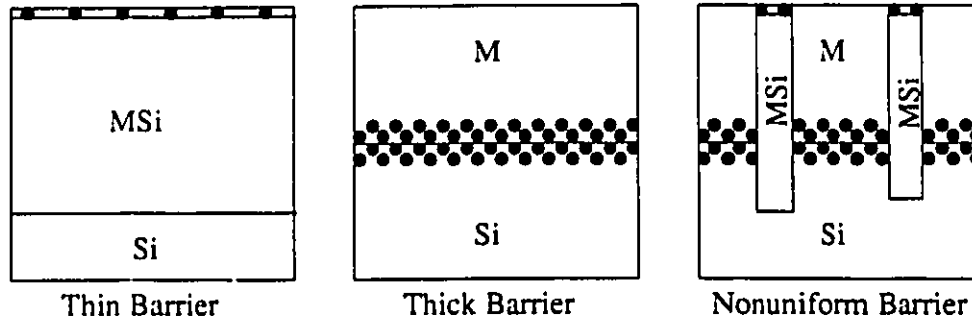
Figure 2-17   Effect of immobile interfacial impurities on silicide formation

easily seen that impurities in the mobile layer are more significant to the formation of silicide layers than are impurities in the stationary layer. Not only may growth be altered, as seen in the figures, but Schottky barrier heights may be affected significantly[31]. In the case of nonuniform silicide formation, the Schottky barrier height may be variable. A corollary to this result exists when silicon is mobile. The silicon - silicide interface suffers a build up of property altering impurities. This interface is often the primary concern for silicide use, making this a serious consideration in silicide formation.

The effect of interfacial impurities is analogous to the effect of impurities in the mobile reactant, where an accumulation of impurity creates a barrier to interdiffusion. Three possibilities likewise exist. When interfacial barriers are thin, they are eventually pushed to the silicide - moving species interface. If the moving species is the metal thin film, the impurity layer will eventually be pushed to the surface of the silicide. If the species is the underlying silicon, the impurity layer will be buried underneath the silicide. When the barrier is thick, silicide reaction is simply precluded. For nonuniform barriers silicide formation occurs only in thin regions, and laterally nonuniform layers evolve (Figure 2-17). Comparison of figures 2-16 and 2-17 show the similarities in the effects of interfacial impurities and those within the mobile layer.

Perhaps the most significant impurity effect on thin film reactions is oxygen contamination. Remarkably low concentrations of oxygen strongly affect the sequence of phase formation. By correlating increased film resistance with the oxygen content present during an anneal, Ottaviani and Nobili have concluded that even the oxide which grows during transportation from deposition chamber to annealing environment is enough to significantly contaminate a metal film[15]. The strong affect of oxygen is seen in the Pt-Si system (Figure 2-18). Concentrations of 0.1% are sufficient to slow silicide formation, and concentrations of 3% can stop growth completely. Researchers[30] have investigated the redistribution of dopants (mainly As and P) in silicon during silicide formation, and found that, although many dopants have low diffusivity at low annealing temperatures, part of the dopant is accumulated at the silicon - silicide interface, and another part in the
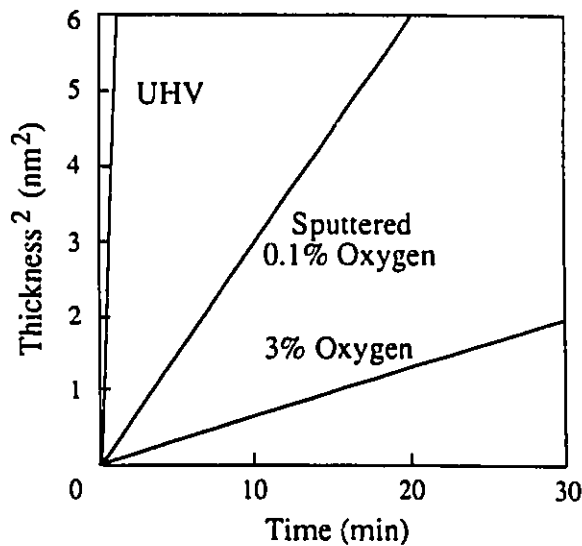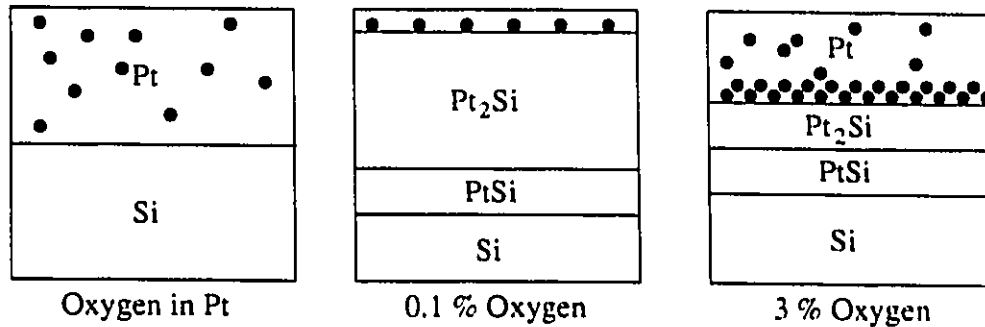
Figure 2-18 Effect of oxygen on silicide formation in platinum - silicon diffusion couple. Low concentrations of oxygen in the platinum film cause an accumulation of oxygen at the Pt - Pt_2Si interface which slows formation. Concentrations of 3 atomic % cause sufficient built up of oxygen to stop silicide growth. Thickness of Pt_2Si formation at 315°C for three sample purities is shown also. (From Ottaviani and Mayer[32])

silicide itself. This phenomenon cannot be explained by the previous model. Another model has been proposed to explain this result[33], in which defects generated in Si adjacent to the interface enhance the diffusion of dopants. This accumulation of dopants has been used to alter the height of Schottky barriers and reduce the contact resistance between silicon and silicide to form ohmic contacts[34].

In addition to immobile impurities there are some impurities which exist which are mobile during silicide formation. Impurity redistribution is due to diffusion of the impurity and/or the kinetic processes of silicide formation. The previously explained model is not sufficient in and of itself to completely explain the nuances of redistribution for impurities of this sort. Such mobile impurities are important when considering the redistribution of impurities in stable silicides, and affect the properties of a silicide more than the formation of the silicide.

2.2   Substrate Cleaning

Before metal is deposited on a silicon substrate, the substrate must be cleaned. It is important to get the substrate surface into a "known" condition to assure consistent and predictable growth of phases, as even slight amounts of impurities can significantly affect the kinetics of silicide growth, and alter the kind of compound formed[35,36]. At the very least, surfa particles may interfere with the uniform growth of a silicide layer[37].

Two types of contaminants are found on a substrate surface; particulates and films. Particulates are "any detectable shape on the surface of a wafer that has readily definable features" while a film is any "detectable layer of foreign material, generally random in character". Particulates are generally more easily detected than films–a result of their discrete presence on the surface–and may be either organic or inorganic. Films have a more continuous character than particulates, making them harder to detect. Examples of films are solvent residues, oil films, silicone films and metallic films[38].

Proper cleaning generally involves two or three steps[36]: the removal of gross contamination such as inorganic particulates, the removal of contaminants such as organics or oxide layers, and an in situ clean in the deposition chamber to remove contaminants that arise during transportation to the chamber. In situ cleaning techniques vary, but usually take the form of a controlled back etch to remove a thin surface layer[36].

Often particles are held on a surface by no more than van der Waals forces, and may be removed by simply immersing the substrate in water[37]. Submicron particles may be difficult to remove, as the bonding forces to the surface may be high with respect to their mass[37]. These may be removed in a variety of ways, including the use of solvents, etching, high pressure liquid spray, or ionized gas blow off[36]. The most effective technique for removing particulate contamination seems to be a high pressure spray followed by a brush off under liquid and flow off using condensing anhydrous alcohol vapor[36]. Etching may be used to remove some of the surface material along with the contaminants and is an excellent way to get the surface into a known condition. Surface layers such as oxides or films are removed along with contaminants that are difficult to remove by other methods.

Organic contamination and films may be removed by the application of solvents or oxidation techniques. Solvents may vary in their ability to dissolve organic material and their effectiveness needs to be determined by discovering the solubility parameter[36] for any contaminants to be removed. The use of such "wet chemistry" tends to leave behind residues[37]. One solution to this problem is to simply burn off the material in an oxidation tube at temperatures from 900 °C to 1200 °C. Alternatively, surface contamination may be removed using a dry etch plasma gas to remove a thin surface layer with out leaving a residue behind[37].

One of the most useful surface cleaning techniques when dealing with organic contamination is that of UV/ozone oxidation[36,39]. It is a simple, inexpensive process that can be used in an air or vacuum environment. By placing precleaned surfaces within a

few millimeters of an ozone producing UV source, the process can produce near atomically clean surfaces in less than 1 minute[39]. In the process, a surface is exposed to oxygen and subjected to ultra violet radiation. Two wavelengths of radiation are used, 184.9 nm and 253.7 nm[39]. The first of these is absorbed by oxygen and leads to the generation of ozone. The second of these is not absorbed by oxygen, but is absorbed by ozone and hydrocarbons. The absorption of the radiation by ozone leads to its destruction. The continual creation and destruction of ozone leads to the formation of atomic oxygen, which is a very strong oxidizing agent[39]. In the presence of this atomic oxygen, the surface of the substrate is quickly oxidized, along with any hydrocarbons that may be present on the surface. A surface layer will rapidly form which contains any organic impurities that were present on the surface. The material is then subjected to a high temperature anneal which evaporates off the oxide, leaving a perfectly clean substrate surface. The oxide layer may also be removed in a hydrofluoric acid dip.

Another useful and very common cleaning procedure for use on silicon substrates specifically is the RCA clean, involving a complex series of solvents based on hydrogen peroxide[40]. It is however an overly complex procedure. A simple variation is the use of a sulfuric acid and hydrogen peroxide bath, known as a "piranha" dip. When the two materials are mixed, a violent reaction occurs which removes any organic contamination of the surface of a wafer dipped in the mixture.

2.3   Formation of Iron Silicide

The first stage of iron silicide formation is the deposition of iron onto a silicon substrate. Conflicting reports exist as to the structure of evaporated iron. Okamoto et al report that on an unspecified substrate evaporated iron forms a layer possessing a columnar structure, the texture and density of which can be varied by altering the evaporation rate and angle of incidence of the iron[41]. Conversely, Urano et al[42,43] have found that thin evaporated iron films can be grown epitaxially on a Si(111) substrate. These thin layers have been found to maintain the ferromagnetic nature of bulk iron[44].

According to the iron–silicon phase diagram, two phases of iron silicide are stable below 800 °C: FeSi and $FeSi_2$ (Figure 2-19). Of these phases it is iron disilicide ($FeSi_2$) that is of the most interest, as it has been found to possess semiconducting properties valuable to the electronics industry. The most common method by which iron silicide is formed is the solid state reaction of a thin iron film on a bulk silicon substrate. This is possible as iron disilicide is the most thermodynamically stable phase in the presence of excess silicon. It has been found that the first phase to form in a iron - silicon diffusion couple is FeSi; formation occurring between 325 and 450 °C[45-48] with silicon being the primary diffusion species in a diffusion limiting reaction[48]. There is some indication of Fe_3Si formation occurring in the same temperature range as FeSi[47]. Confirmation of this may be steeped in confusion as silicon is reported to dissolve in iron prior to compound
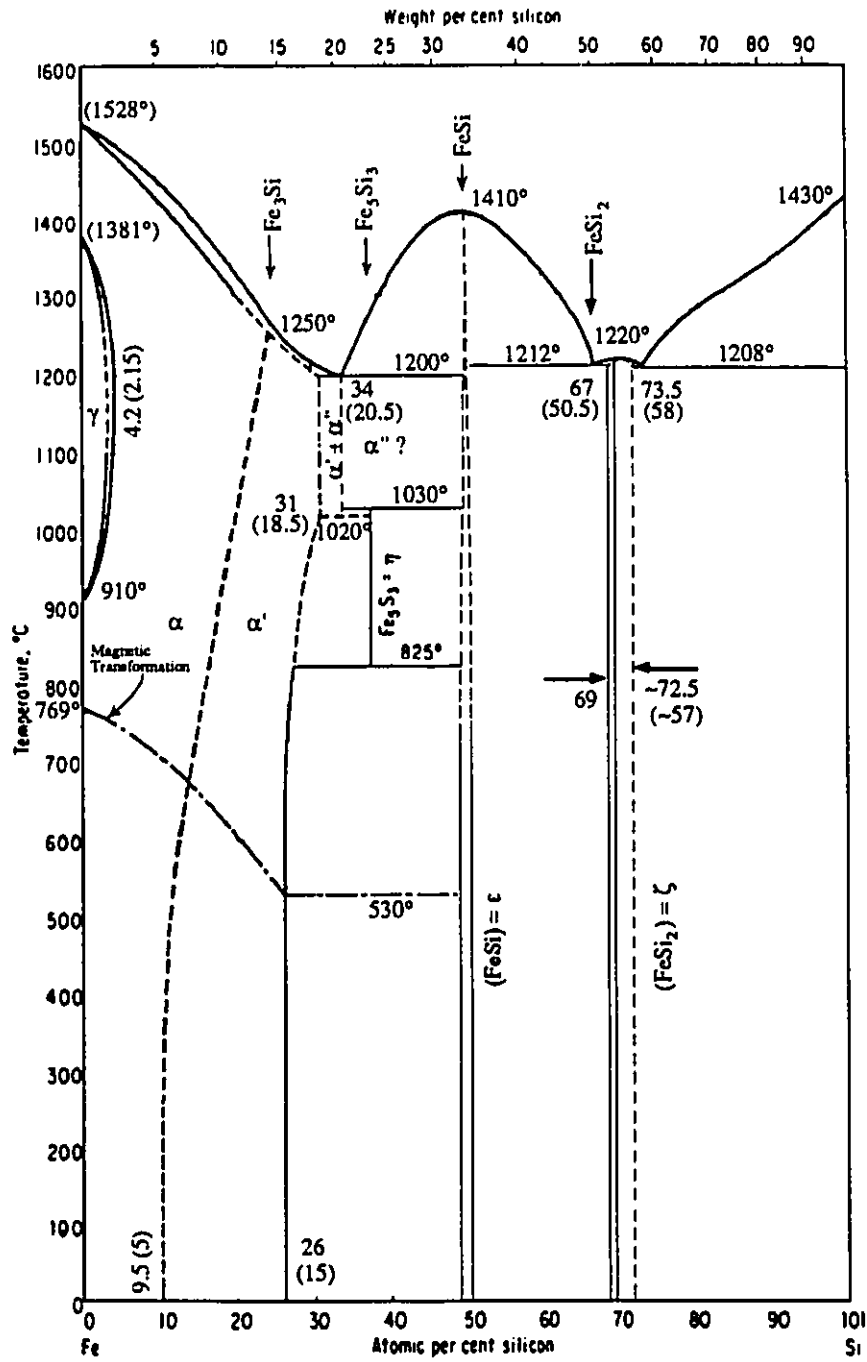
Figure 2-19   Iron Silicon Phase Diagram ("Constitution of Binary Alloys", Mcgraw-Hill Book Company, 1958)

formation, with a disordered to ordered transition occurring as silicon reaches 25 at %
concentration[48]. Orthorhombic β FeSi$_2$ forms from FeSi above 450 to 550 °C[45,46,47,48,49].
From a survey of the literature it would appear that the lower formation temperatures
correspond to improved vacuum conditions during deposition and annealing, with the
best results being obtained when the vacuum is not broken between these steps. FeSi$_2$
appears to grow laterally in patches from a nucleation controlled reaction[50]. Lower
temperature growth and cooling rates yield semiconducting layers of better quality[50,51],
with smaller grain sizes, less stress and less surface roughness. Sapphire substrates
produce smoother surfaces than silicon substrates due to the match of the thermal
expansion coefficient of sapphire to the silicides[50]. The β disilicide phase remains stable
until approximately 670 °C, at which point annealing produces a disruption of thin films
into individual islands, a process known as agglomeration[45,46,52]. The literature is unclear
on whether agglomeration occurs in the iron layer prior to silicide formation, or in the
silicide layer after formation.

At a temperature which is in some dispute, being reported at various values
between 900 °C and 960°C[53-56], β FeSi$_2$ transforms to the tetragonal α phase. This phase
is not semiconducting, but rather metallic in nature. It is important to note that this
transition temperatures lies in the typical range for the thermal growth of silicon dioxide
(SiO$_2$), which is an important material in the production of integrated circuits. SiO$_2$ is
grown between 900 - 1050 °C in current microelectronic processes, and the tendency for
FeSi$_2$ to transform away form the semiconducting β phase may make the material
difficult to integrate with electronic devices.

At temperatures near the transition point from β to α disilicide, thin iron layers of
less than 1000 Å appeared to favor formation of the α phase, while thicker layers of
greater than 1500 Å favor formation of the β phase[53]. Additionally, it was found that
radial symmetry in the variation of α and β phases over the 4 in diameter wafers used as
the substrate corresponded to the radial variations in the sputtering thickness. The
concentration of β phase as compared to α phase is greater near the center of the wafer
where the initial iron layer is thicker. These results agree with the tendency for the α
phase to be slightly deficient in iron[53,54].

Chapter 3

Electronic Properties of Silicides

Silicides can be subdivided into two classes based on their electronic character: metallic and semiconducting. These silicides are used for drastically different purposes and require distinct properties to make them suitable for practical application. These properties are discussed in the following sections, as they relate to each silicide class.

3.1 Metallic Silicides

3.1.1 Resistivity

For metallic silicides such as $CoSi_2$, $TiSi_2$, and α $FeSi_2$ the most obvious quality to consider is the resistivity of the silicide, as most of these materials could be used as interconnects between devices or for metallic gates in high speed and specialized devices. With a decrease in line width to sub-micron levels, the use of low resistance interconnects is becoming necessary to reduce resistance dependent delays and power consumption in large scale integrated circuits. The higher temperature stability of silicides and their high resistance to electromigration make them particularly suitable to large scale integrated circuits. The continued use of metals for interconnect material has been hampered by a number of difficulties, including electromigration, high diffusivity in silicon and poor stability at high temperatures[1]. While silicides will likely never achieve the low resistivities of metals currently used as interconnect material, they neatly circumvent the physical deficiencies associated with these metals while offering a lower resistivity than the currently used alternatives such as polysilicon.

Table 3-1 lists the resistivities for selected polycrystalline metal silicides. A dependency can be seen on the method of silicide formation. In most cases the silicides were formed by reacting a thin metal film with a silicon or polysilicon substrate. The few exceptions, in which the silicide was formed through cosputtering of the metal with silicon, show higher resistivities than the reacted films. The reason may be a reduced number of grain boundaries in the reacted silicides, owing to interdiffusion and grain growth during the reaction process. These values may be compared to those in Table 3-2 for single crystal silicides, which possesses much lower resistivities.

Silicide	Resistivity ($\mu\Omega$·cm)		Silicide	Resistivity ($\mu\Omega$·cm)	
TiSi$_2$	13-16		MoSi$_2$	100	cosputtering
	25	cosputtering	WSi$_2$	70	cosputtering
ZrSi$_2$	35-40		α FeSi$_2$	1000 +	
HfSi$_2$	45-50		CoSi$_2$	18-20	
VSi$_2$	50-55			25	cosputtering
NbSi$_2$	50		NiSi$_2$	50	
TaSi$_2$	35-45			50-60	cosputtering
	50-55	cosputtering	PtSi	28-35	
CrSi$_2$	600		Pd$_2$Si	30-35	

Table 3-1 Resistivities of selected metal silicides[27]

Silicide	Direction	Resistivity ($\mu\Omega$·cm)		Anisotropy of thermal component	Thermal Resistivity Ratio ρ 273 K / ρ4.2 K
		4.2 K	273 K		
TiSi$_2$	[001]	0.09	11.3	1.23	126
	[100]	0.08	11.0		138
	[010]	0.08	9.19		115
VSi$_2$	[2$\bar{1}$0]	8.59	79.3	1.88	9.23
	[0001]	5.03	42.7		8.49
CrSi$_2$	[2$\bar{1}$0]	338	739	1.75	2.19
	[0001]	252	481		1.91
MoSi$_2$	[100]	0.17	17.9	1.42	105
	[001]	0.13	12.6		96.9
α FeSi$_2$	[001]	250	267	1.18	1.07
	[100]	230	250		1.09
CoSi$_2$	[111]	4.33	20.9	1.29	4.83
	[100]	3.77	17.2		4.56
	[112]	3.27	16.1		4.92

Table 3-2 Resistivities of single crystal metal disilicides[57]

Material	Typical Sheet Resistance[58] Ω /□	Approx Resistivity[59] $\mu\Omega$·cm
Metal (Al)	0.05	3.5
Diffusion	25	1250
Polysilicon	50	5000
Silicides	3	300

Table 3-3 Resistivity values for materials currently used in silicon based microelectronics.

Table 3-3 contains typical resistivities for currently used interconnect materials. Due to the proprietary nature of such information, the values quoted are approximate[59]. It is easy to see that silicides offer an advantage over materials such as polysilicon and diffusion (highly doped n or p type substrates), although they fall far short of the resistivity obtained with aluminum. In most instances disilicides possess lower resistivities than other silicides, even though they contain more of the nonmetallic element[27]. Most disilicides possess resistivity values that are only an order of magnitude greater than pure metals. An explanation for this lies in the nature of the metal to metal and metal to silicon bonding in these compounds. Bonds tend to be ionic in metal rich silicides but covalent or metallic in silicon rich silicides. Fe and Cr disilicide seem to be exceptions to this rule, displaying resistivities substantially larger than than other silicides. These exceptions have been attributed to the magnetic properties of the two disilicides, although this has not been substantiated[27].

3.1.2 Ohmic Contacts

It is unlikely for resistivity to be the sole requirement of a conducting material. It is also important to consider the ease with which a material produces good contacts to silicon. One must consider the Schottky barrier height between silicon and the interconnect material. A high Schottky barrier acts much like a silicon p-n junction, rectifying current and creating a non linear current - voltage characteristic. Figure 3-1 shows a typical I-V curve for a Schottky barrier. Traditionally, it has been stated that a good contact must possess a linear current to voltage relationship, symmetric about the origin of the I-V curve. Resistance attributable to a contact should be low, such that the voltage drop across a contact is small when compared to the voltage drop across the devices it connects. Contacts of this nature are termed ohmic. This criterion is inaccurate, however, as a contact can be considered ohmic as long as it can supply the current demanded by the devices it connects without affecting the operating voltage of those devices. The non-linear characteristic shown in Figure 3-1 is therefore not a problem as long as contact resistance is small[60,61].
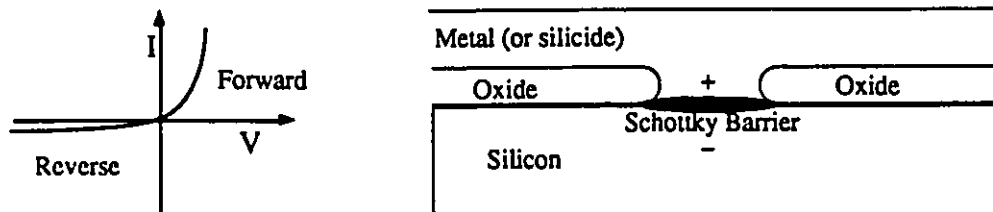
Fig 3-1 I-V characteristics through a Schottky barrier

Contact resistance arises when a metallic material placed in contact with silicon forms a Schottky barrier diode. Current through such a diode can be expressed as it would for a pn junction,

$$I = I_0(e^{qV/kT} - 1)$$

where I_0 is the saturation current, q is the electronic charge, k is Boltzmann's constant and T is temperature. As the curve is non-linear (see Figure 3-1), a differential resistance is defined at each point along the curve as dV/dI. As an ideal contact would have a linear curve symmetric about the origin, contact resistance r_c is defined at the origin as

$$r_c = \frac{\partial V_0}{\partial I} \qquad (V=0)$$

Current density J is used in lieu of the current I to define a specific contact resistance R_c that is independent of contact area. Therefore

$$R_c = \frac{\partial V_0}{\partial J} \quad \text{and} \quad r_c = \frac{R_c}{A}$$

where A is the contact area. Completing the differentiation gives

$$R_c = \frac{kT}{qJ}$$

When doping levels are lower than 10^{17} atoms/cm^3 current flow across a metal - semiconductor junction is due to thermionic emission and can be described as

$$J = A^{**}T^2 e^{-q\phi_B/kT} \times (e^{qV/kT} - 1) \text{ [60]}$$

where A^{**} is the Richardson constant and ϕ_B is the Schottky barrier height in volts. The specific contact resistance at zero volts becomes

$$R_c = \frac{\partial V_0}{\partial J} = \left(\frac{k}{qA^{**}T}\right) e^{q\phi_B/kT} \qquad (3.1)$$

The exponential dependency of contact resistance on the Schottky barrier height can be seen in equation 3.1. Table 3-4 lists Schottky barrier heights on silicon for some important silicides. As a comparison, Table 3-5 shows the barrier height of various metals on n and p type silicon. An indication of what this means to the contact resistance can be seen in Table 3-6, where contact resistances for various Schottky barrier heights are calculated from equation 3.1. A contact is considered ohmic if its resistance is approximately 1-2 $\mu\Omega$ / cm^2 [60], so it would appear that few materials produce an ohmic contact to silicon. In practice this is not the case, as the saturation current I_0 is often

Silicide	ϕ_β (V)	Silicide	ϕ_β (V)
HfSi	0.53	$TiSi_2$	0.60
MnSi	0.76	$CoSi_2$	0.64
CoSi	0.68	$CrSi_2$	0.57
NiSi	0.75	$ZrSi_2$	0.55
Ni_2Si	0.75	WSi_2	0.65
RhSi	0.74	$MoSi_2$	0.55
Pd_2Si	0.74	$TaSi_2$	0.59
Pt_2Si	0.78	$NiSi_2$	0.70
PtSi	0.87	HfSi	...
IrSi	0.93	$FeSi_2$	...
Ir_2Si_3	0.85	$NbSi_2$	...
$IrSi_3$	0.94	VSi_2	...

Table 3-4 Schottky barrier heights of important silicides on n type silicon[27]

Metal	ϕ_β (V) - n Si	ϕ_β (V) - p Si
Al	0.72	0.58
Au	0.80	0.35
Cr	0.61	
La	0.40	0.70
Mo	0.68	0.42
Pt	0.90	
Ti	0.50	0.61
W	0.67	0.45
Y	0.40	0.70

Table 3-5 Schottky barrier heights of selected metals on n and p type silicon[60]

ϕ_β (V)	R_c ($\Omega \cdot cm^2$)
0.85	4.7×10^5
0.70	1.4×10^3
0.55	4.3
0.40	1.3×10^{-2}
0.25	4.0×10^{-5}

Table 3-6 R_c values for n-type silicon Schottky Diodes[60]

orders of magnitude greater than theory predicts, greatly reducing R_c[60].

Many materials, such as Al, are commonly used as ohmic contacts to silicon even though equation 3.1 predicts a high resistivity, even when I_0 reduces R_c by two or three orders of magnitude. An ohmic contact can be created in any region with high recombination rates, including highly doped or damaged regions. It is clear that a mechanism exists to lower the contact resistance. This mechanism involves altering the Schottky barrier between silicon and the contacting material. Engineering the height of the barrier has proven to be impractical, but barrier width is easily controlled. The width of the space charge region is proportional to $N_D^{-1/2}$, so by increasing the doping level the width of the space charge region is reduced. This is seen in Figure 3-2. If the space charge region (or *depletion region*) is sufficiently narrow electrons can pass directly through. Conduction through this region is commonly referred to as quantum tunneling or field emission. When the doping level reaches about 10^{19} atoms/cm^3, instead of being proportional to $e^{q\phi_B/kT}$ the contact resistance becomes

$$R_c \propto e^{B\phi_B/\sqrt{N_D}}$$

$B = 4\pi/h \sqrt{\varepsilon m^*}$, where h is Plank's constant, ε is the dielectric permittivity, and m^* is the effective mass of the charge carrier. N_D is the number of charge donors. At these doping levels, the contact resistance can drop by as much as five orders of magnitude[60].

Upon deposition many materials display significant interdiffusion with silicon, leading to autodoping of the region near the interface. Metal atoms which have diffused into the silicon may donate or accept electrons to increase the number of charge carriers at the junction. If a metal increases the charge carriers in n type silicon it will deplete the charge carriers in p type silicon, so contacts to one type of silicon will generally require additional doping.

For silicides to be used successfully as ohmic contacts to silicon devices, it is important for them to possess similar contact resistance to both n and p type silicon. This ensures an equal current supply to n and p devices. Refractory metal silicides have nearly equal Schottky barrier heights for n and p type silicon, making them particularly suitable for use as contacts to microelectronic devices. Noble metal silicides, however, have high barrier values on n type material, making them suitable for contacts to p type silicon only. Contacts made with these silicides may require additional doping for n type material.
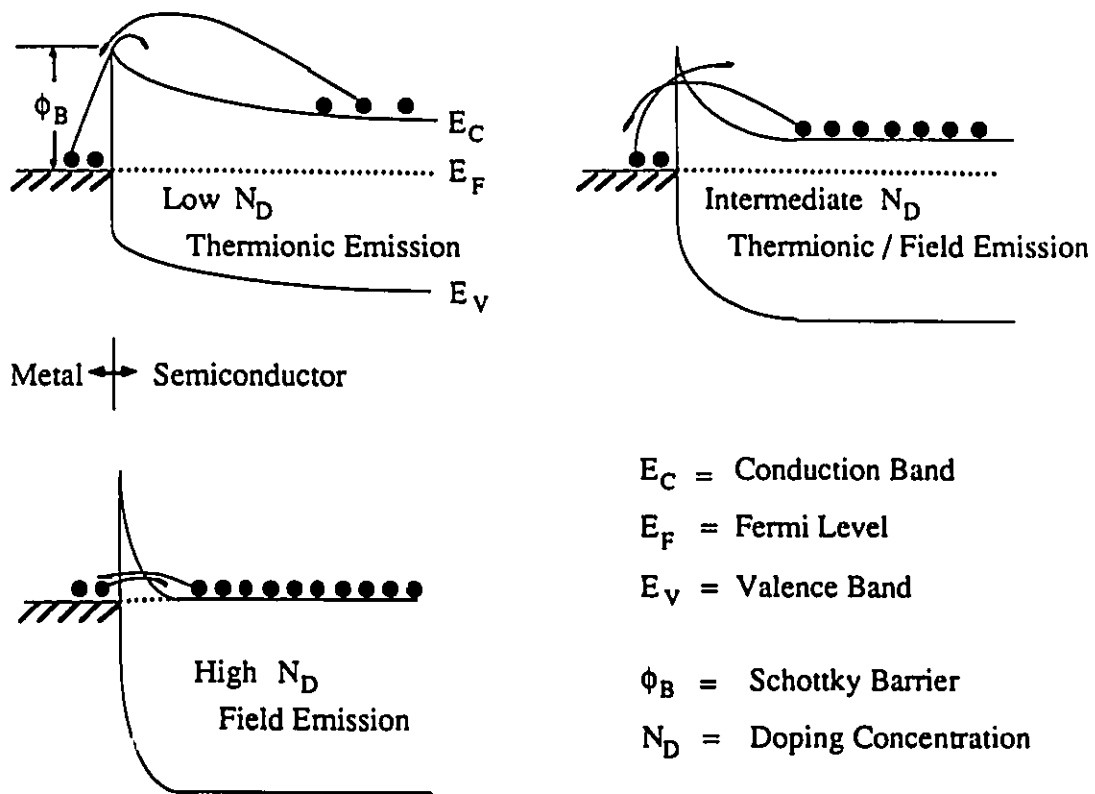
Figure 3-2 Schematic of Schottky barrier between metal and n-type semiconductor for various semiconductor doping levels. Shown also are the conduction methods that dominate at each level[61]. Effects for p-type semiconductors are similar.

3.2   Semiconducting Silicides

A number of silicides possess forbidden energy gaps which make them suitable for use as semiconductors. These energy gaps often lie in a range suitable for optical devices, particularly those operating in the infrared range. Because of the potential for integrating silicide structures with conventional microelectronics processes, these semiconducting properties offer possibilities for the integration of optical and electronic devices on a single substrate. Unfortunately, relatively little work has been done to characterize the optical and semiconducting properties of most silicides, and most information currently available pertains to bulk silicide samples. Table 3-7 shows the energy gap for several silicides which are known.

One of the most interesting concepts of optical integration in electronics is that of electro-optic interconnects. Because of the extremely high operating speeds of leading edge integrated circuits, significant delay is attributed to the interconnections within and between chips. A solution to the problem could lie in optically coupling devices. The problem at present is that most components are build around silicon technology, and silicon possesses an indirect forbidden energy gap which does not lend itself readily to the construction of optical sources or detectors. As a result there has been a concerted effort to grow, on a silicon substrate, semiconductors which are more conducive to optical use. Silicides have shown great promise in this area for several reasons: many silicides have the potential to be easily grown on silicon substrates[62]; growth is possible under conditions attainable in current microelectronic processing environments; and it is suspected that several silicides have direct energy gaps which make them suitable for development of optical based devices[62]. As stated previously, a complete account of semiconducting properties does not exist for silicides as a whole, so it is unknown if any *one* silicide possesses all the requirements for integration into current silicon technology.

Material	Energy gap eV
$CrSi_2$	0.35
$\beta\,FeSi_2$	0.87
$LaSi_2$	0.19
$ReSi_2$	0.12
$BaSi_2$	0.48
$OsSi_2$	1.8
Ca_2Si	1.9
Mg_2Si	0.78
$IrSi_{1.75}$	1.2
Ru_2Si_3	1.0
$MnSi_{1.7}$	0.65

Table 3-7
Forbidden energy gap of selected silicides[53,62]

3.2.1 Mobility and Conductivity

An important characteristic for any semiconductor is the mobility of its charge carriers. Semiconductors have a resistivity much greater than conducting materials, but this is due to a reduced number of charge carriers and not an inhibition to charge flow itself. Drift mobility is a measure of this ease of travel through the material. Higher mobilities make for faster and less power consuming circuits.

When placed in an electric field charge carriers within a material are affected by a force $F = e\mathcal{E}$, where $\mathcal{E}$ is the field strength and e is the magnitude of electronic charge. This force causes charge carriers to drift with an acceleration

$$a = \frac{e\mathcal{E}}{m^*}$$

m^* is the effective mass of a charge carrier. Ideally a charge carrier passes undisturbed through a material, its velocity increasing continuously. In actuality it continuously encounters scattering centers within the material that stop its movement, causing the charge carrier to undergo a continuous series of accelerations from zero drift velocity. This fixes the velocity at an average value υ_d. The average velocity of the charge can be estimated using the acceleration a and times between collisions τ, whereby

$$\upsilon_d = a\tau.$$

Using the acceleration described above,

$$\upsilon_d = \frac{e\tau}{m^*}\mathcal{E}$$

From this equation the mobility of a charge carrier is defined as

$$\mu = \frac{e\tau}{m^*} \qquad \text{with the units} \quad \frac{cm^2}{V \cdot s}$$

leaving a simple description of the drift velocity.

$$\upsilon_d = \mu\mathcal{E}.$$

Current is the quantity of charge passing through a cross sectional area in unit time. Thus

$$I = \frac{Ne\upsilon_d}{L}$$

where N is the number of carriers in the conductor and L is the length of the conductor. The current density J, as a scalar quantity, is

$$J = \frac{I}{A} = \frac{Ne\upsilon_d}{LA}$$

Property	Electrons	Holes
Charge (q)	- e	+ e
Concentration (charge/cm^3)	n	p
Mobility (cm^2/V • s)	μ_N	μ_p

Table 3-8 Electron and Hole notation

where A is the cross sectional area and LA is the volume of the semiconductor. We designate a charge concentration n for electrons or p for holes (see Table 3-8 for a clarification of notation) as the number of electrons per unit volume, where

$$n = \frac{N}{LA} \quad \text{or} \quad p = \frac{N}{LA}$$

For electrons the current density can be written as

$$J = ne\upsilon_d \quad \text{or} \quad J = ne\mu\mathcal{E}.$$

As the electric field is independent of material, the conductivity of a sample is defined as

$$\sigma = ne\mu$$

and

$$J = \sigma\mathcal{E}.$$

Similar equations may be written for holes. Most semiconductors possess both charge carriers, and mobility is defined as the mobility of electrons + the mobility of holes,

$$\mu = \mu_N + \mu_p \quad \text{and} \quad \sigma = ne\mu_N + pe\mu_p$$

In extrinsic semiconductors, where one conduction mechanism dominates due to a much larger number of charge carriers, it is common to approximate conductivity as either $ne\mu_N$ or $pe\mu_p$. Table 3-9 shows the mobilities of electrons and holes for some common

Semiconductor	μ_N (cm^2/V•s)	μ_p (cm^2/V•s)
Silicon	1500	450
Gallium Arsenide	8500	400
Germanium	3900	1900

Table 3-9[63]   Mobilities of electrons and holes for some common semiconductors.

semiconductors. By comparison, the mobility of silver is 50 cm²/V•s, more than an order of magnitude less than that of the semiconductors. The higher conductivity of metals is due not to mobility, but to the large number of charge carriers in the conduction band.

3.2.2 Hall Mobility and the Hall Effect

When a current travels through a magnetic field, a force is exhibited on the charge carriers perpendicular to the direction of flow. This is defined by the Lorentz force law:

$$\bar{F} = q\bar{v} \times \bar{B}$$

where q=-e if the charge carrier is an electron and q=e if the charge carrier is a hole. If the current flows in a bounded region, such as a narrow semiconductor plate, the force deflects the charge carriers and causes an accumulation of charge at the boundary edge[64]. Charge separation produces an electric field perpendicular to both the magnetic field and the direction of current flow to balance the force exhibited by the magnetic field. A voltage equal to the integral of the electric field develops across the width of the semiconductor (Figure 3-3). This voltage is known as the Hall voltage. The electric field that results is known as the Hall field (ε_h), named after the Edwin Hall, the American physicist who first discovered the effect in 1879.

The Hall effect enables the measurement of several semiconductor characteristics, as well as the determination of their n or p nature. Independent of whether a charge carrier is a hole or an electron it will be deflected in the same direction by a magnetic field[65]. Current flow embodies the movement of electrons and holes in opposite directions, which coupled with the opposing charge of the carriers causes their deflection to be in the same direction. This allows the semiconducting type to be obtained by
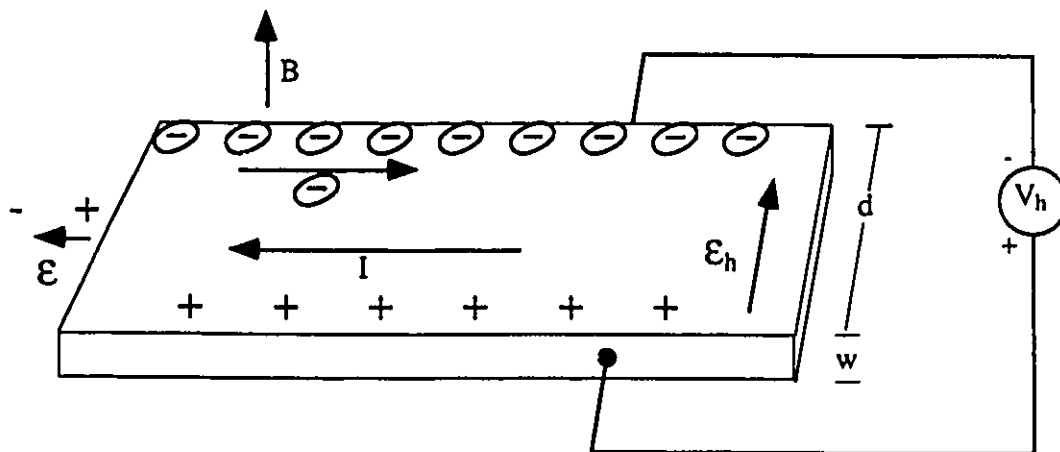
Figure 3-3 Hall effect in an isotropic n type semiconducting plate

determining the polarity of charge separation. In Figure 3-3, the back surface of the plate is charged negatively with respect to the front, revealing that the material is n type. If the material were p type, the polarity of the surfaces would be reversed. A material intrinsic in nature, possessing equal numbers of electrons and holes, produces no Hall voltage.

Determination of Charge Density and Mobility

An electric field ε_h arises to balance the magnetic force exerted on charge carriers. This balance of forces can be expressed as

$$q\varepsilon_h = -qB\upsilon_d.$$

As $\varepsilon = -\dfrac{\partial V}{\partial x}$, it follows that $\varepsilon_h = -\dfrac{V_h}{d}$.

Current density J can be written as I/wd, so combining equations for an electron leads to

$$V_h = -\varepsilon_h d = B\upsilon_d d = -\frac{BJd}{nq} = -\frac{BI}{nqw}$$

As V_h, B, I and w can all be measured, it is possible to determine the charge density nq. If one charge carrier sufficiently dominates another in terms of shear numbers then conduction in a material will be dominated by conduction of that charge carrier. Thus, since we know that $\sigma = ne\mu$, and we can measure conductivity, we can determine the mobility of the dominant charge carrier. It is convenient to define a Hall coefficient as

$$R_h = \frac{1}{ne} = \frac{V_h w}{BI}$$

and represent the charge concentrations as

$$n = -\frac{1}{qR_h} \quad \text{and} \quad p = \frac{1}{qR_h}.$$

and mobility as

$$\mu = \sigma \mid R_h \mid.$$

The sign of R_h shows whether a material is p or n type. When both holes and electrons are present, a complex relationship exists for R_h, which becomes

$$R_h = \frac{\left[(p - b^2 n) + (\mu_n B)^2 (p - n)\right]}{q\left[(p + bn)^2 + (\mu_n B)^2 (p - n)^2\right]}$$

where $b = \mu_n / \mu_p$. As $B \to 0$

$$R_h = \frac{(p - b^2 n)}{q(p + bn)^2}$$

and as $B \to \infty$

$$R_h = \frac{1}{q(p - n)}$$

For semiconductors with low mobilities and low b, ($100 - 1000$ cm^2 / V • s, $b \approx 3$ to 10) the Hall coefficient varies little with magnetic field. Semiconductors with high mobility and high b have a Hall coefficient which varies noticeably with the magnetic field[61].

The previous equations require the assumption that scattering is independent of energy considerations. For the most general case, this assumption will not hold true. Removing the assumption alters the equations such that[61]

$$p = \frac{r}{qR_h}$$

$$n = -\frac{r}{qR_h}$$

where r is the Hall scattering factor, possessing a value typically between 1 and 2. It is now required that a Hall mobility be defined as

$$\mu_h = \sigma \,|\, R_h \,|$$

with

$$\mu_h = r\,\mu_n \,, \quad \mu_h = r\,\mu_p.$$

Mobilities determined with the Hall effect most often use the assumption that $r=1$. Although the assumption will normally result in only a small error, Hall mobility can deviate significantly from standard mobility.

3.3   Electronic Properties of Iron Disilicide

In comparison to silicides of other metals, relatively little has been reported in the literature regarding electronic properties of either semiconducting or metallic iron disilicide. Nevertheless, some information describing aspects of the two materials exists.

3.3.1   Metallic Iron Disilicide (α FeSi$_2$)

For a metallic disilicide, α FeSi$_2$ possesses a resistivity that can only be considered high. As seen in Table 3-2, single crystal α FeSi$_2$ ascribes to a room temperature resistivity between 250 and 267 $\mu\Omega$ cm. These values are an order of magnitude greater than those achieved for other disilicides. However, as is also seen in the Table, the silicide possesses a remarkable stability with respect to temperature; its resistivity at 4.2 K is 230 to 250 $\mu\Omega$ cm, a change of only 6 to 8% over a temperature change of nearly 270 K. The silicide also shows a nearly linear temperature dependence from 4.2 K to 300 K[57]. While the absolute resistivity for metallic iron disilicide is at least an order of magnitude greater than many other silicides, its temperature stability is at least two orders of magnitude better. Finally, the carrier concentration (N) in the conduction band of the metallic phase is 4.9 x 10^{22} cm^{-3}.[54]

3.3.2   Semiconducting Iron Disilicide (β FeSi$_2$)

The most prolific avenue of iron disilicide research involves the semiconducting β phase. This material possesses an energy gap (E_g) which is in some dispute. The energy gap has been reported to possess a value anywhere between 0.7 and 1.0 eV.[51,53,54,55,56,66, 67] Until recently, the value reported by Bost et al.[53] of 0.87 eV was most widely considered to be correct, but two new values have emerged from the literature–one from Bost et al. as a correction to their earlier work–to bracket the accepted value with new values of 0.85[67] and 0.89 eV[51]. It is as yet unclear which result should be considered valid. Although dispute again exists regarding the value of E_g, the previously referenced studies seem to agree that the energy gap is direct.

Without intentional doping, β FeSi$_2$ is a p type semiconductor with an electron mobility of 1 cm^2 / V·s at 1210 K. The room temperature hole concentration is ~2 x 10^{18} cm^{-3}, and the Hall mobility is 3 cm^2 / V·s. The character of the conduction mechanism is changed by intentionally doping with aluminum to increase the hole concentration. Doping with cobalt converts the silicide to n type material[54,56]. P type iron disilicide suffers a decrease in conductivity as temperature is increased. At room temperature μ_p = 2 cm^2 / V·s and μ_N=0.26 cm^2 / V·s. The resulting mobility $\mu = \mu_p + \mu_N$ is 2.26 cm^2 / V·s, substantially higher than values reported at higher temperatures. As well, an exponential decrease in the Hall coefficient with increasing temperature is noted[56].

Chapter 4

Epitaxy (Gk; epi - upon + Gk; taxis - ordered)

Epitaxy, as defined by the Concise Oxford Dictionary, "is the growth of crystals on an underlying crystal that determines their orientation". Although most commonly used to describe the growth of one semiconductor on another, epitaxy encompasses the ordered growth of any material on a single crystal substrate. The crystal acts as a seed from which ordered layers of material grow. The process is akin to the well known Czochralski method for producing single crystal silicon. The processes have–perhaps erringly–been differentiated since epitaxial growth can be accomplished below a material's melting point, while the Czochralski method relies on crystal growth from a melt. Liquid phase epitaxy, a well known and oft-used form of epitaxy (q.v.), relies on the same arrangement of crystal and melt used by Czochralski, making it more appropriate to consider this method as a well developed, albeit specialized, occurrence of epitaxy.

The tightly ordered nature of epitaxy often produces an interface between materials with a regular lattice structure down to the atomic level[68]. Such interfaces can be virtually free from dislocations or other defects. In the thin film arena, this means the formation of nearly flawless crystalline films. Common in silicon based technology is the deposition of an epitaxial layer of silicon onto a preexisting silicon crystal. Epitaxy of this nature, in which a seed crystal and growing layer are comprised of synonymous material, is termed homoepitaxy. This applies to the aforementioned Czochralski method. The counterpart to homoepitaxy, heteroepitaxy, grows a layer of material on a foreign seed. Epitaxy in compound technologies, such as the processing of GaAs, where layers such as $Ga_xIn_{1-x}As$ are grown on GaAs substrates, is of the heteroepitaxial sort. The interface between materials formed by heteroepitaxy is referred to as a heterojunction, and the two materials together constitute a heterostructure. These interfaces possess valuable electronic properties, and are essential to devices such as solid state transistors and lasers. Materials are continually sought to produce heterojunctions with improved characteristics. In order to create the many high quality heterostructures demanded of modern microelectronics, epitaxy is essential. Silicides, if they are ever to realize their true potential as materials of choice for novel new devices, are certain to require a heteroepitaxial relationship with silicon; however, such a relationship is often elusive.

4.1 Lattice Match

Although the matter of epitaxial growth is complicated, one factor can be isolated that is of particular relevance[69,70]. It is the matching of the Bravais lattices between two planes of an interface. In the past, epitaxial systems were of a simple nature, such that an epitaxial layer possessed the crystal structure and orientation of the substrate on which it resided. All that was required for lattice matching was to match the lattice parameters of two materials. Accompanying the appearance of more complex materials is the appearance of complex systems and interfaces, leading to a number of important cases in which an epitaxial layer is dramatically different from that which lies beneath it. The old criterion of lattice match, in which the a, b, and c lattice parameters are compared directly, is no longer sufficient. Instead we describe two lattices as matching if the two dimensional lattices formed by crystal translations parallel to the interface possess a common superlattice[69,70]. For example, if in the interfacial plane 10 unit cells of silicon possess the same dimensions as 20 unit cells of gallium arsenide, their lattices would be said to match. A low stress interface arises which has unbonded Ga and As atoms between bonded Ga, As and Si atoms. An additional example of lattice matching may be seen graphically in Figure 4-1. Here the unit cells possess similar size, but markedly different structure. The rules for this situation do not differ, however, and a good match

a)   b)   c)
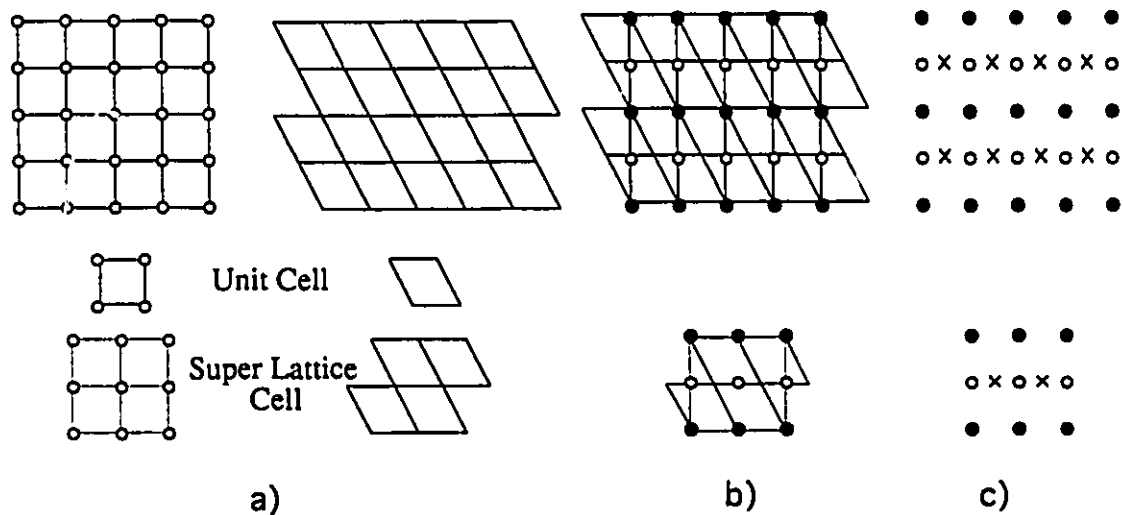
Figure 4-1   a) Shown are two lattices of different structure, with unmatched unit cells. Superlattice cells appropriate for matching are shown, each containing four unit cells of their respective lattice.

b) Superimposed are the two lattices. Solid circles represent atoms of the first lattice which match with those of the second. Open circles are unmatched atoms.

c) Interface atoms of the lattice and superlattice cell. Solid circles are matched atoms. Open circles and crosses show unmatched atoms of the first and second lattice.

between the lattices is still obtained. There is no fixed rule as to the precision with which superlattice cells must match, but it is suggested by Van Der Merwe[71] that if the affinity of a substrate for the atoms of an epitaxial layer is large, a difference of less than 4% in the lattice cells produces good epitaxial results. Stress formed at the interface is small enough to be accommodated by a change in bond angles. When the difference increases beyond ~ 12% the stress at the interface is great and an array of dislocations forms to relieve it. A definitive rule has yet to be established for the maximum area a superlattice cell can have, but it is deemed reasonable that a cell can possess an area of several hundred square angstroms[69,70].

An algorithm has been crafted by Zur and McGill[69] which locates matches to within a given precision and size for any materials of interest. This algorithm is of a systematic nature, lending itself well to automation by computer. A table has been compiled by Zur and McGill to list all the possible matches for transition-metal silicides and silicon; the conditions being a mismatch of 0.5% or less in all three lattice parameters, and a unit cell area of 150 Å or less[70]. A less stringent and more extensive set of tables has been produced with a match of 3% and 150 Å unit cell area. These tables are available at the Physics Auxiliary Publication Service.

The question of lattice matching is of great significance to epitaxial growth; however, *two* criteria dominate the reality of whether epitaxy can be realized in a system. It is often incorrectly assumed that a matching of two crystal lattices satisfies all the requirements of epitaxy. This is not the case, as the chemistry of the local interface always plays a role[69]. Thus the guidelines cited by Van Der Merwe possess the caveat requiring an affinity between substrate and overlayer. This role is not completely understood, but it is suggested that for epitaxial growth to occur the surface energy of a film must be less than the surface energy of the substrate[72]. Examples of the insufficiency of the lattice match condition to alone establish the epitaxial nature of a system are the silicides γ Y_3Si_5 and RuSi on silicon; the two silicides have a mismatch of 0.1% and 0.0% respectively, yet neither displays an epitaxial relationship with silicon[70]. Silicon on sapphire demonstrates the converse, that occasionally a large mismatch can produce single crystal films: the mismatch between silicon and sapphire being 12.5%[73]. Lattice matching may provide only an indication as to whether epitaxial growth is possible between two materials, but should allow for the identification of many systems for which epitaxy cannot occur.

4.2   Methods of Epitaxy

Most methods of epitaxial growth can be classed as either vapor phase epitaxy or liquid phase epitaxy[9]. Epitaxial layers produced by the former condense from a vapor comprised of the materials required to form the layer. The necessary vapor is produced by evaporation of materials directly, or by a reaction of gasses near the substrate surface. These processes are molecular beam epitaxy (MBE) and chemical vapor deposition (CVD) respectively. The latter class, liquid phase epitaxy (LPE), precipitates an epitaxial layer onto a crystal seed immersed in a liquid solution. Metal-organic chemical vapor deposition (MOCVD) and metal-organic vapor phase epitaxy (MOVPE) are additional techniques used in the creation of complex heterostructures; however most processing in silicon technology remains centered around CVD and MBE, and LPE.

4.2.1   Chemical Vapor Deposition (CVD)

The most common epitaxial process is chemical vapor deposition. MOCVD and MOVPE are closely related to CVD, being descendants of original CVD technology adapted to the deposition of metallic compounds. Chemical vapor deposition occurs when reactive gasses are mixed in a deposition chamber containing single crystal substrates. These gasses possess all the elements of a layer intended for deposition. Chemical vapor deposition can be readily understood by examining the process as it occurs for silicon[63].

One of four sources is traditionally used to deposit silicon through CVD: silicon tetrachloride ($SiCl_4$), dichlorosilane (SiH_2Cl_2), trichlorosilane ($SiHCL_3$) and silane (SiH_4). Using silicon tetrachloride as an example, the overall reaction required for deposition is

$$SiCl_4 \text{ (gas)} + 2H_2 \text{ (gas)} \rightarrow Si \text{ (solid)} + 4HCL \text{ (gas)}$$
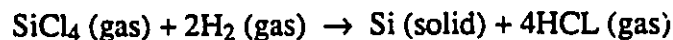
(A number of intermediate steps actually describe the reaction as written, since the epitaxial process itself is not an equilibrium reaction. These steps are not required for an understanding of CVD.) When reactants are introduced to the chamber, an epitaxial layer is grown from the resulting vapor through adsorption of silicon by the substrate. Similarly, a metal-organic reaction can be described for the growth of GaAs, wherein

$$Ga(CH_3)_3 + AsH_3 \rightarrow GaAs + 3CH_4$$
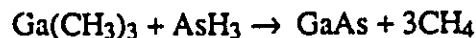
The chemical vapor growth process is by nature quite complex, but numerous schemes have been developed to accommodate the growth of a large number of materials. A dangerous disadvantage with this system is the volatile and toxic disposition of many of the reactants. Silane, for example, is pyrophoric, exploding upon contact with air. When compared with other methods, the process does possess the advantages of being relatively quick and well understood, once a reaction is worked out.

4.2.2 Molecular Beam Epitaxy (MBE)

Historically, molecular beam epitaxy has not been classified as vapor phase epitaxy, possessing a method of deposition substantially different from that described above. However, as with chemical vapor deposition actual growth takes place from a vapor phase, so justification exists for its inclusion in this class. This reflects more current thinking; although admittedly, the point is purely semantic.

Molecular beam epitaxy has been known since the early 1960s, although it was not until the early 1980s that it achieved serious consideration for device fabrication. Difficulties were a lack of commercial equipment and a quality of growth far below that required for devices of the day. Advances in vacuum technology and an increased industrial base have opened the door wide enough for this method to become a dominant force in modern epitaxy.

MBE can best be described as a highly controlled, ultrahigh vacuum evaporation process[9]. Components of an epilayer are evaporated under ultrahigh vacuum conditions from individual resistance heated crucibles known as Knudsen or effusion cells. Effusion cells have a small aperture from which vapor must escape, confining evaporated material in a tight molecular beam. These beams are directed towards a heated substrate mounted above the effusion cells. The flux of atoms escaping through the aperture to impinge on a substrate can be controlled to alter the composition of a growing layer.

Currently, a number of advantages exist for the use of MBE. Deposition temperatures are low compared to CVD, minimizing outdiffusion and autodoping in thin layers. Additionally, MBE provides more precise control over doping due to its immunity to time constant considerations[74]. High quality epitaxial layers can be grown with very little contamination, although the process may be prohibitively slow. The expense of an ultra high vacuum system may discourage many who would use this technique.

4.2.3 Liquid Phase Epitaxy (LPE)

Liquid phase epitaxy is a simple method in which a seed crystal is bathed in a melt of supersaturated liquid. The liquid is subjected to a temperature gradient, and if solution and crystal are similar in lattice constant and structure epitaxial layers will grow when atoms in the melt solidify on the surface of the seed. Usually the major constituent of the solution is a component of the seed crystal, and is dilute in all components save one. The technique is relatively easy, but less precise than other methods[75].

LPE is commonly used in the formation of heterostructures for lasers and photodetectors, while MBE and MOVPE are used to grow multiple quantum well structures and superlattice structures[9]. Of the detailed techniques, MBE produces the best overall results[75,68]. Methods are being developed to combine aspects of various methods of epitaxial growth[9], which may eventually displace current techniques.

4.3   Epitaxial Silicides

A number of silicides meet the conditions required for epitaxy–both conditions which are known and conditions which may yet remain unknown. Epitaxial silicides offer a provocative avenue of research; they may be created through solid phase epitaxy. Silicide phases subjected to heat treatment often transform to match the lattice of the underlying silicon crystal. In a family of silicide phases only the one stable with respect to silicon is susceptible to epitaxy in this form, but in all other manners the principles governing epitaxial growth remain unadulterated. Table 4-1 displays the lattice mismatch and orientations for some of the more commonly grown silicides, while Figure 4-2 displays the silicides for which epitaxy has been achieved. Also displayed in the table are the reduced resistivities of the epitaxial silicides over their polycrystalline counterparts. Unfortunately, epitaxial silicide must form directly upon a silicon substrate, whereas most current technologies require a thin insulating layer of silicon dioxide between metal layers and silicon. Epitaxial silicides will not replace polycrystalline silicides in their entirety, but remain limited in use to specialized niches which require a direct interface of silicon with silicide.

4.3.1   Formation of Epitaxial Silicides

The literature describes a number of epitaxial silicides which have been formed through solid phase epitaxy (SPE)[76-83]. It is undisputed that such formation is possible; the main point to note is that epitaxy through SPE seems to be consistent. Resulting films possess good crystallinity and few defects.

The cleanliness of a substrate surface, as well as the purity of a film during silicide formation is of paramount importance to the quality of the film grown[84,85]. Growth in less than ultra high vacuum environments, or on substrates that are not atomically clean, shows a degradation in crystallinity. This is equally true for films exposed to an atmosphere for periods as short as one day before annealing. It has also been noted that many silicides prefer growth on <111> oriented silicon substrates. Silicides grown on <100> or <110> oriented silicon tend to show a discontinuous

Silicide	PtSi	Pd$_2$Si	CoSi$_2$	NiSi$_2$	
Lattice Mismatch	9.5 %	2.2 %	1.2 %	0.4 %	
Substrate	(111)	(111)	(111)	(111)	(100)
Orientation	<100>	<001>	<111>	<111>	<100>
Resistivity (μΩ cm)					
Polycrystalline		30-35	18-20	50	
Epitaxial films		25	15	35	

TABLE 4-1 Properties of Epitaxial Silicides[68]

IIA										IIIB
Be	Conducting			Semiconducting						B
Mg	IIIA	IVA	VA	VIA	VIIA	VIII	VIII	VIII	IB	IIB	Al
Ca	Sc	Ti	V	Cr	Mn	Fe	Co	Ni	Cu	Zn	Ga
Sr	Y	Zr	Nb	Mo	Tc	Ru	Rh	Pd	Ag	Cd	In
Ba	La	Hf	Ta	W	Re	Os	Ir	Pt	Au	Hg	Tl

Figure 4-2 Silicides displaying an epitaxial relationship with silicon

interface possessing crystallographic facets. These facets are most often oriented along (111) silicon planes[85,76,77].

Despite the ease with which epitaxial silicides are formed through solid phase epitaxy it has been found that silicides formed through molecular beam epitaxy display a much bette: crystallinity that those formed through SPE. Of interest to this process is the fact that a stoichiometric deposition ratio of metal and silicon is not required to produce crystalline silicides. In fact, a flux of pure metal vapor on the surface of a silicon substrate can produce crystalline silicides. This has been attributed to the high reaction kinetics of the silicides involved. It has been found, however, that growth from such non-stoichiometric deposition results in crystalline films of reduced quality, as does growth at higher deposition rates[86].

4.3.2 Double Heteroepitaxy

Historically, semiconductor-metal-semiconductor structures have been useful for specialized devices such as the metal base transistor, permeable base transistor, and the buried-metal-gate static induction transistor[85]. These structures also are important in the consideration of three dimensional integrated circuits. Refinements in three dimensional processing could be invaluable to technologies such as high speed and high capacity dynamic memory, which traditionally crave monumental amounts of real estate on an integrated circuit. Attempts to process buried metal layer devices have encountered such difficulties as interdiffusion between films and the need to grow single crystal semiconductors over the metal[72,85]. The increased temperature stability of silicides, along with their natural epitaxial rapport with silicon, neatly circumvent these problems.

An interesting difficulty exists for the creation of alternating epitaxial layers of materials. One of the criteria required for epitaxial growth is for the surface energy of a film to be less than the surface energy of its substrate, a result of the principle of minimization of surface energy[72]. If the surface energy of the film is greater than that of the substrate, the film tends to agglomerate as it grows. If an epitaxial structure of the

form A/B/A/B is to be grown, it would appear that of necessity this principle is violated: if B wets A, then A cannot wet B and one of the films must agglomerate. Such multiple layer structures have been grown with materials possessing very similar surface energies, such as GaAs and GaAlAs, but this is simply not the case with silicon and silicides. Thus, it should not be possible to grow such structures.

However, an unparalleled advantage possessed over other materials is actually the ease with which epitaxial silicon may be grown over a silicide layer. Double heteroepitaxy has been confirmed for both $CoSi_2$ and $NiSi_2$[85,86]. The degree to which these silicides lend themselves to the overgrowth of silicon seems to be empowered by the outdiffusion and segregation of silicon on the surface of a silicide. Evidence has been found for both $CoSi_2$[87,78] and $NiSi_2$[88-90] that during the annealing required to form epitaxial layers of silicide, silicon outdiffuses through the silicide layer and forms a thin epitaxial cap on the surface. It is from this layer that epitaxial growth of silicon may occur. The successive growth of a silicon film on silicide films has in all cases been accomplished at low temperatures through molecular beam epitaxy, although initial silicide films can be formed through any means available. Attempts to achieve silicon overgrowth by solid phase epitaxy have not met with success. Dissociation consistent with that predicted by surface energy considerations occurs. It is proposed that the MBE technique avoids the surface energy problem as the high surface mobility of depositing Si gives rise to the rapid growth of crystalline silicon[86]. This crystalline development is no doubt accentuated by the presence of epitaxial silicon on the silicide from the outset.

4.4 Epitaxial Iron Disilicide

Iron silicide is one of the assemblage of silicides with which epitaxy is possible. Substrates of both <100> and <111> oriented silicon display epitaxially grown silicide overlayers, although epitaxy on <111> oriented silicon wafers has proven much easier to achieve. The reasons for this distinction are not fully understood, although it could be noted that interdiffusion rates of iron and silicon are higher for the <111> case. It is dubious that this factor alone would differentiate between the two substrates, as it has previously been asserted that epitaxial silicides do not of necessity grow from a silicon substrate, but rather transmogrify to the epitaxial form from a polycrystalline precursor. Lattice match conditions, detailed in Table 4-2, would seem to indicate that the <100> substrate is more susceptible to epitaxy than the <111> substrate. It seems that a preference of epitaxy on <111> substrates presents an intriguing conundrum.

4.4.1   Epitaxy on Silicon <111>

Epitaxial layers of iron silicide were first achieved by Cheng, Yew, and Chen[81,47, 82], whose initial successes were limited to <111> substrates. Cheng's group achieved epitaxy through the heat treatment of silicide layers on standard silicon wafers, finding that at ~900°C a transformation from polycrystalline to epitaxial ordering occurred in grains of both orthorhombic β $FeSi_2$ and tetragonal α $FeSi_2$. Grains of varying size and orientation were achieved through a number of different heat treatments, but in no cases did more than 40% of the film display epitaxy, and the semiconducting phase was never obtained on its own. Subsequent research, described below, has found methods for reducing temperatures of formation to a level conducive to the exclusive formation of the semiconducting phase. The achievement is of note as silicides possessing a split semiconducting-conducting character are of little worth.

The factor of greatest import to the formation temperature seems to be the purity of the system from which a silicide first grows. This includes the purity of the initial iron film, the purity of the initial iron-silicon interface, and the contamination of the film during annealing. Cheng's initial depositions were performed in a vacuum between 3 and 7×10^{-7} torr, with iron layers capped by either SiO_2 or Si to protect them from oxidation. Substrates were dipped in dilute hydrofluoric acid prior to their placement in the vacuum environment, and annealing occurred in either a vacuum furnace or dry flowing nitrogen. Cherief et al. [49] reduced the transformation temperature and isolated the semiconducting β phase by first increasing the quality of the vacuum to $\sim 10^{-10}$ torr. Substrate cleaning occurred in situ, as did annealing. Epitaxial layers formed at temperatures as low as ~800 K (525°C) and remained stable up to ~950 K (675°C), at which point they began to disintegrate. These layers were solely of the semiconducting phase.

Material	Epitaxial Plane	Directions Si	FeSi$_2$	Direction Mismatch	Unit Cell Area		Mesh Area Mismatch
		Silicon <001>					
β FeSi$_2$	(100)	110	010	1.45 %	Si	58.97	3.48 %
		$\bar{1}$10	001	2.00 %	FeSi$_2$	61.02	
		Silicon <111>					
	(101)	$\bar{1}$10	010	1.45 %	Si	102.14	3.93 %
		$\bar{1}\bar{1}$2	$\bar{1}$01	5.30 %	FeSi$_2$	98.13	
	(110)	$\bar{1}$10	001	2.00 %	Si	102.14	3.61 %
		$\bar{1}\bar{1}$2	1$\bar{1}$0	5.50 %	FeSi$_2$	98.43	

Table 4-2
Epitaxial relationships for semiconducting iron disilicide and silicon

In their own attempt to reduce the temperature of epitaxy, Cheng *et al.* introduced a thin layer of Ni between the iron and silicon[82]. $NiSi_2$ provides a better match with silicon and displays an epitaxial relationship at much lower temperatures. Nickel silicide is similar to β $FeSi_2$ in structure, and the idea is for epitaxial $NiSi_2$ to form at lower temperatures and act as a transitional layer for iron silicide, making a match easier. Success was achieved for thin nickel layers; the temperature of formation was reduced from 975°C to 800°C, and better quality films were formed. This system also promoted epitaxy on Si<100>. Attempts to combine this process with better vacuum and annealing processes have not occurred, even though the improved processing environments have become nearly standard in silicide formation.

4.4.2   Epitaxy on Silicon <100>

A set of results similar to those obtained with <111> silicon was eventually obtained on silicon <100>[52,83,46]. Initial successes with the epitaxial formation of iron disilicide on <100> oriented silicon utilized thin layers ~25 Å thick. Conditions again require ultrahigh vacuum deposition and annealing. However, a variation in substrates enlists silicon wafers that are both planar and stepped. Deposited layers subjected to multiple annealing steps at temperatures increasing from 500 to 950 K show that at 800 K a stable semiconducting phase of iron disilicide forms. This phase remains stable until 950 K, at which point disruption of the overlayer occurs. The silicide formed at 800 K shows no sign of epitaxial growth on planar silicon; it is entirely polycrystalline. The same overlayer formed on stepped silicon is epitaxial. The effect of the steps is not understood, but it is suggested that they "act as a nucleation site for the growth of silicide islands with fixed orientations."[83] The importance of steps is also noted by Akinci[91] on the epitaxy of $NiSi_2$ on Si<111>.

In a departure from the nearly exhausted avenues of solid phase epitaxy, Mahan *et al.*[52] create much thicker epitaxial layers on even planar Si<100> by means of reactive deposition epitaxy (RDE) and molecular beam epitaxy (MBE). RDE deposits iron onto hot silicon substrates painstakingly prepared to ensure atomically clean surfaces. MBE codeposits iron and silicon in stoichiometric quantities onto the same silicon substrates. Both methods require ultrahigh vacuum conditions—10^{-9} to 10^{-11} torr is typical—and achieve similar results. Films that range from several hundred to several thousand Å in thickness have been grown on planar <100> silicon by these methods. Evidence is once again seen in thinner films of a tendency towards the formation of islands, while relatively thick films show a deterioration in the epitaxial relationship. Formation temperatures are similar to the lowest achieved by solid state epitaxy (~500°C).

4.4.3   Epitaxy of α FeSi₂

When considering iron silicide for epitaxy, the presence of the α phase has been generally considered a nuisance. However, important merits in growing this phase do exist. A heteroepitaxial relationship between silicon and α silicide would facilitate its use for interconnects, ohmic contacts, or other devices.

One potential reason for little effort being directed towards α disilicide is its high temperature nature. Many researchers report difficulties with the stability of films at temperatures above 600°C[45,46,52]. They have alleviated these difficulties by perfecting their recipes to achieve epitaxy below this threshold. The higher temperatures required to form α disilicide make it difficult to create a stable epitaxial layer. It is possible that this problem could be overcome by the application of a passivation layer on top of the iron layer to prevent disintegration of the silicide layer during annealing. This technique has been used by many researchers to solve similar problems (q.v.).

Most work on the epitaxial nature of iron disilicide is a refinement of work begun by Cheng et al., in which epitaxial silicides of both phases were grown. An examination of the lattice parameters of iron silicide and silicon shows a small mismatch, indicating that it is not implausible that heteroepitaxy should occur. From this and the awareness that researchers are growing the semiconducting phase epitaxially on <100> substrates, given improved vacuum conditions and refined epitaxy techniques, it is reasonable to generalize that growth could occur for α silicide on <111>, <100> and <110> silicon. Since Cheng's study, no reports of the epitaxial nature of the α phase are in evidence. It is of necessity that on this one set of writings, as well as on theoretical considerations, conclusions regarding α phase epitaxy must be based. Thus, it is important to note that these conclusions are to be treated with skepticism until further study is conducted.

4.4.4   Epitaxial Relationships of Iron Silicides on Silicon

The techniques described previously achieve varying degrees of success in producing epitaxial layers of iron disilicide. However, regardless of the technique used, the heteroepitaxial relationship between silicon and silicide presents a constant face. Table 4-3 shows the lattice parameters for silicon and iron disilicide. It can be seen that the orthorhombic semiconducting phase has two very similar lattice parameters, and

Material	a_0 (Å)	b_0	c_0	Structure
Si[92]	5.4301			Diamond Cubic
FeSi₂ (β)[93]	9.863	7.791	7.833	Orthorhombic (Cmca - D_{2h}^{18})
FeSi₂ (α)[92]	2.69		5.08	Tetragonal

Table 4-3   Lattice parameters for silicon and iron silicide

FeSi₂ (100) on Si (001)

FeSi₂ (101) on Si (111)

FeSi₂ [010]
Si [110]

FeSi₂ [101]
Si [112]
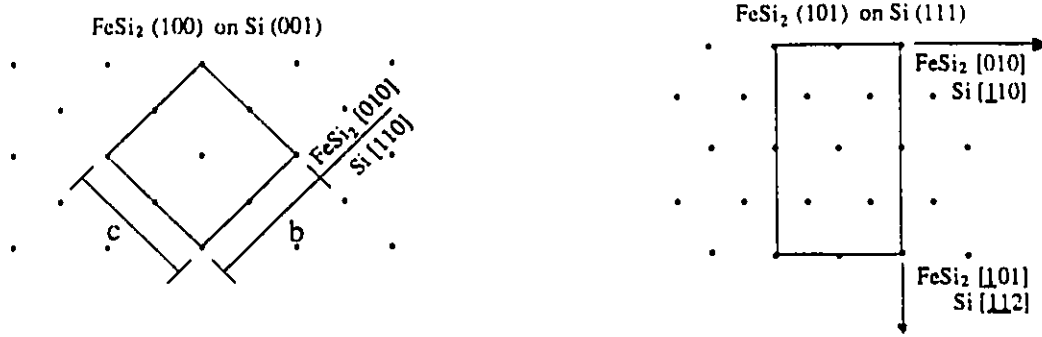
Figure 4-3
Possible Epitaxial relationship for β FeSi₂ on Si <100> and <111>

could almost be considered tetragonal. As a result, dual epitaxial planes are possible for the semiconducting phase on <111> silicon . This effect of multiple epitaxial planes is not seen on <100> silicon, as one epitaxial plane contains both similar lattice directions at once. Figure 4-3 shows a possible orientation of β FeSi₂ on <100> and <111> silicon.

The two epitaxial planes of β FeSi₂ on <111> Si are indistinguishable through electron diffraction, but have clearly been seen to coexist in a single sample through transmission electron microscopy[49]. In addition to the presence of the dual epitaxial planes, the threefold symmetry of the <111> Si substrate allow for three equivalent and equiprobable azimuthal orientations. These orientations are shown clearly in Figure 4-4. Multiple orientations also exist for the silicide on <100> Si. Due to the fourfold symmetry of the silicon, two orientations are possible, and are also shown in Figure 4-4. These multiple orientations are likely to be problematic as they should lead to the formation of rotation twins. This difficulty is demonstrated by Cherief *et al.* for <111> Si[49]. It is more difficult to identify twins on <100> Si, possibly due to the minor 0.5% discrepancy between the b and c lattice parameters of the silicide[83]. This factor does provide for one advantage of epitaxy on <100> as opposed to <111> silicon.

Silicon <111>

Silicon <100>
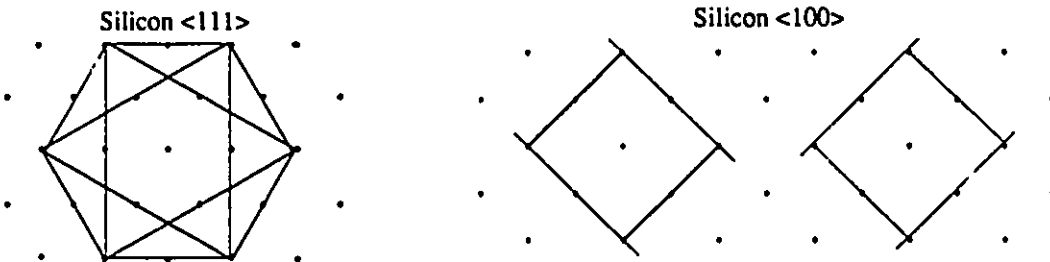
Figure 4-4
Azimuthal orientations of Iron Disilicide

Thin Film Failure

Film stability is an important concern for thin films of all materials, and is an important factor in the reliability of microelectronic devices[94]. A thin film of an otherwise useful material, under various conditions, may undergo severe distortion through hillock formation, hole formation, or complete or partial dissociation of the film. Additional difficulties arise when a thin film reacts with an adjacent layer to form compounds or structures that were not indented. Various mechanisms contribute to thin film disruption; electromigration (electrotransport), thermomigration (thermotransport), thermal grooving (grain boundary grooving), and diffusion being principle among them[94,95]. Figure 5-1 depicts some of the difficulties facing thin film metallizations.

5.1 Metal Migration

Electromigration occurs when mass transport is stimulated by an applied electric field. Two competing mechanisms can lead to failure through electromigration. Positively charged metal ions tend to drift toward the negative cathode under the electrostatic force induced by the electric field[95]. This causes an accumulation of material near the cathode which is possible only through the depletion of material surrounding the anode. This depletion is most often in the form of holes. In a metallic conductor, where conduction occurs through a large flux of electrons, an *electron wind force* pushes the metallic ions in the direction of electron flow. In metallic conductors the electrostatic force is thought to be negligible with respect to the electron wind[95]and metal tends to migrate towards the anode, leaving holes to form near the cathode. Electromigration is commonly referred to in the semiconductor industry as metal migration, and is a well recognized problem facing the production of small scale integrated circuits. As current flow occurs through metal lines smaller than 1μ in diameter, hole formation results in a large increase in local current density which further increases migration, and may lead to a break in the metal line. This problem is particularly pronounced when current flow encounters a region of reduced diameter, such as at sharp corners or contacts to various layers, where metal tends to migrate more rapidly at these points due to the increased carrier density. These
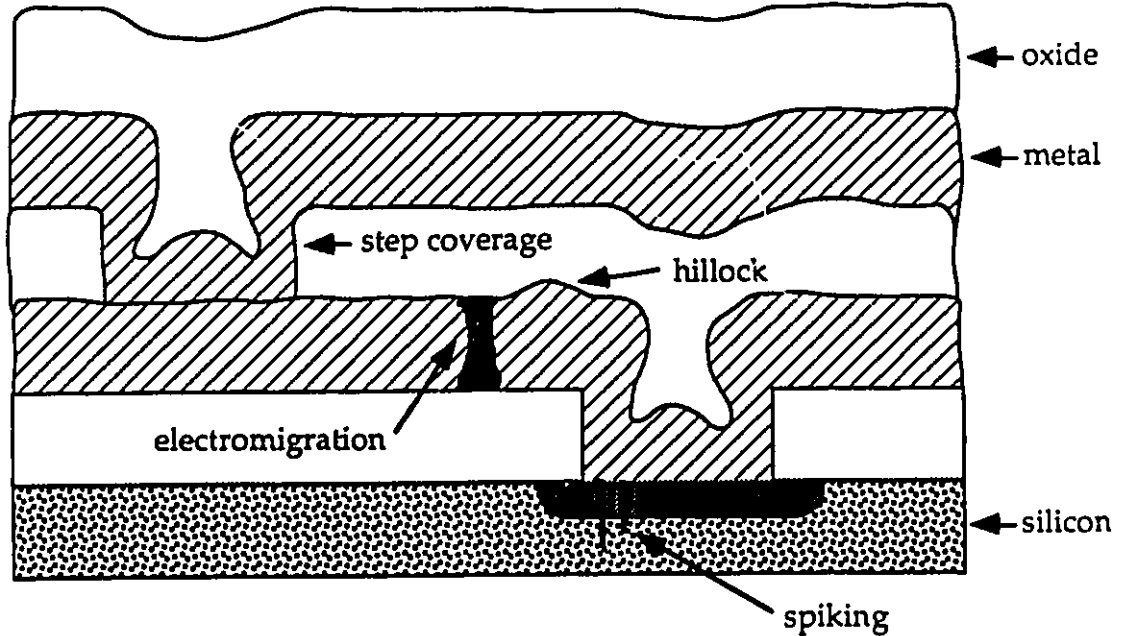
Figure 5-1   Thin Film Failure Mechanisms (Niall Tait, University of Alberta)

affects can be seen in Figure 5-1. If metal migration does not result in a break in the conductor, the pile of material can result in hillocks sufficiently large that they impinge on adjacent conductors, resulting in a short circuit. Either of these eventualities, hillock or hole formation, may result in circuit failure[96].

Most metal films are polycrystalline in nature, and diffusion of atoms occurs most often at grain boundaries within the films. By increasing the grain size of a conductor the number of grain boundaries in any given volume is decreased and electromigration decreases. An additional gain is achieved as it has been found that a reduction in grain boundaries can lead to an improvement in resistivity[97]. Silicides are expected to have a substantially increased resistance to electromigration than metals as the activation energy for the electromigration process can be correlated with the melting point of the metal or silicide in question. This correlation is reasonable as mass transport is likely diffusion limited. It has been shown that metals with a higher melting point resist migration more than metals with a lower melting point, and this trend is expected to continue for silicides[1]. Thermotransport is a process similar to electrotransport, where mass transport is induced by a temperature gradient along a material. Depending on the material, atoms may migrate towards either the hot or cold end, forming hillocks and holes in the process. Less work has been done to characterize thermotransport, but if the relationship between electrotransport and melting point holds true, it is reasonable to assume that the same relationship holds for thermotransport as it too is likely a diffusion controlled process.

5.2   Interdiffusion

Any reaction between a metallization layer and silicon is undesirable. Unfortunately, all of the metals suitable for use as electronic metallization have a high interdiffusivity with silicon, which can lead to a number of problems. The first of these is the doping of silicon with the metallization material. Metal interdiffusing with silicon in a contact region can have severe effects on the Schottky barrier height of the contact. The metal acts as a dopant to produce donor or acceptor levels in the silicon band gap. This effect may often be useful to reduce the height of the barrier, but often can lead to unwanted doping of the silicon layer. A related effect occurs when the interdiffusion of materials leads to compound formation. The uncontrolled formation of any material in an electronic circuit can lead to unpredictable and possibly failure inducing results.

An additional difficulty exists when silicon diffuses into the metal at a contact region. Silicon diffusing into the metal in sufficient quantities leaves behind pits. These pits can be of sufficient size to penetrate shallow p-n junctions, an effect known as spiking. This is shown in Figure 5-1. A number of methods, from the doping of metal with silicon to the addition of a barrier layer between them has been used to control the problem of spiking[96]. Many silicides, however, being metal silicon compounds already are in nature stable with respect to silicon. No additional processing is required.

5.3   Agglomeration

The most serious failure mechanism for silicide thin films may actually occur during solid state formation. Thin films subjected to annealing temperatures often display catastrophic dissociation of the thin film layer into isolated islands on the substrate surface (Figure 5-2). This difficulty is not unique to silicides, however, as it affects any thin film at high temperatures. Films affected in this way are useless as electronic materials as they possess no continuity. A number of thin films have shown various stages of dissociation, including gold[94,95,98,99], silver[100,101], nickel[98], platinum[102,103] and copper[104]. These materials have, under various conditions, displayed varying degrees of hillock and hole formation in the thin films, as well as dissociation into individual islands. This dissociation is commonly referred to as agglomeration. The tendency for agglomeration has hampered the use of metals in integrated circuit technology as no high temperature processing may occur after metal deposition has taken place. This eliminates the possibility of using metal in self-aligning processes as diffusion temperatures are often in excess of 1000 °C and currently used metals are not stable at those temperatures.

The driving force for the agglomeration process may be varied, and includes such effects as gravity, van der Waals forces, electrostatics and surface tension. The latter of these, known more properly as capillarity, weighs the most heavily on the thin film
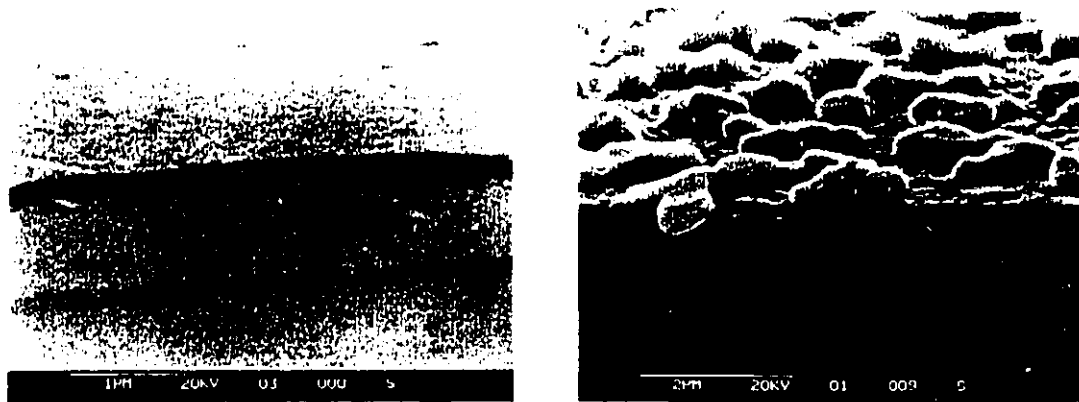
Figure 5-2   SEM photos showing the agglomeration of iron. The picture on the left is an iron thin film prior to being subjected to higher temperatures. The picture on the right is the same thin film after being annealed at 900 °C.

condition[105]. Driven by capillarity, the solid surface transforms into a collection of beads not through the accumulation of material at the bead locations, but rather through the formation and growth of small voids[105,106-108] in the surface of the thin film. It is the growth of these holes, which, upon reaching sufficient size to impinge upon one another and pinch off regions of the film, form the eventual islands of metal. The study of this phenomenon dates back to researchers such as Lord Rayleigh, who first determined that amplitude fluctuations in the surface of a cylinder would grow if the wavelength of the fluctuations exceeded $2\pi R$, where R is the radius of the undisturbed cylinder[109] (Figure 5-3). This same result was obtained more recently by Nichols and Mullins on a similar study of the instability of an infinitely long cylinder[110]. However, in a previous work Mullins had already shown that similar fluctuations in a planar surface would not grow, regardless of their frequency[111]. There is, in contrast, a tendency for a surface to relax to flatness. It has therefore been assumed that a flat surface will only decompose if the fluctuations in its surface are sufficiently great that the film is penetrated[106]. It is well known that should this eventuality occur the voids formed by the film penetration will grow, leading eventually to the breakup of the film into localized islands. A detailed kinetic and energetic analysis of this problem has been performed by Srolovitz and Safran[105,108].
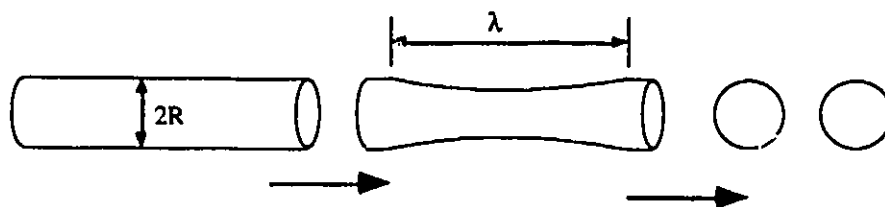
Figure 5-3   Degeneration of a cylinder into spheres. The cylinder remains stable as long as the wavelength of the amplitude fluctuations is less than $2\pi R$.

The thin films reported in the previously referenced literature are without exception flat in relation to their thickness when annealing commences. It must therefore be assumed that for agglomeration to occur fluctuations of sufficient amplitude must grow after the fact. This contradicts the assertion that the tendency of a planar surface is to relax to flatness. The solution to this lies in the mechanism of thermal grooving. For an amorphous or liquid film, thermal grooving cannot occur and the surface will indeed relax to flatness. It is well known that wherever a grain boundary intersects the surface of a hot polycrystal[112] a groove will develop. This thermal grooving is the result of the establishment of an equilibrium between the surface tensions of adjoining grains and the grain boundary tension between them.[112] The required equilibrium angle, shown in Figure 5-4, can be determined using the result $2\gamma_g \sin\beta = \gamma_b$, where γ_g and γ_b are, respectively, the surface and boundary free energies[113]. The equilibrium angle is established by atomic migration in the region immediately around the grain boundary, leading to the formation of sharp ridges. These ridges erode through preferential evaporation and surface diffusion to continually upset the condition of equilibrium established between grains. The result is a continual deepening of the groove[112].

Groove deepening is clearly dependent on the erosion of the ridges bordering the grain boundary, as the establishment of the equilibrium angle occurs rapidly through atomic migration at the intersection between grains. As previously mentioned, this erosion is the result of the dual mechanisms of evaporation and surface diffusion. In a study on the theory of thermal grooving[112], Mullins has proposed that when each effect dominates a different time dependent profile of the surface groove can be determined. For erosion due to evaporation, the groove deepens as the square root of time, while for surface diffusion the groove deepens as the fourth root of time. It is his supposition that it is possible to realize one of the two effects through the careful selection of appropriate annealing conditions. Surface diffusion dominates for short periods of time and low temperatures, but evaporation begins to dominate as time and temperatures increase. The addition of an inert atmosphere reduces evaporation and favors the process of surface diffusion. (For the process of evaporation it has been assumed that a metal film is in quasi-equilibrium with its vapor. Thus we assume that condensation accompanies evaporation in the system, and that conservation of volume applies.)
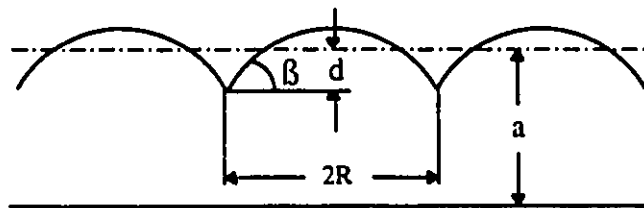
Figure 5-4[105]   Surface equilibrium of a film showing thermal grooving effects where ß is the equilibrium angle, d is the groove depth, a is the film thickness and 2R is the grain diameter.

The theory of thermal grooving presented by Mullins suggests that the depth of a grain boundary groove will increase infinitely as either the forth root or square root of time, implying that eventually every groove is destined to penetrate the film. This is not the case. Srolovitz and Safran have shown that a finite depth exists which is dependent upon both the equilibrium angle and grain size[105]. Film rupture occurs only if the grain size of the film is large with respect to the film thickness. The general shape possessing a minimum surface area and circular base is a spherical cap, so it can be assumed that the shape possessing a minimum surface energy on the thin film would be a spherical cap meeting the grain boundary at the equilibrium angle. If the requirement of conservation of volume is to be met, the condition shown in Figure 5-4 will be constrained by both the angle β and film volume, and can be met only if an equilibrium depth exists such that

$$d = R \frac{2 - 3\cos\beta + \cos^3\beta}{3\sin^3\beta} .$$

[105]

This shows that thermal grooving will penetrate the film only if

$$\left(\frac{R}{a}\right) \geq \frac{3\sin^3\beta}{2 - 3\cos\beta + \cos^3\beta} .$$

[105]

5.3.1   Prevention of thin film failure

A number of steps may be taken to prevent the failure of a thin film. This is especially true of agglomeration. However, eliminating a single failure mechanism does not eliminate the possibility of failure by another mechanism. For example, the doping of gold thin films with indium stabilizes the grain size during annealing to reduce the effect of grain boundary grooving. However, smaller grain sizes result in increased numbers of grain boundaries, which in turn provide pathways for mass flow due to thermotransport and electrotransport. Thus, while agglomeration can be curtailed through the doping of indium, such films are subject to metal migration and a reduced lifetime when used in integrated circuits. Similarly, it has been found that doping gold with sodium increases the thermal grooving effect to the point where heating due to current flow is enough to cause serious grooving.[95]

However, as silicides have shown the potential to remain relatively unaffected by many of the processes that create instability and failure in metal films, the important criteria to focus on is the elimination of agglomeration. A number of simple methods exist to accomplish this, such as increasing the film thickness or doping to limit grain size, but often more complex procedures are required so that properties such as thickness and film purity may be maintained.

Annealing in controlled environment

One of the common methods for controlling the agglomeration of thin metal films is the use of a controlled atmosphere during annealing. As previously asserted, agglomeration depends on surface energy considerations more than on any effects between the metal layer and its substrate. This assumption has been verified by the observations that agglomeration of Gold, Nickel and Copper occurs independent not only of substrate material, but independent of whether a substrate is present[98,114]. Altering the atmosphere surrounding a thin film during annealing should affect the surface energies, and therefore the processes of thermal grooving and agglomeration. This has been shown for many materials. Silver annealed in the presence of oxygen has shown grooving which disappears when annealing occurs under nitrogen[115]. Similar studies have shown that annealing in vacuum, helium and argon will produce hillock formation in silver films, but only annealing in oxygen will produce agglomeration[100]. Silver appears to have a high surface mobility on an oxygen covered silver surface. Conversely, the break up of tin films annealed in vacuum can be prevented by the addition of slight amounts of oxygen[107,116]. It was suggested that the formation of one or two monolayers of surface oxide reduces the surface mobility of the tin.

Capping Layers

In addition to annealing in a controlled environment, surface energy considerations can be altered by the addition of a capping (passivation) layer to a thin film diffusion couple. The capping layer should not react with the thin film to alter the kinetics of compound formation, nor should it alter the ultimate result of reaction. Capping layers have been utilized in silicide formation to control the oxidation of metal layers. Molybdenum and tungsten layers have been used to protect cobalt thin films from oxidation before silicidation occurs[117], and silicon and silicon dioxide layers have been used to protect iron[47]. At the temperatures at which silicide forms in a silicon-cobalt diffusion couple neither material (Mo or W) mixes with cobalt. Upon completion of the reaction Mo, W and their oxides can be etched away without removing the underlying silicide. These capping layers have also been used to alter the capillarity conditions that drive thermal grooving, as well as by limiting the mass transport at the surface of the film. $ErSi_2$ formed under a passivating layer of amorphous silicon has been found to possess none of the surface pits that are typical of its formation without such a layer[118]. It was found that the amorphous silicon layer reacted quickly with erbium to produce a planar silicide with little or no reaction between erbium and the underlying substrate.

It has been found that indium *underlays* in thin gold films can also prevent the agglomeration of the film[94]. This novel approach results in the diffusion of indium through the gold layer to form an oxide on the surface which limits mass transport. The indium and indium oxide also serve to pin grain boundaries and impede grain growth.

Characterization

A variety of methods were used to investigate and characterize the experimental work performed for this thesis. These methods included the use of x-ray diffraction, scanning electron microscopy, transmission electron microscopy, ellipsometry, spectrophotometry and line profilometry.

6.1 Thickness Measurement

A crystal thickness monitor was used in situ to control the thickness of films during deposition The monitor provides information on deposition rates and times, as well as cumulative film thicknesses. Assuming the density and z-factor (which must be entered into the monitor prior to deposition) of the material being deposited are known, the crystal thickness monitor provides readings which may be assumed accurate to approximately 20%. Table 6-1 lists the density and z-factor for the materials deposited during this research. Line profilometry was used to verify the thickness results obtained with the crystal thickness monitor by measuring the deflection of a stylus dragged across the edge of a masked region on the sample surface. A profile of the film edge is produced from which the thickness of the film can be determined This method is accurate to approximately 50 Å. Multiple readings were obtained for each wafer and averaged to account for any inconsistencies in the film thickness. Cross sectional TEM and SEM were used also used to measure film thickness. This was particularly useful when a surface layer existed on top of a film, an occurrence which makes profilometry impossible.

	Iron (Fe)	Silicon (Si)	Oxide (SiO_2)
Bulk Density (gm/cm^3)	7.86	2.32	2.20
Z-Factor	0.349	0.712	1.070

Table 6-1 Bulk Density and Z-Factor Values

6.2   Etching of Silicon Dioxide

Before a sample could be studied it was often necessary to remove a silicon dioxide capping layer which was used to protect the iron film during annealing (q.v.). SiO_2 was removed with the use of a buffered oxide etch (BOE) of hydrofluoric acid (49%) and ammonium fluoride (40%). The solution used was 1 part hydrofluoric acid (HF) to 10 parts ammonium fluoride. The HF accomplishes the etching, while the ammonium fluoride acts as a buffering agent to replace fluoride ions that are lost to the reaction. This maintains a constant concentration of hydrofluoric acid and insures constant, predictable etch rates.

Although BOE is an oxide etch, etching of silicon and possibly silicide will still occur. The rate of this etching is substantially reduced, however. To prevent etching of the layers beneath the oxide cap, the etch rate and thickness of the oxide must be known to determine proper etch times. To determine the etch rates of electron beam evaporated SiO_2, an oxide layer was deposited on a clean silicon substrate partially masked to produce a sharp interface in the oxide layer. The thickness of the oxide was determined by line profiling the step with an Alpha Step, and confirmed through ellipsometry of the silicon and oxide layer. Etch rates were then determined by immersing the oxide in a BOE solution and monitoring the time required for the oxide to completely disappear. The exact interval at which the oxide was removed was determined two ways. Oxide color fringes, easily identified by the naked eye, fluctuate as the thickness of the oxide changes. When the oxide is removed, the color fringes disappear. For accuracy, partially masked samples were used so that bare silicon was present as a color reference during etching. Secondly, BOE sticks to oxide, but does not wet silicon. The surface of a sample removed from an etching solution can be identified as silicon if BOE beads form on the surface. If a sample is removed immediately prior to the completion of oxide removal, a change in the surface can be observed as the sheet of BOE adhering to the oxide beads and runs off the sample. This corresponds to the point at which oxide etch concludes.

The etching times determined are only accurate for the as deposited samples. Annealing of the oxide layer increases the density of the oxide and decreases its etch rate. Samples etched after annealing required slightly longer etch times to compensate for the density change.

Etching required 150 seconds to remove 7200 Å of oxide, corresponding to an etch rate of 48 Å/s. This is substantially faster than the etch rate for annealed CVD deposited oxide, which is approximately 8 Å/s.

6.3   X-ray Diffraction

X-ray diffraction was used to determine the identity of phases formed during annealing. When a beam of x-rays strikes a sample (Figure 6-1) it is diffracted in all directions[11c]. When x-rays diffracted from different atomic planes are detected such that the angle of incidence is equal to the angle of diffraction (Figure 6-1), a phase shift results which is dependent on the difference in distance traveled by each x-ray (distance a-b in the figure). If the extra distance traveled is a multiple of the wavelength of the incident x-rays, diffracted x-rays remain in phase and produce an intense x-ray beam. When this is not the case, diffracted x-rays interfere destructively with one another and a weak beam results. The phase shift can be shown by geometrical considerations to be dependent on the interplanar spacing d, and a relationship known as Bragg's law shows that for x-rays to be in phase

$$\lambda = 2d\sin\emptyset.$$

λ is the wavelength of the incident x-rays, d is the spacing between crystal planes and $\emptyset$ is the angle between the crystal plane and x-ray beam (Bragg angle). If a set of planes is oriented such that the Bragg condition is satisfied, incident x-rays will leave the sample at an angle of $2\emptyset$ (with the transmitted beam) with sufficient intensity to be easily detected. If a sample is rotated in an x-ray beam, diffracting planes will be moved one at a time into an orientation which satisfies their Bragg condition. A detector rotating with the sample (Figure 6-2) will detect a peak in the diffracted x-ray intensity. If the intensity of the detected x-rays is charted against the angle between the x-rays and the sample, a plot results with peaks corresponding to the interplanar spacings of the sample (x-ray spectrum).
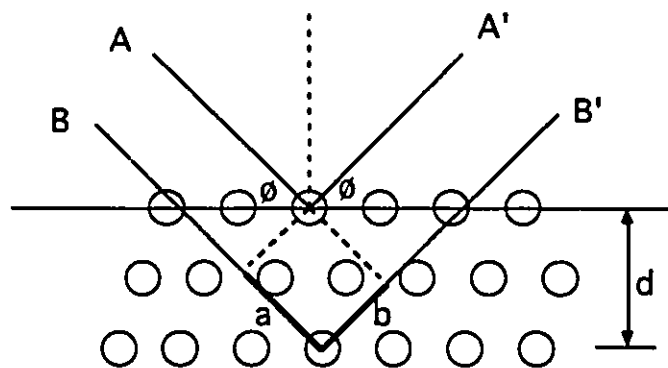
Figure 6-1   X-ray Diffraction
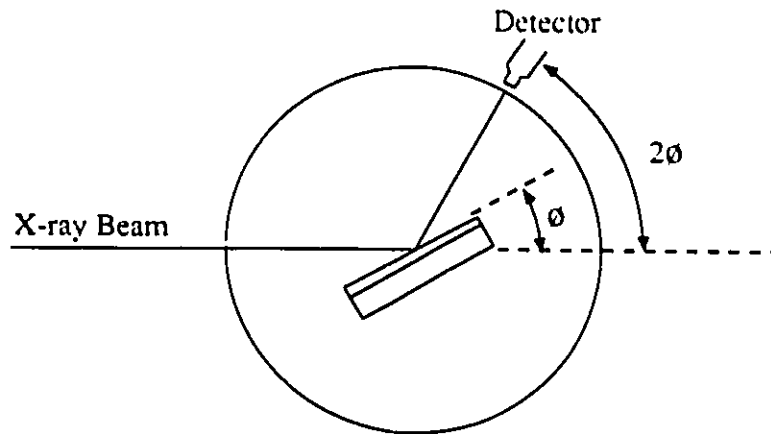
Figure 6-2 X-ray diffractometer

The interplanar spacings for different materials are tabulated in the ASTM X-ray powder diffraction files. These files are a tabulation of crystallographic data of most known materials. The x-ray spectra obtained during this research were compared to the spectra for compounds thought to exist in the films; iron, silicon, iron silicides, iron oxides and silicon oxides to determine the identity of each thin film layer.

Homogeneous strain in a thin film either expands or contracts the interplaner spacings of the diffracting planes[120]. By comparing the interplanar spacing found in the powder diffraction files to the interplanar spacings determined by x-ray analysis the expansion or contraction of the the thin film lattice can be determined[121].

X-ray diffraction produces a sharp peak only for the plane that is parallel to the sample surface. Amorphous material produces a broad, diffuse peak. For this reason samples are often powdered to produce a large number of randomly oriented crystals which will produce peaks for each diffraction plane in the sample. For this research, however, the dependence on surface orientation was advantageous and no attempts to powder the thin films were made. The size and position of the peaks in the diffraction spectrum provided an indication of the orientation of the crystals in the sample. X-ray diffraction was therefore useful in determining if a sample was amorphous or crystalline. If crystalline, an indication of whether a preferential orientation existed was obtained.

6.4   Electron Microscopy

6.4.1   Scanning Electron Microscopy (SEM)

Scanning electron microscopy was used to study the surface of deposited and reacted thin films. A Cambridge Stereoscan 250 equipped with a secondary electron detector and Robinson backscattered electron detector was the principle instrument used. The microscope was also equipped with a TN 5500 energy dispersive x-ray analysis system (EDX).

Both secondary electron and backscattered electron imaging proved extremely useful in the study of thin film surfaces. Secondary electron imaging revealed surface topography with submicron detail, and allowed for the study of thin film cross sections by revealing structural differences such as grain size and orientation in film layers. Layers as thin as 100 nm were successfully viewed in this manner. Backscattered electron imaging allowed for the determination of the composition of various regions within a sample. While this technique does not provide information regarding the actual composition of a region, it provides image contrast based on the difference in atomic number between the elements in various regions.

In addition to its use in imaging samples, the Cambridge SEM was capable of energy dispersive x-ray analysis (EDX) which allowed for composition analysis of deposited films. Although a small small spot size is possible for the electron beam, scattering of the beam results in the detection of x-rays from a region of approximately 1 μm^3. As the thin films studied were all substantially thinner than this detection region the exact composition of a layer could not be determined by this method. Instead, the relative composition of elements within various regions of a sample were detected. Therefore, if a lump were present on the surface of an iron film, it could be determined if the lump was more rich in silicon than the surrounding thin film, but the exact ratio of silicon to iron could not be determined. Finally, only elements heavier than atomic number 10 were detected, as the SEM was not equipped with a light element detector (x-rays were absorbed by the Be window). This eliminated the study of thin film purity, as oxygen and carbon, the two most likely contaminants, could not be detected.

Specimen Preparation

Specimen preparation for the SEM is a simple matter. A diamond scribe is used to drawn scribe lines along a <110> direction, and samples are easily cleaved along these lines. This produces a clean fracture surface which could be observed in the SEM. Non conductive films were covered with a thin layer of sputtered gold to prevent charging of the film during imaging. The gold layer is thick enough to conduct electrons away from the sample surface but still sufficiently thin to escape having a presence in SEM imaging.

XXXXXXXXXXXXXXX

6.4.2 Transmission Electron Microscopy (TEM)

Transmission electron microscopy is useful for high resolution imaging of specimens that is not possible with conventional scanning electron microscopy. A resolution of ~2 Å was possible with the TEM, whereas only 50-60 Å resolution was possible with the SEM. TEM was used to detect the intermediate silicide layers that formed during the processes of annealing. The microscopes used were a Hitachi H-7000 (125 kV), and H-600 TEM/STEM (100 kV) with a Be window x-ray detector (KEVEX).

Energy Dispersive X-ray Spectroscopy (EDX)

The Hitachi H-600 was used for energy dispersive x-ray spectroscopy (EDX) to analyze the composition of individual layers within the diffusion couples. In a thin film, the composition of a given phase can be determined by the application of the formula[122]

$$\frac{C_{Fe}}{C_{Si}} = K_{Fe/Si}\,\frac{I_{Fe}}{I_{Si}}$$

where C_{Fe} and C_{Si} are the concentrations of iron and silicon (weight percent), I_{Fe} and I_{Si} are the intensity of iron and silicon characteristic x-rays in the EDX spectra, and $K_{Fe/Si}$ is the Cliff-Lorimer proportionality factor. This factor is independent of specimen composition and thickness, but is dependent on instrument conditions. Tables of K factors exist which can be used for a rough estimate of the proportionality constant. For an accurate application of the above equation, the K factor should be measured from standards. A limited number of phases, with known composition, were present in this research, so only an approximate composition was required to identify a phase.

Specimen Preparation

Although difficult and time consuming, specimen preparation for the TEM is straight forward and methodical. Standard techniques have been adopted for specimen preparation, and are well documented in the literature[123,124]. A seven step procedure was followed for each specimen[125].

1)   The desired thin film sample was cut into 1.5 mm by 4 mm sections. Ordinary silicon slabs of the same dimension were also cut to use as filler material.

2)   Two sample sections were glued together, such that the thin films were face to face, with a silver loaded epoxy which required elevated temperatures to set. Two slabs of filler material were glued to each side of the sample pieces (Figure 6-3).

3)   The structure was gently squeezed in a small vice to produce thin, bubble free
      glue layers. The vice and sample were then cured in a furnace at 90 °C for 1h.

4)   After curing, the structure was polished with 400 and 600 grit SiC paper down to
      a thickness of approximately 400 μm. A 3 mm disc was cut from the structure
      using an ultrasonic disc cutter. This sample was polished down to approximately
      200 μm with 600 grit SiC paper.

5)   Using a Gatan Dimple Grinder, one side of the sample disc was dimpled to
      approximately half the samples thickness. 2-4 μ diamond polishing paste was
      used initially, and the sample was polished with 1 μ polishing paste and a special
      polishing wheel to produce a shiny surface.

6)   The opposite side of the sample was dimpled until either a very small hole
      appears, or red light could be seen through the center of the sample. The sample
      was then polished with the same paste and wheel used in step 5.

7)   The sample was ion milled using an Ion Tech or Gatan Ion Mill, using a cold
      stage and a vacuum of 10^{-6} torr. The cold stage was kept cold with liquid
      nitrogen. Specimen cooling minimized preferential sputtering of different layers.
      Actual sputtering required the use of two Ar^+ ion guns working at 3 kV and 0.6
      mA. Sputter times varied depending on the amount of milling desired and the
      specimen was rotated throughout the process.
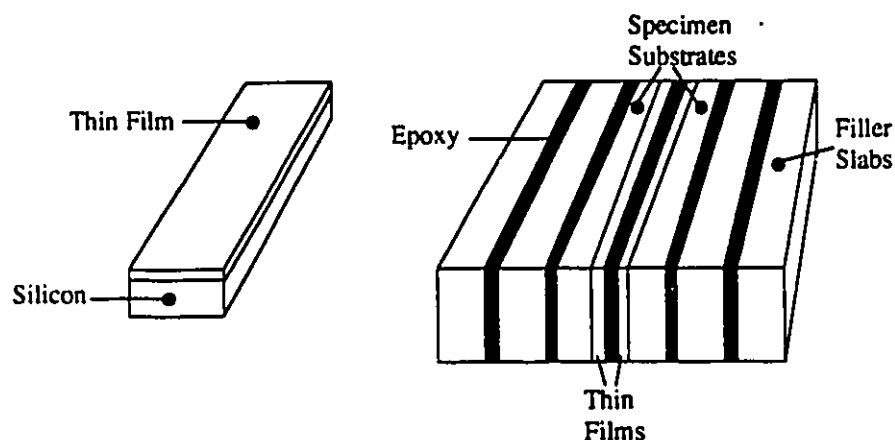
Figure 6-3   TEM specimen preparation

6.5 Spectrophotometry

The energy gap of a semiconductor may be measured through the optical absorption of varying wavelengths of light. Light will be more strongly absorbed if its photons possess sufficient energy to excite an electron from the valence to the conduction band. For a direct gap material, an absorption coefficient, dependent on the energy of the incident photons and the materials energy gap, can be expected to follow the relationship

$$\alpha = A(E\text{-}E_g)^{1/2}$$

where α is the absorption coefficient, A is a constant, and E is the energy of the incident photons[126]. The energy gap can be determined by plotting α^2 vs the energy of the incident light. Such a plot contains a linear region for energies above the energy gap and an exponentially decaying region for energies near or below the gap. Extrapolating the linear region to a zero absorption coefficient yields a materials' energy gap (Figure 6-4).

Values of the energy gap determined through this method are considered an effective energy gap, as they can vary with the composition and structure of a material. This is due to changes in the allowed states near the bandgap and not to changes in the material itself[127-129]. The measured energy gap should not be considered equivalent to the intrinsic band gap of the material, but can be considered a good estimation.

The absorption coefficient can be determined experimentally by measuring the transmission and reflection of light from a semiconducting sample. The absorption coefficient can be determined from the approximation that

$$\frac{T}{1\text{-}R} = e^{\text{-}\alpha d}$$
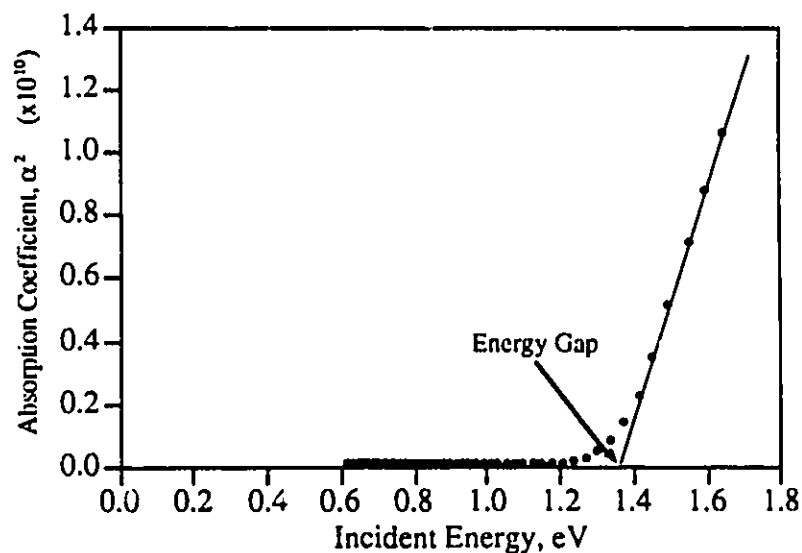
Figure 6-4   Band gap determination using optical absorption coefficient

where T is the percent transmission of light through the semiconductor, R is the percent reflected light off the semiconductor and d is the thickness of the semiconductor. This approximation is good only for strongly absorbing samples. If the band gap is determined graphically, the semiconductor thickness is unimportant. The approximation assumes that multiple reflections within the semiconductor do not occur, and that the semiconductor does not rest on an absorbing substrate. This assumption may result in an error in the absorption coefficient of nearly 5%[121].

The transmittance and reflectance of semiconducting samples were determined for this research using a Cary 2400 UV-NIR spectrophotometer. Values were determined for transmission and reflection separately, for wavelengths between 750 nm and 2500 nm. Wavelength can be converted to an energy value using the relationship

$$E = hc/\lambda$$

where h is Planck's constant, c is the speed of light, and λ is the wavelength of the incident photons. Transmittance is determined by placing a semiconductor between a light source and detector, and varying the wavelength of the light. Reflectance requires a complex arrangement known as a "v-w" geometry (Figure 6-5). Light reflects off a set of three mirrors before being received by the detector. The spectrophotometer calibrates itself to register 100% reflectance with no sample. When a sample is placed within the beam, the center mirror is moved to the front of the sample, and light reflects off the sample, to this mirror, and off the sample a second time before arriving at the third mirror in the setup. The location of the mirrors is designed so that the light reflects from the sample at the same angle it reflected off the mirror when the spectrophotometer calibrated itself, and so that the distance traveled by the light is constant. As this requires two reflections from the semiconductor sample, R^2 is measured instead of R.
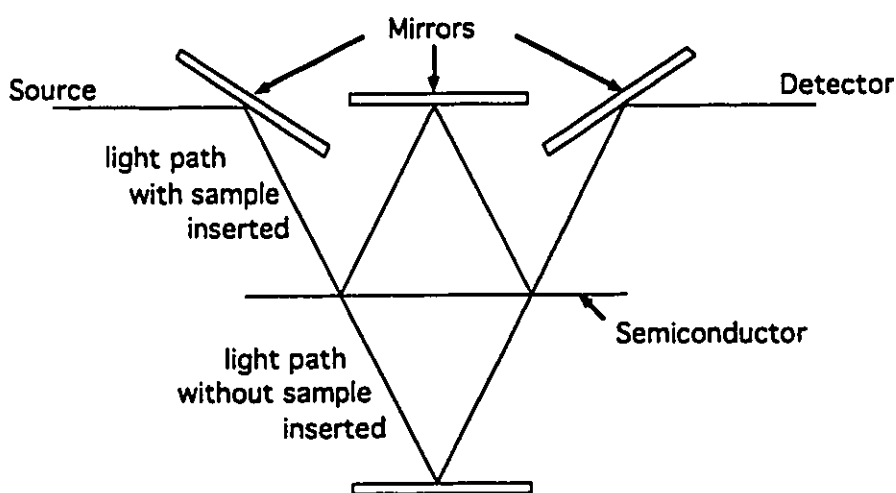
Figure 6-5   Reflectance Measurement

Thin Film Deposition

Thin films of iron, silicon and silicon dioxide were deposited to create a variety of thin film couples from which silicide formation could take place (Figure 7-1). The simplest of these diffusion couples was iron deposited on a silicon substrate. Deposition was through thermal and electron beam evaporation, and occurred on substrates of both <100> and <111> orientation. More complex films of iron and silicon were created by 1) the RF sputtering of silicon on thermally deposited iron thin films 2) electron beam evaporation of iron and silicon successively without breaking vacuum 3) successive electron beam evaporation of iron and silicon dioxide and 4) electron beam evaporation of iron, silicon and silicon dioxide. The latter three methods eliminated the need to expose the iron film to an atmosphere before depositing a second layer.

Details of the various thin film depositions can be found in Table 6-1.
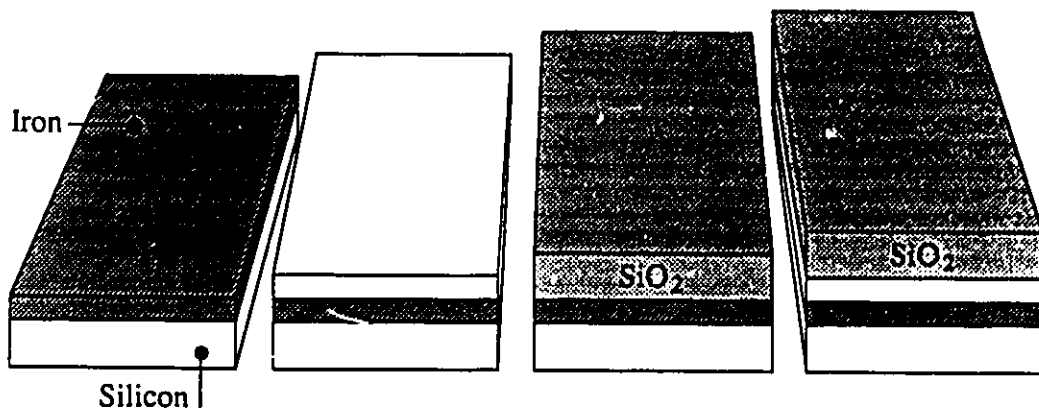
Figure 7-1   As deposited thin film structures

Dep	Method	Pressure	Max Rate(Å/s)	Dep Current	Duration (seconds)	Thickness (Alpha Step)	Material
A	Thermal Evap	5×10^{-6}	2.0		900	1850 Å	Fe
B-1	Electron Beam	5×10^{-7}	4.3	65 mA	420	1000 Å	Fe
B-2	Electron Beam	9×10^{-8}	10.4	165 mA	270	1700 Å	Fe
C	Electron Beam with heat		4.0		663	1400 Å	Fe
D	Sputter Silicon on samples from deposition B						Si
E	Electron Beam	2×10^{-6}	7	30 mA	1150	7240 Å	SiO_2
F	Electron Beam	2×10^{-6}	16	280 mA	130	1797 Å	Fe
		7×10^{-7}	5	20 mA	1000	5020 Å	SiO_2
G	Electron Beam	3×10^{-6}	15	280 mA	40	500 Å†	Fe
		7×10^{-7}	17	240 mA	24	500 Å†	Si
		8×10^{-7}	5	25 mA	1500	7000 Å†	SiO_2
H	Electron Beam	5×10^{-7}	22	350 mA	26	525 Å†	Fe
		3×10^{-7}	50	350 mA	6	474 Å†	Si
		1×10^{-7}	2-3	20 mA	800	2000 Å†	SiO_2
I	Electron Beam	3×10^{-6}	22	350 mA	46	980 Å†	Fe
		1×10^{-6}	40	350 mA	21	1034 Å†	Si
		5×10^{-7}	3-4	25 mA	700	2011 Å†	SiO_2

Table 7-1 Deposition details for experimental thin films

(† thickness estimates from crystal thickness monitor)

7.1   Deposition Systems

7.1.1   Electron Beam Evaporator

The electron beam evaporator was the primary method of deposition used throughout this research, as this was the method through which the highest purity films could be formed. The evaporator used a roughing pump backed by a diffusion pump and was capable of producing a vacuum of approximately 1×10^{-7} torr. The evaporator was equipped with ultraviolet lamps capable of raising the temperature of a substrate two to three hundred degrees during deposition. Bakeout heaters were installed as part of this research in the form of resistance heat tape on the sides of the evaporation chamber. Baking out the chamber prior to deposition by heating the walls and substrate holder improves the vacuum by facilitating the outgassing of water vapor and oxygen. If the

chamber is not baked out prior to deposition, energy lost to the chamber will cause it to outgas during deposition. By limiting outgassing during deposition more power can be pushed into the target material to increase the rate of deposition without increasing the pressure in the system. A faster deposition rate means less reaction with the remaining oxygen and water vapor can occur, and the film is deposited with increased purity. To further improve the quality of the vacuum, a nitrogen back fill was performed to assist in the removal of water vapor from the chamber walls, and a liquid nitrogen cold trap condensed water vapor out of the vacuum. Careful preparation of the vacuum system using the enhancements described above obtained in the best case a much improved vacuum of 2×10^{-8} torr.

The evaporator used a Temescal electron gun which possessed four rotating, water cooled copper crucibles. Each crucible could be loaded with source material and rotated one at a time under the electron beam. The three crucibles not under the beam are covered by a copper plate to protect them from contamination. The electron beam was generated beneath the crucible and curved $270°$ by a magnetic field which also served to confine and sweep the beam. The Temescal setup allowed for the deposition of multiple materials without compromising the vacuum in the chamber.

The system contained an Inficon crystal thickness monitor to supply information during deposition, and a ion gauge located near the cold trap to measure chamber pressure. The location of the ion gauge produced readings that may be slightly lower than the actual pressure in the system.

7.1.2 RF Sputtering System

A High Vacuum Systems Inc. RF sputter system was used sparingly as part of the deposition equipment in this research. The system contained two planar magnetron sources which used 5" by 8" by 0.25" targets, and a magnetron gun which used 2" diameter targets. The sources were arranged around a rotating carousel which contained 8 facets on which substrates could be placed. Each facet held a box containing the actual substrate, and when placed on the carousel each box could be opened or closed individually. The rotating carousel allowed for the inclusion of multiple substrates which could be rotated one at a time into position in front of a magnetron source. Multiple depositions could be made without having to reload and repump the vacuum system.

The pumping stack consisted of a CTI Cryo-Tor 8 cryopump. An ion gauge and a residual gas analyzer measured the pressure in the high vacuum range and a Baratron model 127 capacitance manometer measured pressures in the sputter range. Bakeout heaters and quartz lamps for substrate heating were also part of this system, but were not used in this research. The RF supply was an Advanced Energy RFX 600 (13.56 MHz) supply with a 500 W matching network.

7.1.3 Thermal Evaporator

Iron was thermal evaporated by resistively heating iron flakes in a tungsten boat. The deposition system contained a pumping stack consisting of a diffusion backed roughing pump, but was only capable of producing pressures on the order of 10^{-6} torr. No bakeout or substrate heaters were present for conditioning the chamber, nor was a crystal thickness monitor present to control deposition. Only a single deposition source could be present in the system at any time, making the deposition of multiple layers impossible unless the vacuum was broken and the substrates were exposed to atmosphere. The limited capabilities of the thermal evaporator made its use minimal, and the films deposited with this instrument are of suspect quality.

7.2 Substrates and Substrate Cleaning

A number of different substrates were used during deposition. Silicon wafers with orientations of <111> and <100> were used to study silicide formation and develop a method of forming the semiconducting β phase. Both n and p type wafers were used, with a resistivity of approximately 5 $\Omega \cdot cm$. Similar wafers, oxidized to produce a layer of SiO_2 0.5 to 1 μm thick were used to study the electrical properties of the thin film layers. To determine the band gap of semiconducting iron disilicide, ultra thin silicon wafers were used to minimize absorption by the substrate. The wafers were 75 μm thick, n type <100> wafers with a resistivity of 100 $\Omega \cdot cm$. The ultrathin wafers were polished on both sides to reduce scattering during the optical measurements. Finally, standard microscope slides were included during every deposition to provide expendable material from which characteristics of the deposition could be measured. Such characteristics included uniformity of the deposition, deposition rates and deposition thicknesses.

Before deposition of a thin film, the substrate upon which deposition occurred was thoroughly cleaned to remove organic and particulate contamination, and in the case of the unoxidized wafers, to strip off any oxide layer on the surface. To clean the silicon substrates, one or more of three methods were employed. The first method was a piranha clean to remove organic contamination form the surface of the wafer. Teflon boats were used to withstand the effects of the piranha mixture. The second method of cleaning was a two minute dip in semiconductor grade hydrofluoric acid to remove oxide and particulates from the surface. Wafers dipped in HF were rinsed in 10 $M\Omega$ distilled water and blown dry with pure nitrogen. The third method of cleaning was a dip in 10:1 hydrofluoric acid or buffered oxide etch to remove the oxide from the wafer. In all cases the wafers were placed in the deposition chamber for evacuation as quickly as possible.

Slides were cleaned ultrasonically and in acetone, isopropyl alcohol and distilled water. All substrates were blown dry with nitrogen prior to placement in the deposition system. A section of each substrate was masked with a microscope coverslip to produce an edge from which the film thickness could be profiled.

7.3 Iron Deposition

Metal was deposited through the thermal or electron beam evaporation of bulk iron onto a single crystal silicon substrate. To maintain the purity of the iron film, deposition was carried out in the best vacuum environment possible, on the cleanest substrates possible. Techniques were refined to improve vacuum conditions from 10^{-6} to 10^{-8} torr, and deposition rates were maximized to limit the reaction of oxygen and iron during deposition. The best rates obtained approached 22 Å/s.

7.3.1 Evaporation Source

Different source material was used for the thermal and electron beam evaporation of iron. Electron beam evaporation utilized 99.95% pure iron pellets. Considerable conditioning of the iron was required prior to thin film deposition. The iron pellets were melted a few pieces at a time by a low power electron beam to facilitate the amalgamation of the iron into a melt. Continuously massaging the melt with the electron beam stimulated the desorption of gases from the iron surface. Severe outgassing of iron occurred, suggesting that the iron traps large quantities of oxygen, and the melt required several runs to condition. Material that is not degassed in this manner is subject to spitting during deposition, as gas bubbles out of the melt.

Thermal evaporation required iron shavings of 99.99% purity in a tungsten boat. The quality of the iron was uncertain as the shavings had been exposed to the atmosphere for several months prior to their use. Unlike the iron used in the electron beam evaporator, the thermally evaporated iron was not degassed prior to its use. Iron, being soluble in tungsten, quickly melts through the tungsten boats used in thermal evaporation, so insufficient time was available to degas the iron.

7.3.2 Deposition

Prior to each deposition in the electron beam evaporator, the iron melt was degassed with the shutter closed to protect the substrate from erroneous deposition of iron. This additional degassing insured that any oxygen in the melt during the loading and unloading of previous samples was removed. This step was necessary as the evaporator is not equipped with an airlock and the chamber must be exposed to the atmosphere for loading to occur. During degassing, iron coats the chamber walls and acts as a getter pump to remove additional oxygen, but the net result is nevertheless an increase in pressure due to the escape of gasses from the iron melt, as well as in increase in the temperatures of the gasses remaining in the system (PV=nRT). Deposition occurred only after the vacuum again dropped to a stable level.

The deposition rate was limited by the tendency for iron to spit from the melt, as well as by increasing pressures during faster deposition. The increase in pressure is attributed to increased outgassing from the chamber and substrate holder, which increase in temperature as more power is input into the evaporation system. The problem with spitting is attributable to the nature of the material used and could not be eliminated. It was reduced, however, through conditioning the melt as described previously. In an attempt to increase the rate of deposition, attempts to evaporate iron were made with the iron placed directly in contact with the copper crucible as well as with a boron nitride liner placed in the crucible. The boron nitride liner provides thermal insulation between the iron melt and the water cooled copper crucible, the idea being to maintain the quality of the melt by preventing energy loss through the crucible. As boron nitride is a large band gap semiconductor, it electrically insulates the iron melt as well, leading to problems with electrical charging of the iron. Iron, possibly due to its magnetic nature, displayed increased spitting with the crucible in place. Rates were limited to only a few Å/s. It is suggested that such liners be abandoned for use with iron, and that deposition takes place in an electrically conducting crucible.

Iron, being a ferromagnetic material, affected the magnetic containment and sweep of the electron beam. As the iron in the crucible was heated, the beam position changed, so care was required to insure the beam maintained its position in the melt, and did not fall on the crucible itself. An abrupt and severe shift in beam position occurred before the iron began to melt, and it has been suggested[130] that this is a result of the iron reaching the Curie point. Fixed magnets used to adjust the width of the electron beam required adjustment to produce the proper beam width in the iron melt.

7.3.3 Thermal Evaporation

Deposition of iron layers was initially attempted with the thermal evaporator, due simply to the availability of equipment. Because of the high solubility of iron in tungsten, there was a tendency for an iron melt to eat through the boat used in thermal evaporation. Films were put down quickly to prevent contamination with tungsten, and it was not possible to produce thick films.   The vacuum, measured before deposition, was approximately 2×10^{-6} torr. Deposition rates were slow, requiring approximately 15 minutes to deposit an 1850 Å film. The quality of the films deposited thermally is not considered to be good, as the slow evaporation rates and poor vacuum conditions increase the likelihood of contamination. The exact details of deposition could not be obtained, as there was no gauge which could measure the vacuum pressure during deposition, and no crystal thickness monitor to provide feedback as deposition occurred. The vacuum may therefore have been substantially worse than the estimated 2×10^{-6} torr, and it is uncertain whether the deposition occurred at a constant rate.

7.3.4   Film Characteristics

Figure 7-2 shows the surface and cross sections of thermally and electron beam evaporated iron films. Both films are smooth; any fluctuations in their surface are small in comparison to the thickness of the films. The nodular growth that is occasionally observed in the films can be attributed to contamination of the silicon substrate[1][1], as neither of the films shown in the figure were subjected to extensive cleaning procedures. The cross sections reveal that iron is deposited with a fine grained columnar structure, and x-ray diffraction suggests a random grain orientation with respect to the substrate.

Thermally Evaporated Thin Film

Electron Beam Evaporated Thin Film

Figure 7-2   Thermal and electron beam evaporated thin iron films. The upper pictures show a TEM cross section and SEM surface view of a thermally deposited iron layer. Below is an SEM image of the surface of an electron beam deposited iron film.

7.4   Silicon and Silicon Oxide Deposition

In addition to iron, various attempts were made to deposit silicon and silicon dioxide thin films. Deposition occurred in both an RF sputter system and electron beam evaporator. The RF system possessed the advantage of forming films at low temperatures, while the evaporator allowed for the deposition of silicon onto iron without breaking vacuum.

7.4.1   RF Sputtering of Silicon

Initial attempts to sputter silicon required a home made target for use in the smaller gun, created by cutting a 2.5" silicon wafer down to 2" in diameter and gluing it to a metal backing plate. The target was presputtered (burned in) for 30 minutes to remove any contamination from the surface. Deposition of silicon occurred for another 30 minutes. Amorphous layers of silicon were successfully deposited, although the layers were extremely thin. The thin nature of the wafer, coupled with the need for a good burn in of any sputter target made it unlikely that a target could last sufficiently long to produce a series of thicker films. The films were grown with a base pressure of 1 x 10^{-6} torr, with an argon flow of 10.6 sccm (standard cubic centimeters per minute) at a pressure of 4.2 mtorr. The forward power was 95 watts. Due to imperfect impedance matching to the target the reflected power was 3 watts, resulting in a power input of 92 watts to the target. Additional power input was not deemed reasonable as larger and more durable silicon targets have been shattered at higher power levels.

Further attempts to sputter silicon were made with a 99.999% pure polycrystalline silicon substrate obtained from Metron Incorporated. The target was used in the planar magnetron sputter guns, and was 5" by 8" by 1/4" thick as required. Much more power could be pushed into this target without the risk of shattering it. Silicon was deposited at 400 watts, with 10.6 sccm of argon at a pressure of 2 m.:orr. The initial base pressure was 1 x 10^{-6} torr. Deposition rates obtained during this run were approximately 6.3 Å/s, as obtained by the crystal thickness monitor attached to the sputter system. As the larger target and planar magnetron gun produced better deposition rates, and likely better films, this method was used to sputter silicon for use in the research.

7.4.2   Electron Beam Evaporation of Silicon

Attempts to deposit silicon in the electron beam evaporator met with good success. Silicon of 99.9999% purity was used as source material, and conditioning similar to that performed for iron was used to create a pure and coherent melt. Once a good melt was obtained, deposition rates of 50 Å/s were achieved. Depositions that occurred prior to complete conditioning of the melt were limited in rate due to sudden bursts of outgassing which resulted in large fluctuations in the vacuum chamber pressure.

Films grown under these conditions displayed a muddy brown color, suggesting they were composed primarily of silicon oxide and not pure silicon. Films grown from a well conditioned melt appeared shiny and metallic.

7.4.3 Deposition of SiO₂

Deposition of SiO_2 occurred exclusively in the electron beam evaporator, from crushed quartz pieces of 99.99% purity. Although SiO_2 possesses a high melting point, it lends itself well to deposition of this sort due to its low thermal conductivity. Little energy is lost through heat conduction to the cooled crucible. Because of the low thermal conductivity of SiO_2, the quartz does not form a cohesive melt. Only the top layers of the pieces melt as the beam passes over them, and evaporation occurs from this layer. The low thermal conductivity allows the top to remain molten, as little energy is conducted away. Thus, even though SiO_2 has a high melting point, evaporation can be performed with little power and relative ease. A disadvantage is that evaporation tends to follow the sweep of the beam, and evaporation rates may suddenly change as the beam passes over and melts small quartz pieces. This leads to a slightly unstable evaporation rate.

During evaporation, pressures quickly rose an order of magnitude as severe outgassing occurred when the quartz was heated. Some oscillation of the pressures occurred initially, but subsided after the quartz had time to heat. Initial heating occurred slowly, as quartz pieces tended to jump out of the crucible when large amounts of power were input when they were cold. Good rates were possible with the input of relatively little power, but deposition was kept intentionally slow. Rates between 2 - 3 Å/s were used. Too much power inputted into the quartz causes dissociation of silicon and oxygen, resulting in the growth of a film displaying poor stoichiometry. This may be monitored by observing the color of a film as it grows. Films displaying good stoichiometry display characteristic SiO_2 color fringes for varying thicknesses. Poor films possessed a dull brown color, similar to poor films produced during Si deposition.

An advantage with the deposition of SiO_2 was the reduced requirement for good vacuum conditions. Deposition improves if it occurs with a slight oxygen ambient.

7.4.4 Film Characteristics

Unlike the deposited iron films, SEM and x-ray analysis of the deposited silicon and silicon dioxide films suggest that the films possess limited, if any structure. It is most likely that both materials are deposited with an amorphous structure. This is consistent with findings for other processes such as chemical vapor deposition which state that silicon deposited under 600 °C is amorphous[132].

7.5 Multiple Layer Depositions

Deposition of multiple layers of material was possible in the electron beam evaporator due to the rotating crucible setup. Target materials could be placed in one of four crucibles, each capable of being rotated into a position under the electron beam. In all cases iron was the first material deposited, and was followed by either silicon or silicon dioxide. Iron deposited on the chamber walls served to getter pump the vacuum prior to silicon deposition, facilitating the creation of good vacuum conditions for silicon deposition. A similar result was obtained after silicon deposition; silicon acting as a getter pump prior to oxide deposition. This result was less important however, as the deposition of silicon dioxide proceeds better in a slightly oxygenated atmosphere.

Sputtered layers of silicon were also deposited on electron beam evaporated iron. This procedure was put to limited use as the exposure of the iron layer to the atmosphere prior to silicon deposition was believed to be detrimental to silicide formation.

Formation of β FeSi$_2$

8.1 Annealing

A number of annealing procedures were carried out on samples obtained from the deposited thin films. Annealing occurred in nitrogen, flowing nitrogen, forming gas, and vacuum environments. Samples were annealed between temperatures of approximately 400 and 1100°C, for times between 5 min and 48 hours. The results of annealing are found in the sections following this one. Details of the annealing process follow directly.

Sample wafers were diced with a Micro Automation model 1100 Wafer Dicing Saw. The wafers were cut into sections from 1 to 1.5 cm square. Selected samples were sealed in Pyrex and Quartz tubes in a vacuum of approximately 10^{-4} torr, with a limited number being sealed in Quartz under a nitrogen atmosphere. Prior to either sealing or annealing, samples were cleaned ultrasonically in acetone, isopropyl alcohol and distilled water to remove gross contamination from the surface.

8.1.1 Flowing Nitrogen and Forming Gas

Silicide formation was attempted under flowing gas in a Thermco Products Corporation "Mini Brute" 10 KW annealing furnace. The furnace possessed two gas feed lines; one connected to high purity nitrogen, and the other connected to forming gas, a mixture of 90% nitrogen and 10% hydrogen, supplied by Linde. The nitrogen used was from the Alberta Microelectronic Center's inhouse main lines, possessing a purity of 99.9987%. The gas was dried on site in dual moisture removal systems, and put through a trace oxygen removal system to insure that impurities included no more than 1 ppm moisture (H$_2$O) and 3 ppm oxygen. The total level and composition of the impurities can be seen in table 8-1. As the nitrogen traveled several hundred feet from the processing facilities to the annealing furnace it is possible that additional impurities were absorbed undetected. The impurity levels of the forming gas was unknown.

The furnace possessed a central temperature controller variable from 400 to 1400°C, with deviation controllers for the furnace ends which were adjustable by ± 50°C to compensate for furnace nonlinearity. An independent K-type thermocouple was used

Impurity	Max Acceptable Level (ppm)	Impurity	Max Acceptable Level (ppm)
Carbon Dioxide (CO_2)	1	Oxygen (O_2)	3
Carbon Monoxide (CO)	5	Total Hydrocarbons	1
Hydrogen (H_2)	2	Water (H_2O)	1

Table 8-1 Specifications for semiconductor standard bulk liquid nitrogen (N_2)

to provide an accurate reading of the furnace temperature. Flowing nitrogen through the furnace at annealing temperatures removed latent oxygen and moisture prior to annealing. Upon completion of annealing samples were generally air cooled, although furnace cooling to 400°C was used with high temperature annealing to prevent oxidation. Excess gas was vented through a burn box to eliminate the possibility for uncontrolled combustion or explosion.

For annealing in flowing nitrogen, samples were placed in a hot furnace only after nitrogen had been passed through it for a short period of time. Samples annealed in forming gas were placed in room temperature and preheated furnaces flushed with pure nitrogen. The gas was switched to forming gas prior to the insertion of a sample.

8.1.2 Vacuum

Thin films were annealed in vacuum under varying conditions. Low temperature anneals (below 650°C) used samples 1.0 - 1.5 cm² sealed in Pyrex tubes under a vacuum of 10^{-4} to 10^{-6} torr. Most of the experimental work was done on samples in the 10^{-4} range. As the vacuum gauge was located close to the vacuum pump and not the sample tube, the vacuum in the sealed tubes may be as low as 10^{-3} torr. Higher temperature anneals (above 650°C) were carried out in quartz tubes under the same 10^{-4} torr vacuum.

Actual annealing occurred in two Lindberg furnaces, and was monitored with a K type thermocouple for accurate temperature control. To maintain the consistency of the annealing process samples were placed on a metal stage located in the front center of each furnace. Samples that rolled off of this stage were labeled as invalid as it was unsure how their annealing temperatures compared to the rest of the experiments. Sufficient differences in the reaction rates of those samples justifies their removal from the results. After annealing, samples were air cooled for one minute before being quenched in room temperature water. Air cooling was necessary to prevent shattering of the sample tube upon quenching. Selected samples were annealed at high temperatures and furnace cooled to, and held at, lower temperatures in an attempt to bring about a transformation from the high temperature to the low temperature silicide phases. These samples were subsequently air cooled and quenched.

8.1.3 Nitrogen ambient

A limited number of anneals were carried out in sealed quartz tubes under a nitrogen ambient. Sample sections were placed in quartz tubes which were evacuated, back filled with nitrogen, re-evacuated, and refilled with nitrogen to slightly below atmospheric pressure. The reduced pressure in the sample tube facilitated the sealing of the tube as the partial vacuum would draw in the molten quartz as the tube was pinched off. Ultra high purity (UHP) nitrogen was supplied by Linde, possessing less than 3 ppm each of moisture and oxygen. Samples were annealed in the same Lindberg furnaces detailed above, and again were air cooled and quenched to room temperature.

8.2 Agglomeration of Iron Thin Films

A serious obstacle to the formation of iron silicide is the agglomeration of iron in the thin film couple. Agglomeration is known to occur at temperatures above 650 °C[45,46, 52], and was found to occur at the temperatures required for silicide formation in this work. Significant distortion of the iron surface required only 5 minutes at 800 °C, with complete disruption of the film occurring shortly after 1 hour. Given sufficient time, the : iron films turned into a collection of spherical beads on the surface of the silicon substrates. The agglomeration process can be clearly seen through the series of SEM photos in Figure 7-1. The agglomeration steps are outlined below;

- Initially the surface is continuous and completely flat

- After 5 minutes small spherical caps have formed

- At 10 minutes the caps have grown significantly in size

- After 20 minutes small perforations have appeared in the film. Spherical caps can still be seen, but are beginning to disappear

- After 1 hour, perforations have grown and threaten to pinch off portions of the film. The surface of the iron has become very smooth

- Longer anneals (2 - 4 hours) show a film that has broken into isolated islands, and is no longer continuous

The process detailed above fits well with the theory of agglomeration outlined in Chapter 6. As the film is annealed grooves develop along surface grain boundaries, and deepen until the grains form spherical caps on the surface. As the deposited iron film is thin, some of these grooves penetrate the film before a stable cap forms. The resulting holes grow until they impinge upon one another, causing the surface to dissociate into islands. When small grains at the surface are absorbed by larger grains (either on the
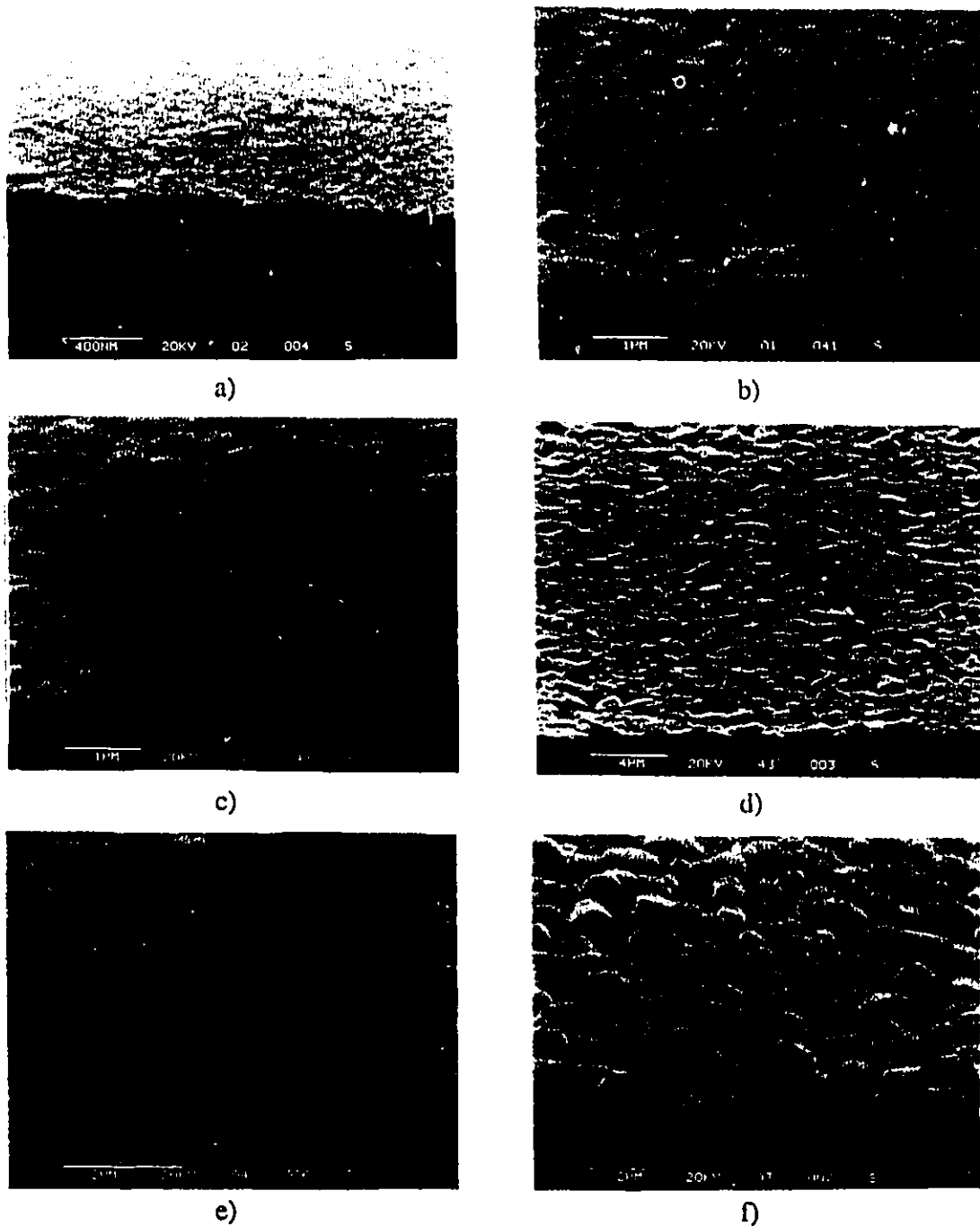
Figure 8-1   Agglomeration process at 800°C, as seen by the SEM. a) Unannealed iron thin film. b) After 5 minutes small spherical caps have formed on the surface. c) At 10 minutes the caps have grown substantially in size. d) After 20 minutes perforations can be seen in the film surface. e) At 1 hour the perforations have grown and threaten to pinch off portions of the films. f) At two hours, the film has broken into isolated islands.

surface or within the film), the surface begins to relax to flatness, and the islands become relatively smooth. Eventually, most islands transform to spherical beads as this is their most stable shape. Extremely long islands will not become spherical unless grooves exist and are spaced more than $2\pi \times$ the island radius. This effect can be seen in Figure 8-2, which shows a high temperature anneal of 1000°C (40 hours). The thin films have formed completely spherical beads on <100> substrates, and a combination of beads and cylinders on <111> substrates.

X-ray analysis of samples annealed at 800 °C for two hours shows no evidence of materials other than iron and silicon, suggesting that agglomeration occurs prior to silicide formation. Agglomeration of iron occurred on all silicon substrates, regardless of surface preparation or deposition conditions. This is consistent with the assumption that agglomeration of the iron layer is an effect of the surface energy of the iron with respect to the atmosphere, and not an effect at the interface between the iron and silicon substrate (Agglomeration, Chapter 5).

8.2.1 Formation in Nitrogen Ambient

Being dependent on surface energy considerations, agglomeration effects can be altered by changing the nature of the surface. This was done by introducing a controlled atmosphere to the annealing process. Silicon–iron diffusion couples were sealed in nitrogen to alter the conditions at the surface of the iron layer, and the couples were annealed in the same manner as vacuum sealed couples. The nitrogen ambient succeeded in slowing agglomeration, but was unsuccessful in preventing its occurrence. As long times were required to form iron silicide from the thin film samples prepared in this research, the use of a nitrogen atmosphere to prevent agglomeration was rejected.
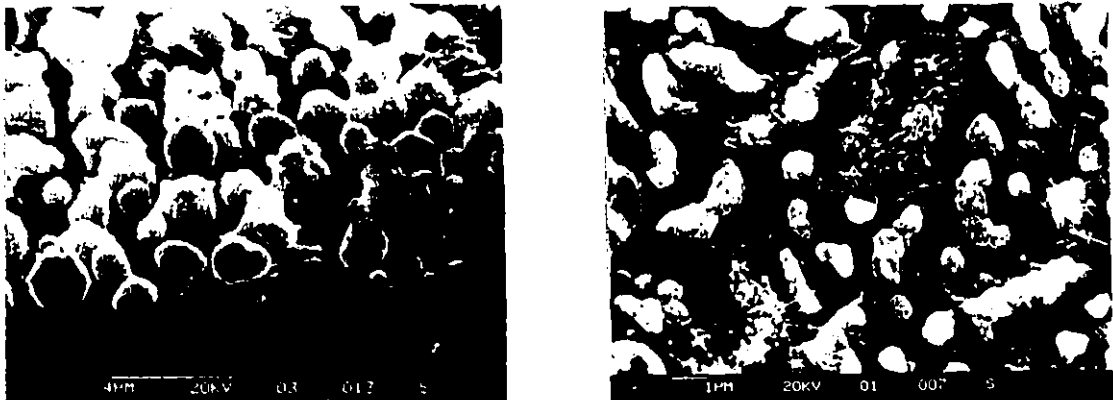
Figure 8-2   SEM micrographs showing high temperature agglomeration of iron on <100> and <111> substrates. <100> substrates (left) show a tendency towards the formation of spherical beads, while <111> substrates (right) show mixed bead and cylinder formation. Formation temperature was 1000°C.

8.2.2 Capping Layers

In addition to annealing in a controlled environment, surface energy considerations can be altered by the addition of a capping (passivation) layer to a thin film diffusion couple. The capping layer should not react with the thin film to alter the kinetics of compound formation, nor should it alter the ultimate result of reaction. Capping layers have previously been utilized in silicide formation to control the oxidation of metal layers. Molybdenum and tungsten layers have been used to protect cobalt thin films from oxidation before silicidation occurs[117]. At the temperatures at which silicide forms in a si :on–cobalt diffusion couple neither material (Mo or W) mixes with cobalt. Upon completion of the reaction Mo, W and their oxides can be etched away without removing the underlying silicide.

Capping layers of silicon and silicon dioxide were used as passivation layers for iron thin films. The materials were selected for the ease with which they could be deposited, as compared to metals such as molybdenum and tungsten, which posses high melting points that make them difficult to evaporate. Additionally, a covering layer of silicon on iron thin films provides an additional interface at which silicide formation may occur, thereby decreasing the diffusion distance and time required for silicon formation. As the final product desired from annealing was FeSi₂, silicon layers were generally made slightly thinner than iron layers to insure complete consumption of the silicon during silicide formation. This would leave a single silicide layer on the wafer, covered in some instances by an SiO₂ layer which could be easily removed. The possibility of agglomeration of the silicide after removal of the capping layers was not considered.

Sputtered Silicon

Silicon was sputtered onto previously evaporated iron thin films to form passivation layers that would also assist with the interdiffusion of iron and silicon to form iron disilicide. The iron thin films were electron beam evaporated onto HF dipped silicon wafers, and the films were cleaned in acetone and ethanol prior to the sputtering of silicon. Silicon in excess of the amount required to form stoichiometric β FeSi₂ was deposited onto the iron to insure that a good passivation layer was created. Excess silicon was intended to be etched away upon completion of silicidation. The resulting diffusion couple was annealed in flowing nitrogen, as the silicon passivation layer protects the iron from oxidization by forming an oxide itself, and a vacuum environment is unneeded.

Limited success was achieved with sputtered capping layers. Figure 8-3 shows the resulting film after annealing, at a fractured edge. It can be seen that the silicon overlayer is relatively flat, but regions of the silicon layer that have been removed during fracturing reveal that localized agglomeration has occurred beneath the it. These regions of agglomeration exist between large regions of unagglomerated iron. The detection of backscattered electrons with the SEM allowed for an image to be formed from atomic
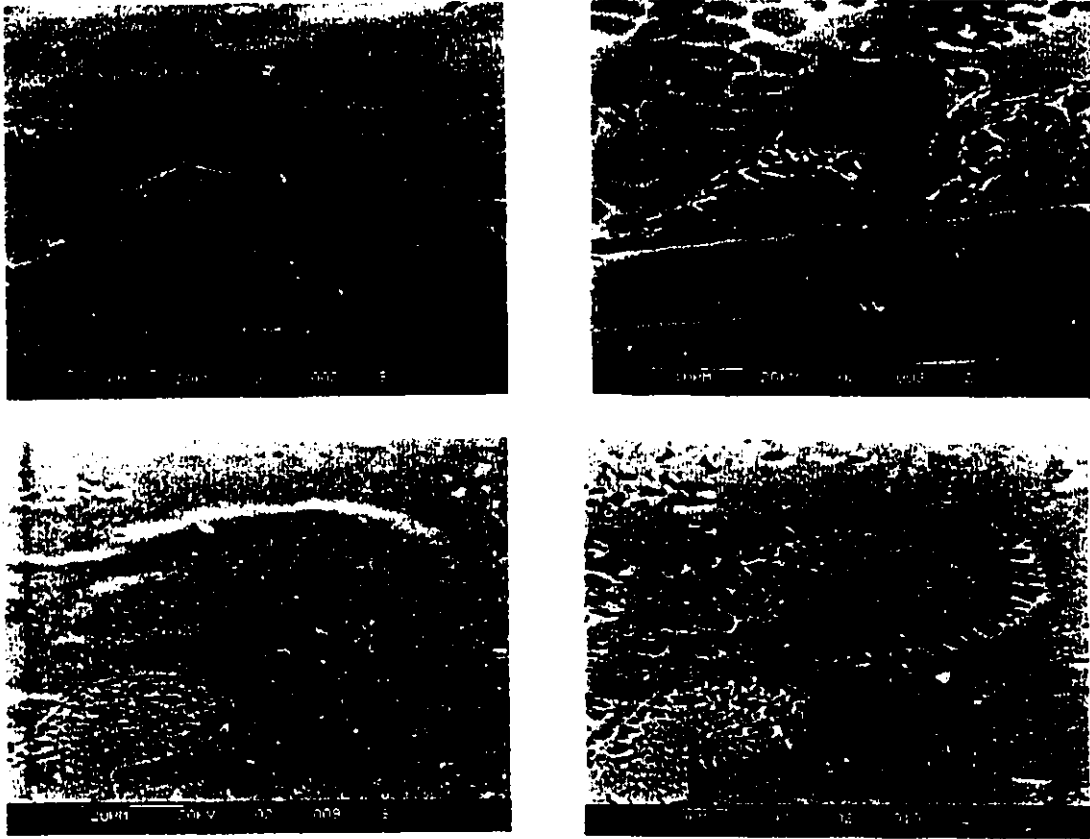
Figure 8-3   Sputtered silicon passivation layers. The above photos show SEM images of iron layers covered with sputtered silicon, after annealing at 800°C. The pictures on the left use secondary electron imaging to reveal surface topography. The pictures on the right use backscattered electron imaging to reveal surface composition. Brighter regions are iron rich, while darker regions are deficient in iron.

number differences in the surface of the thin films. Regions of high iron concentration appear brighter than the silicon background. These images reveal that the regions of unagglomerated iron continue under the silicon capping layer, as iron can be seen to have diffused into the silicon evenly in these areas. Dark patches on the surface of the film are regions in which agglomeration has taken place, and iron has not diffused significantly into the silicon layer. Figure 8-3 shows backscattered and secondary electron images of the same regions to allow for a comparison of surface topography and composition.

The unexpected result of localized agglomeration is possibly due to the presence of oxygen in the iron thin film prior to silicon deposition. As the iron thin films spent significant amounts of time in an uncontrolled atmosphere it is assumed that considerable reaction with oxygen has taken place at the thin film surface, and it is not inconceivable that particulate or organic contamination found its way into the diffusion couple. This contamination may have caused the intermittent "bubbling" of the surface that can be seen in the photos, as well as having an affect on silicide reaction and thin film stability.

Evaporated SiO₂

Evaporated layers of silicon dioxide (SiO₂) were used as capping layers for iron thin films annealed in flowing nitrogen and vacuum environments. Diffusion couples passivated with SiO₂ and annealed in flowing nitrogen oxidized in much the same manner as unpassivated thin iron films. Couples annealed in vacuum, however, showed a marked improvement in stability. Figure 8-4 shows cross sections for diffusion couples capped with SiO₂. The top photographs show diffusion couples which have been etched to thin, but not remove, the passivating oxide layer. Considerable surface roughness exists on the oxide layer, a result of the etching process and not silicide formation. However, it is seen that the surface is continuous, and smooth with respect to its thickness. Beneath the oxide layer the catastrophic disruption of the iron thin film seen in earlier photographs has been alleviated. However, the SiO₂ capped layers still show significant disruption in the form of pinholes throughout the surface. Although these layers are continuous, the pinholes present concerns with using such films for electronic applications as they will seriously affect the conductivity of a film, as well as exacerbate instability effects such as electromigration.
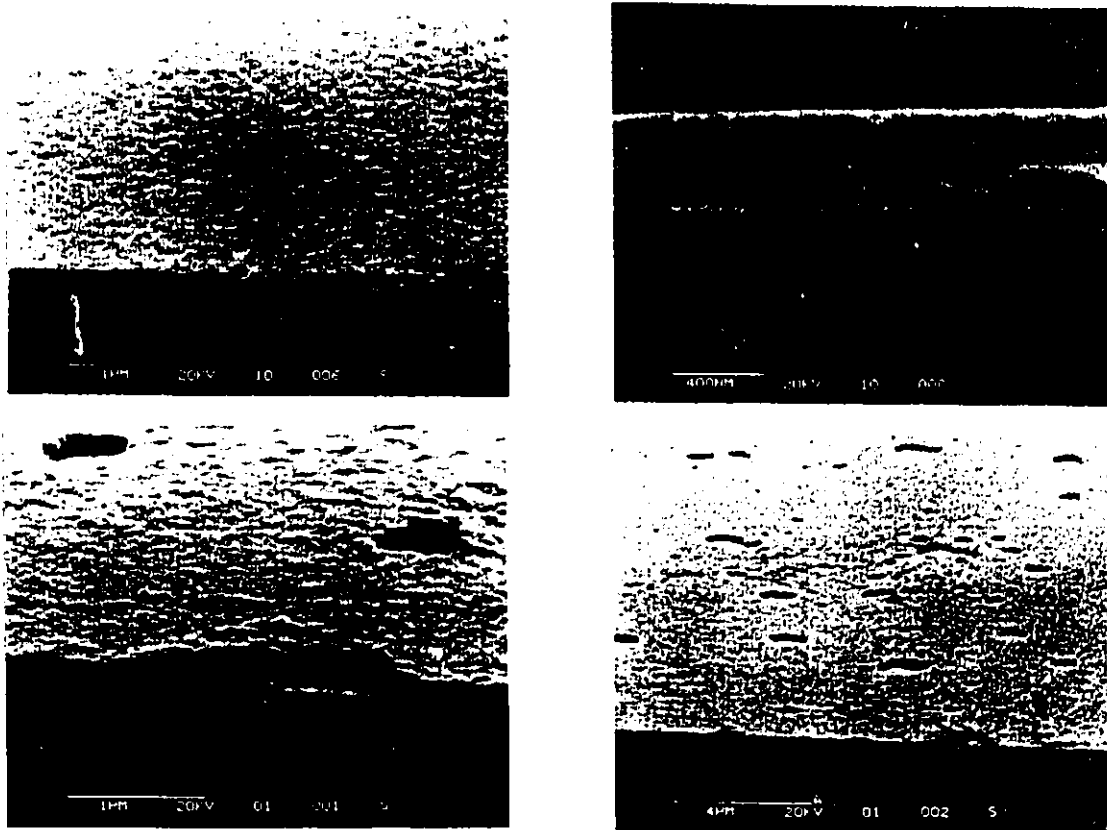
Figure 8-4 SiO₂ capped thin iron films. The top film (shown in surface view and cross section) was annealed at 800 °C and etched to partially remove the oxide layer. The bottom photos show a film which was annealed at 600 °C and etched to remove the entire oxide layer. All photos are from the SEM.

Evaporated Si/SiO₂

Combined layers of silicon and silicon dioxide proved to be the most effective passivation scheme for the prevention of oxidation and disruption of iron–silicon diffusion couples. These layers protected iron films from oxidation in both flowing nitrogen and vacuum environments, although better results were still obtained with annealing in a vacuum. Figure 8-5 shows diffusion couples annealed in vacuum and protected by Si/SiO₂ capping layers. Again, the photos show diffusion couples with a partial oxide layer remaining on the surface. Figure 8-9 shows the surface of a reacted diffusion couple after the protecting oxide layer has been completely removed. Annealing conditions for the thin films were similar to those used for the oxide protected films of Figure 8-4. Unlike the films displayed in the previous figure, these films possess continuous layers with no defects. The slight surface roughness is due either to the oxide etching or the tendency for nucleation controlled formation to produce rough surface topography. It has been previously asserted that iron silicide formation is nucleation controlled[50]. The reason for the improved results with Si/SiO₂ capping layers over straight SiO₂ layers is unclear at this time.
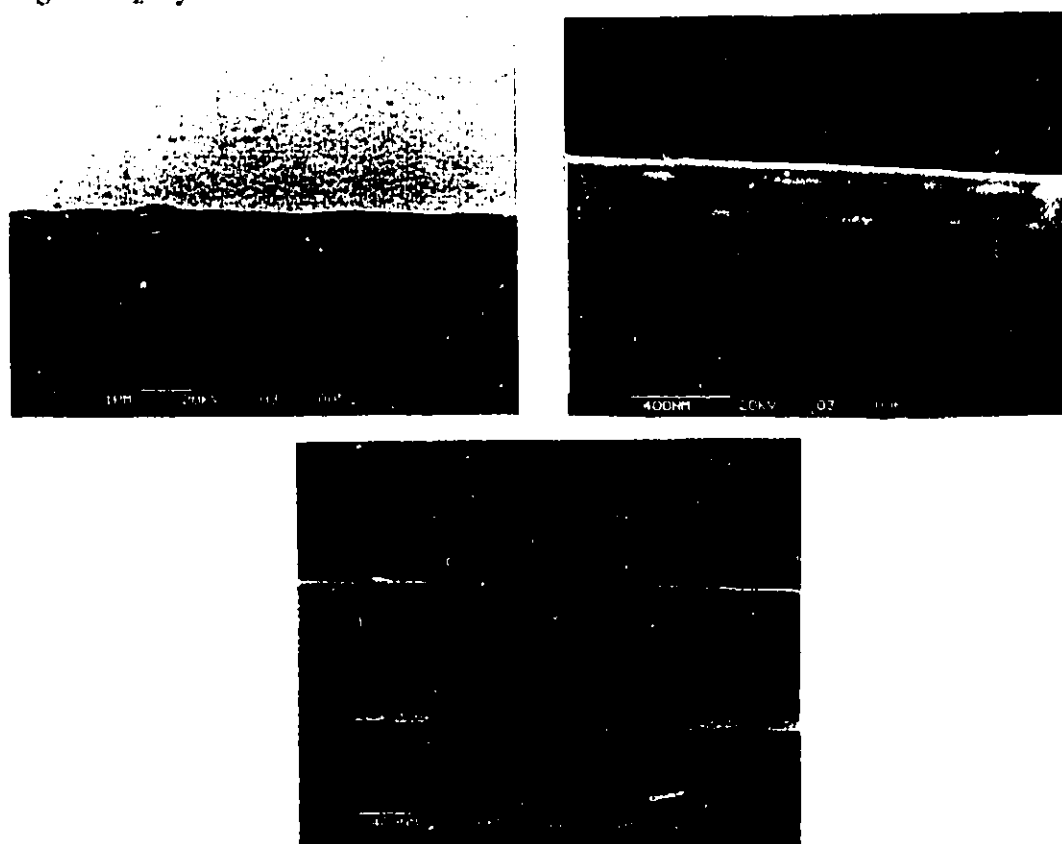
Figure 8-5   Si/SiO₂ capped thin iron films. The photos above show SEM images of an annealed iron layer that was passivated with silicon/silicon dioxide. The top photos show the film after the oxide layer has been partially etched away, while the lower photo shows the film with the entire oxide layer. As can be seen, the iron layer is flat.

The thin films shown in Figure 8-5 show distinct layers on the silicon substrate. The top layer, seen only in the top photographs, is the remaining silicon dioxide layer. The next layer, seen in all the photographs, is believed to be β iron disilicide (FeSi$_2$), as x-ray diffraction shows this to be the only phase present in the samples. The lack of additional layers between the silicide and oxide suggest that the silicide is stable with respect to silicon dioxide, allowing it to be used in silicon dioxide passivated processes.

Silicide formation likely occurs at both interfaces in the silicon–iron–silicon diffusion system (Figure 8-6). Because of the amorphous nature of the top silicon layer, the silicon in this layer is likely bound less tightly than that in the substrate, and likely diffuses much quicker into the iron layer[118]. Thus the silicon capping layer should be consumed quickly. This rapid silicide formation may assist in protecting the iron layer during silicide formation, as silicides have been shown to possess higher thermal stability than metals (see Chapter 5, Thin Film Instabilities).

The necessity of the silicon dioxide overlayer is not confirmed by this work. No evidence exists to suggest that the prevention of agglomeration is due to factors other than the presence of a silicon layer above the iron. While iron agglomerated beneath the sputtered silicon, the silicon layers remained intact, suggesting film disruption was a result of the interface between the iron layer and the silicon capping layer. Silicon layers subjected to sufficient oxygen during annealing should display no effect other than the formation of silicon dioxide, an occurrence that would grow the same Si/SiO$_2$ formation that was deposited in this experiment. It is therefore suggested that silicon capping layers, if sufficiently thick to withstand any oxidation that occurs during the annealing process, should be sufficient to passify iron thin films. Finally, as annealing was performed for times considerably greater than that required for silicide formation with no degradation in the silicide layer, it can be concluded that iron disilicide is stable with respect to silicon dioxide as well as silicon.
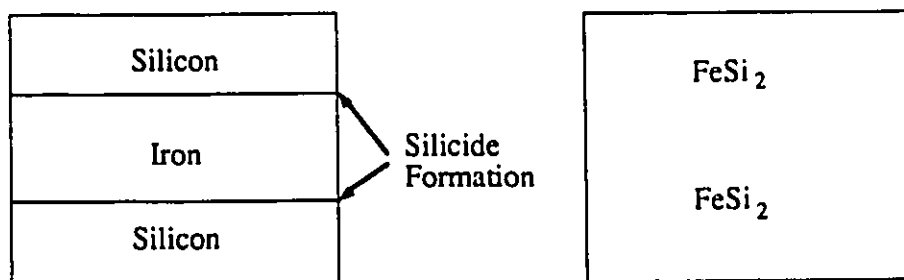
Figure 8-6   Silicide formation in silicon–iron–silicon diffusion system. Because the density of the silicon layer above the iron is less than that of the silicon beneath the iron, this layer likely reacts more quickly to form silicide.

8.3   Silicide Growth

The variety of annealing conditions used to stimulate the growth of silicide met with varied results. Iron films annealed under flowing nitrogen oxidized rapidly regardless of the temperature at which formation took place, and although oxidation was avoided with samples sealed under vacuum or nitrogen, long annealing times (10^+ hours) were required to form silicide. Silicide formation was noticeably quicker for electron beam evaporated iron, and slightly quicker on <111> silicon as opposed to <100> silicon, but never approached the formation times of 1 to 2 hours reported in the literature. Thermally deposited films annealed at temperatures exceeding 900°C for more than 18 hours contained both α iron disilicide and unreacted iron, suggesting that silicide formation is being severely curtailed. This result is likely linked to high impurity concentrations in the iron. Attempts to form β FeSi₂ from early, less pure films, were unsuccessful for anneals of greater than 20 hours at 900°C, while complete formation of iron disilicide was achieved in the same or less time at 800°C for the more pure films deposited in the latter stages of the research. In no instances was iron disilicide detected on its own in a thermally deposited sample. As a result, thermally deposited thin films were rejected for silicide formation.

With improved film qualities and long annealing times, a number of silicide phases appeared. Evidence from cross sectional TEM and x-ray diffraction suggest that Fe₃Si, FeSi and FeSi₂ form simultaneously upon annealing. Table 8-2 shows the phases that formed in this research.

Silicide formation occurs despite agglomeration, and electron microscopy of unprotected films shows silicide formation taking place within individual iron beads. Cross sections of these beads, along with the initial iron layer, are seen in Figure 8-7. A thin oxide layer can be seen between the silicon substrate and initial iron layer. This same oxide layer lies between the silicon and silicide layer after annealing, indicating that silicide formation occurs on the iron side of the oxide. From this observation it is concluded that silicon is, at least initially, the primary diffusing species.

Formation	Compounds Formed	
Temperature (°C)	Thermal Samples	Electron Beam Samples
400	–	
500	–	
600	Fe₃Si	
700		β FeSi₂
800		β FeSi₂
900	Fe₃Si, FeSi, α FeSi₂	β FeSi₂
1000	FeSi, α FeSi₂	α FeSi₂ (944°C)

Table 8-2   Silicide Phases Detected After Annealing

Both TEM and XRD indicate that multiple phases of iron silicide grow simultaneously. This result is unusual for a thin film diffusion couple, but not unheard of. The reason for this growth has not been determined in this research, as the films from which much of the work occurred possess too much impurity to reach an informed conclusion. This impurity may or may not be a factor by slowing interdiffusion to allow for multiple layer growth.

8.3.1   Growth of β FeSi₂

Success in forming β FeSi₂ was achieved with electron beam evaporated iron layers, in a process that was tightly controlled for both film and substrate purity. The final composition of the film was verified as being β FeSi₂ through EDX and XRD. Annealing at 800°C for 20 hours succeeded in forming the silicide phase, and success was achieved on both <100> and <111> oriented substrates. X-ray diffraction patterns for the silicide on the respective substrates can be seen in Figure 8-8. A strong preference can be seen for the formation of (202) and (220) silicide planes on <111> silicon. It is assumed that a degree of epitaxial growth is being observed on the <111> substrates, as epitaxial (202) and (220) planes have previously been observed in the literature (q.v.), and epitaxy has been observed to occur relatively easily on silicon of this orientation (Chapter 4). The <100> substrates show much less sign of preferred orientation, which is consistent with findings that suggest epitaxy on this substrate is difficult. The substantially increased presence of the (202) and (220) planes on the <111> silicon, and the reduced presence of other planes, as compared with silicon <100>, supports the hypothesis of limited epitaxy.
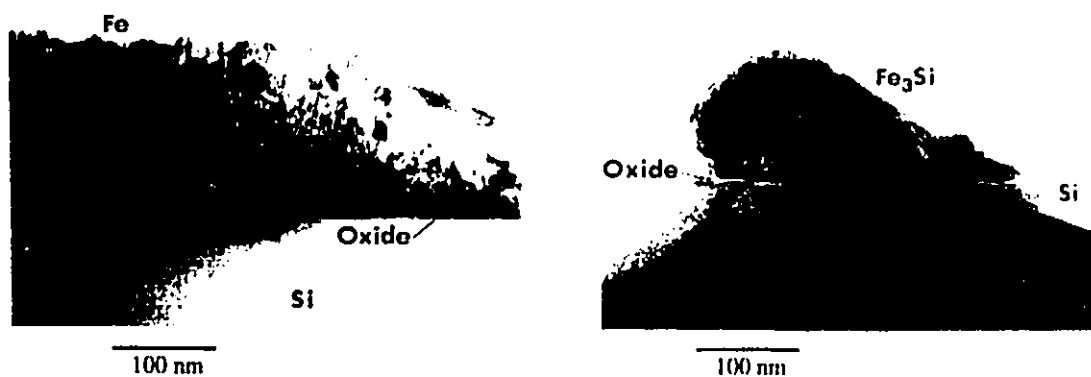
Figure 8-7   Silicide Formation. On the left is a TEM cross section of an unreacted iron thin film on silicon. Between the iron and silicon a thin oxide layer is visible. At right is a TEM cross section of an agglomeration bead, showing silicide formation occurring above the oxide layer.
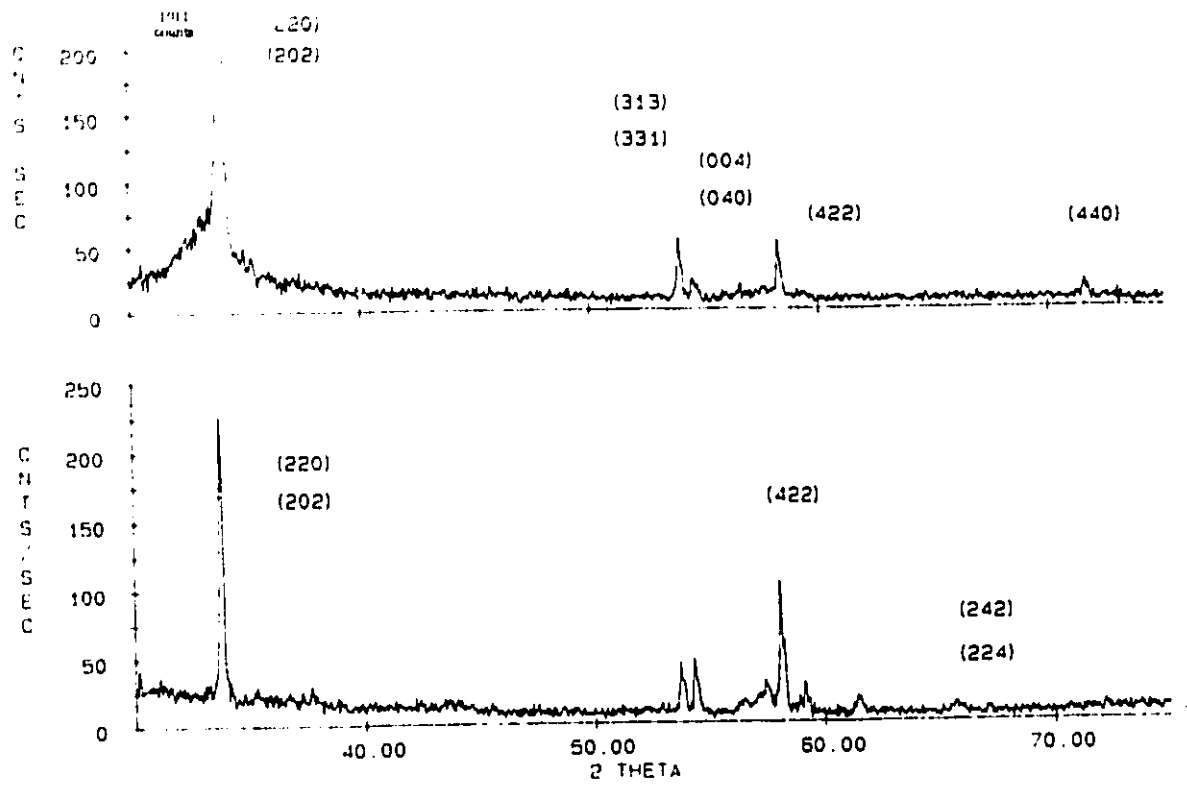
X-ray Diffraction Patterns for <111> silicon (top) and <100> silicon (bottom)
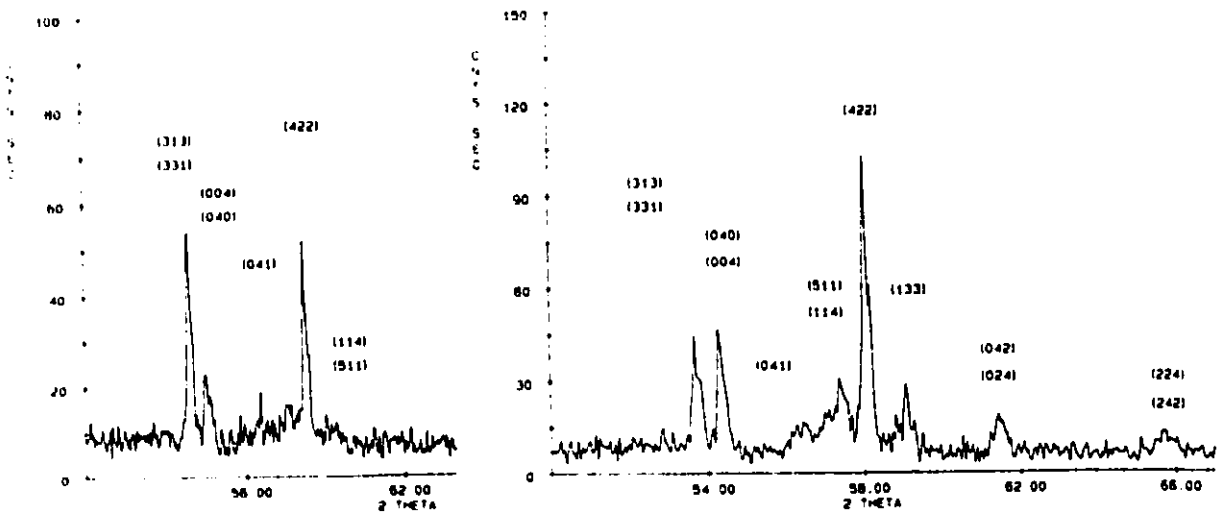
Expanded X-ray pattern for <111> silicon (left) and <100> silicon (right)

Figure 8-8   X-ray diffraction patterns for annealed (800°C 20h) diffusion couples. All peaks represent β FeSi₂.

Figure 8-9 shows a photograph of a continuous silicide film formed through the use of capping layers. The rough surface of the silicide layer can possibly be attributed to two factors. The first is the etching of the silicide layer during oxide removal. It is unlikely that this effect was significant, as long etch times showed limited reaction with iron disilicide; during oxide removal, the silicide surface was only exposed to the etchant briefly. It is more likely that surface roughness is a result of the nucleation controlled growth of iron disilicide. The tendency for a rough surface is consistent with the findings in the literature.[50]

While good silicide films required iron layers deposited in the best vacuum conditions, silicide was successfully formed from poor quality films at higher temperatures. Anneals of 900-1000°C succeeded in producing iron disilicide from all of the thin films studied, but only the α phase was attainable consistently. Attempts to transform this phase back to the low temperature β phase were unsuccessful. These attempts included anneals at 800-850°C for up to 5 hours. The high temperature phase, once formed, appears to be kinetically very stable.

Figure 8-9   Thin film β FeSi₂. Shown is an SEM view of the final silicide layer formed. The fine detail visible on the iron and silicon is gold, which was used to eliminate charging during SEM imaging.

Band Gap measurements of β FeSi₂

The band gap of semiconducting iron disilicide was measured from the thin film depicted in Figure 8-9. Ultrathin (75 μm) silicon wafers were used to minimize absorption by the substrate. Additionally, the wafers were double sided polished to reduce scattering. The reflection and transmission spectra for the film can be seen in Figure 8-10. What appears to be a significant amount of noise in the transmission spectrum, particularly at the higher wavelengths, is a result of interference fringes in the spectrophotometer. This interference phenomenon is created from the high reflectivity of the double sided polished wafers, and it is suggested that such wafers not be used for this sort of work.

The transmission spectrum for silicon can be seen superimposed over the spectrum for iron disilicide in Figure 8-11. Because the value of the silicon band gap is close to that expected for β FeSi₂, the possibility existed for an overlap of the absorption curves for the two materials. Figure 8-11 shows that silicon transmission and reflection begin to decrease near the end of the silicide transmission roll off. This suggests the possibility of an adverse substrate effect. Figure 8-12 shows a plot of the absorption coefficient of the thin film. An intercept can be extrapolated at 1.05 eV, which should correspond to the band gap of the material. The value of this band gap is considerably higher than the reports of 0.85 - 0.89 eV found in the literature.

Transmission and Reflection
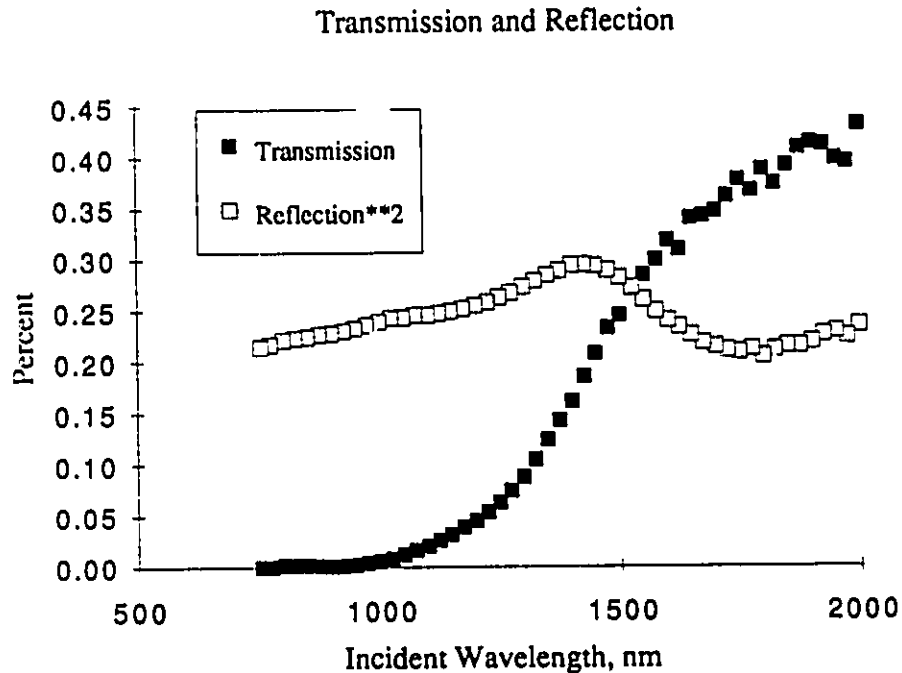
Figure 8-10   Transmission and Reflection curves for β FeSi₂

Reflection and Transmission of Silicon and Silicide/Silicon
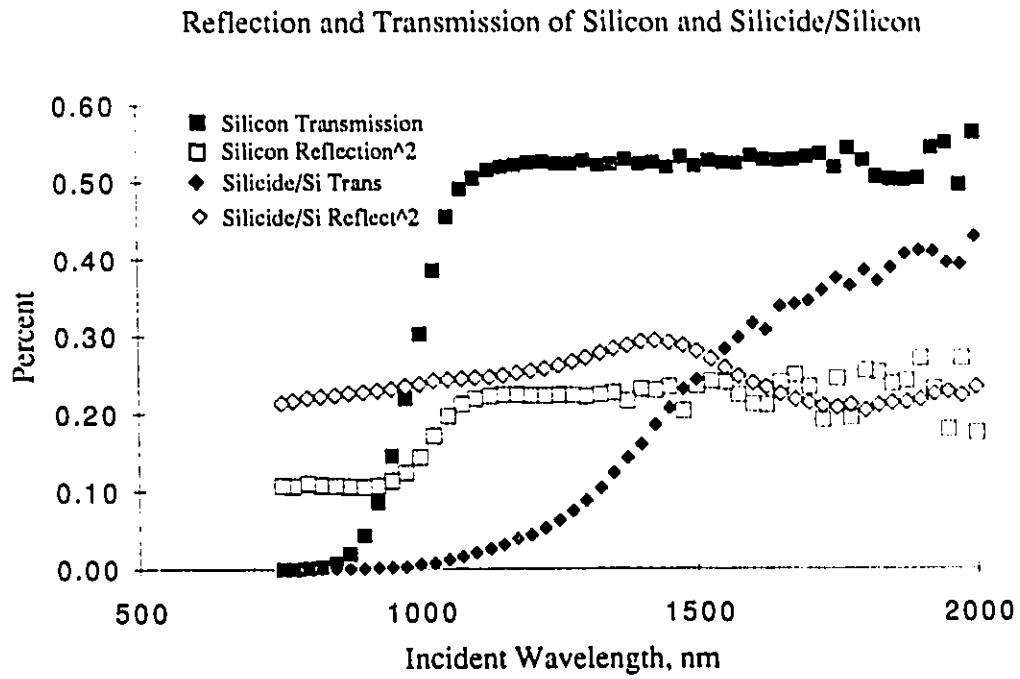
Figure 8-11   Reflection and Transmission data for silicon and silicide/silicon

Absorption Coefficient for Thin Film Silicide
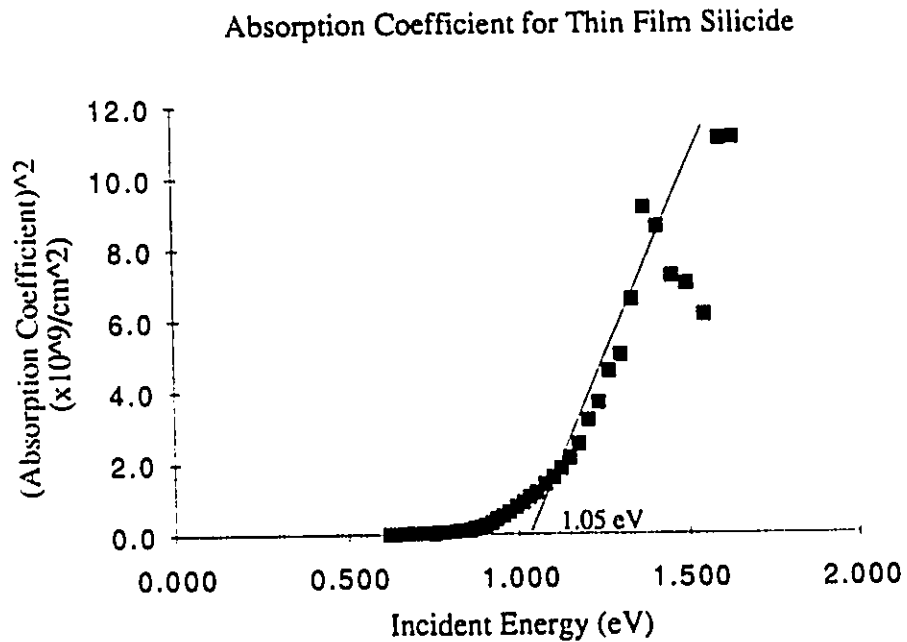
Figure 8-12   Absorption Coefficient for Thin Film Silicide

Figure 8-13 is a plot of the absorption coefficient for the thin silicon substrate used in the spectrophotometry experiments. It is seen that the intercept of this curve would be considerably higher than the 1.1 eV known as the silicon band gap. The reason for this discrepancy is the indirect nature of the silicon band gap, which does not lend itself to measurement by this technique. What can be noticed on the curve is that even though the band gap is indirect, significant absorption begins to occur around 1.2 eV. At this point, the substrate will begin to affect the results obtained from the thin silicide film. Figure 8-14 replots the silicide absorption curve, cutting the curve off at 1.2 eV. When this is done a much more linear curve is obtained for silicide absorption, and an extrapolation to the intercept leads to a more reasonable band gap value of 0.89 eV. As the curve approaches 1.2 eV the beginnings of silicon absorption can be seen. Closer inspection of the curve presented in Figure 8-12 does reveal a piece wise linear nature. The initial linear piece, replotted in Figure 8-14, extrapolates to the silicide band gap. While the second linear piece extrapolates to a value near the silicon band gap, this result is considered to be coincidental. The indirect nature of the silicon band gap and the effects of silicide absorption conspire to prevent an actual measurement of the silicon band gap. To avoid the substrate effect demonstrated in this experiment, it is suggested that the bandgap of iron disilicide would be most appropriately measured on quartz. The higher bandgap of this material should produce no effect on the silicide.

Silicon Absorption Curve
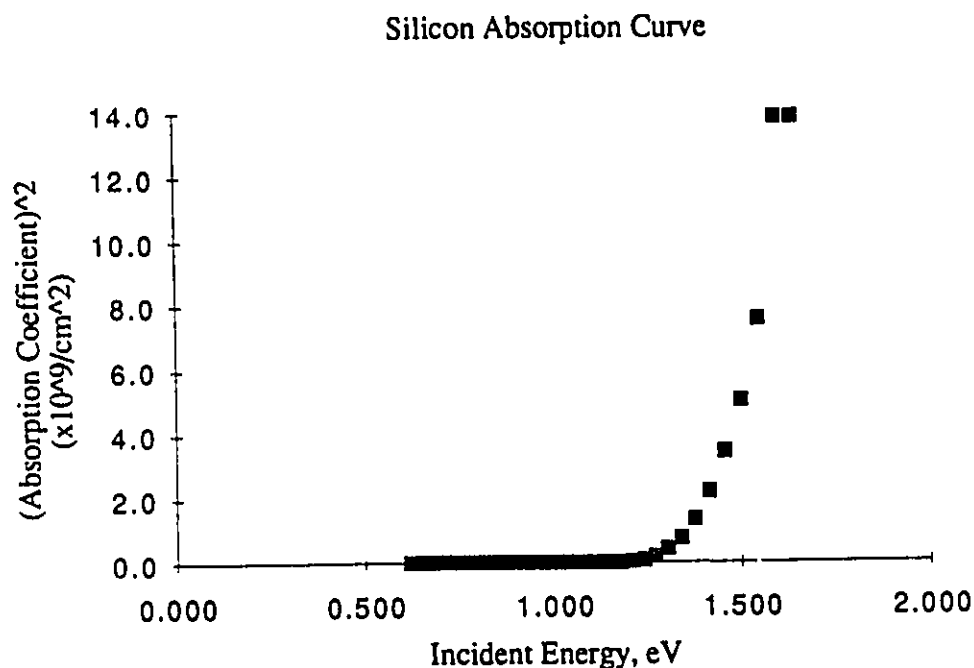
Figure 8-13   Silicon Absorption Curve

Silicide Band Gap Determination
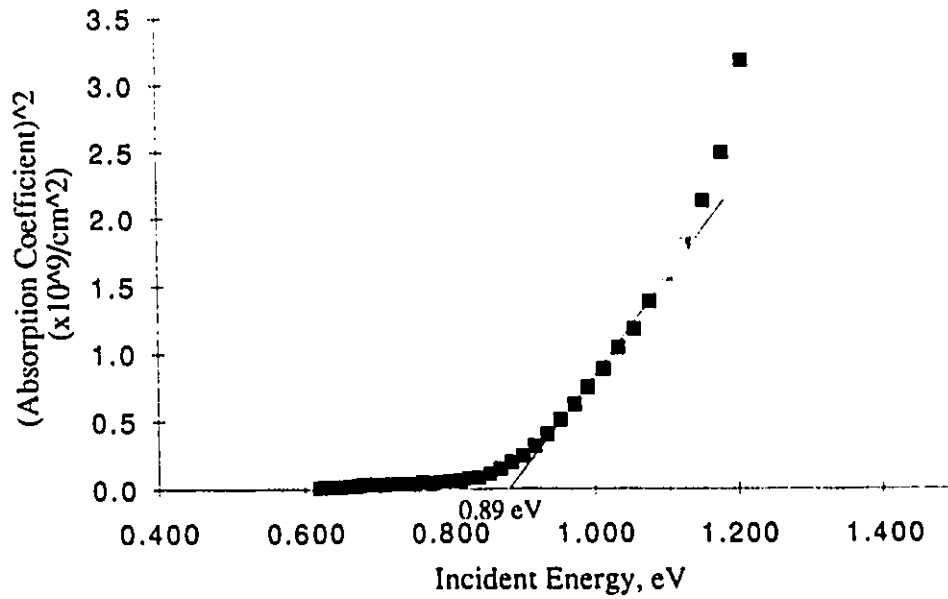
Figure 8-14   Silicide Band Gap Determination

Because of the roughness of the silicide film used for spectrophotometry, error arises from diffuse scattering from the surface. Coupled with error that may arise from absorption in the silicon substrate, the band gap of semiconducting iron silicide is more realistically quoted as 0.9 ± .1 eV, as determined by this work. Though not as accurate, this finding is still consistent with previous work on the material.

Conclusions

The purpose of this research was to form thin, continuous films of β FeSi$_2$, and to determine the bandgap of that material. These goals have been accomplished. It was shown that while iron thin films possess severe problems with agglomeration at high temperatures, continuous silicide layers may be formed through the use of silicon capping layers. These layers alter the surface conditions of the thin film and promote the rapid formation of silicide at the surface. As a result, formation of continuous silicide layers at high temperatures is well documented for the first time. It has also been shown that the vacuum quality during deposition is of tantamount importance to silicide formation, and that annealing must occur in a strictly controlled atmosphere to prevent iron oxidation. A vacuum environment is favorable to flowing nitrogen, as trace amounts of oxygen and moisture in the nitrogen are sufficient to consume the iron. With good conditions, a semiconducting silicide possessing a band gap of $0.9 \pm .1$ eV may be formed.

A number of comments can be made about the silicide formation process.

- During annealing, unpassivated iron tends to break into islands, or agglomerations.

- Despite agglomeration, interdiffusion within individual beads results in the formation of silicide. Most of this interdiffusion occurs after agglomeration.

- Initially, silicon is the primary diffusing species.

- Multiple layer growth occurs in iron–silicon diffusion couples.

- Of the possible silicides (Fe$_3$Si, Fe$_5$Si$_3$, Fe$_2$Si, FeSi, FeSi$_2$) only Fe$_3$Si, FeSi and FeSi$_2$ are confirmed as forming.

- Silicide formation was slow when compared to the literature, where annealing times of less than 2 hours at temperatures between 800 °C and 900 °C have been reported to form pure and stable layers of β FeSi$_2$. Formation of β FeSi$_2$ required nearly 20 hours at 800°C in this research. This is likely attributable to the high level of impurity in the deposited films.

- Silicide formation occurs faster on <111> type wafers than on <100> wafers, and displayed a much stronger epitaxial nature.

- Once formed, the high temperature α phase is very stable, and is difficult to transform to the low temperature β phase.

- Iron disilicide is stable with respect to silicon, as well as silicon dioxide.

Recommendations for further work

A number of avenues of research exist through which this work may be usefully continued.

1)   Study of the kinetics of formation of iron silicides. This would include the determination of the exact series of phases which form at various temperatures, as well the diffusing species during formation. Currently, the primary diffuser is only known for the Fe$_3$Si phase. This study would benefit from a consideration of the affect of impurities.

2)   Study of the effect of high temperatures on iron disilicide. It is known that without capping layers an iron thin film will agglomerate at temperatures above 650°C, but it is not known if this occurrence holds for iron silicide as well. A continuous film of FeSi$_2$ can be formed using the methods described in this work. Etching the protective oxide layer and reannealing the thin films at high temperatures would allow for a determination of the stability of the silicide itself.

3)   Determination of the conditions required to transform the high temperature α phase to the low temperature β phase. If this transformation could be made, silicide formation could proceed at higher temperatures, and the semiconducting phase could be reclaimed. The effects of oxygen impurities in the films would be an interesting avenue to pursue.

4)   It is known that silicon protects iron from agglomeration better than does silicon dioxide, but it is not known why. A study of this effect could include a study of the interaction of iron and iron silicide with silicon dioxide. The possible formation of iron oxide from silicon dioxide could be tested.

5)   A comprehensive study of the electronic properties of α and β FeSi$_2$. In the very least these should include the sheet resistance, mobility, and n or p type nature of the (semiconducting) material.

References

[1]   S.P. Murarka, "Silicides for VLSI Applications.", Academic Press, Orlando, 1983

[2]   K. N. Tu, W. N. Hammer and J. O. Olowolafe, "Shallow silicide contact", J. Appl. Phys. 51, 1663 (1980)

[3]   S. Petersson et al., "IrSi1.75 a new semiconductor compound", J. Appl. Phys. 53, 3342 (1982)

[4]   I. Nishida, "Semiconducting Properties of Nonstoichiometric Manganese Silicides", Journal of Materials Science, 7, 435 (1972)

[5]   I. Kawasumi et al., "Crystal growth of manganese silicide, MnSi1.73 and semiconducting properties of Mn15Si26", Journal of Materials Science, 16, 355 (1981)

[6]   M. C. Bost and John E. Mahan, "An Optical Determination of the Bandgap of the Most Silicon-Rich Manganese Silicide Phase", Journal of Electronic Materials, 16, 389 (1987)

[7]   Ch Krontiras, K Pomoni and M Roilos, "Resistivity and the Hall effect for thin MnSi1.73 films", J. Phys. D: Appl. Phys. 21, 509 (1988)

[8]   K. Y. Ahn et al., "Laser writing on metal-silicon bilayers for optical storage. I. Optical properties", J. Appl. Phys. 53, 3777 (1982)

[9]   James W. Mayer and S.S. Lau, in Electronic Materials Science: For Integrated Circuits in Si and GaAs, Macmillan Publishing Company, New York, 1990

[10]   F.M. D'Heurle and P. Gas "Kinetics of Formation of Silicides" Journal of Materials Research, Vol 1, No 1, 1986

[11]   Lin Zhang, D. G. Ivey, "Reaction kinetics and optical properties of semiconducting MnSi$_{1.73}$ grown on <001> oriented silicon", J. Mater. Sci. Electronics., 2, 116 (1991)

[12]   B.W. Wessals & G.Y. Chin "Advances in Electronic Materials" American Society for Metals, Metal Park, Ohio, 1984

[13]   G. Ottaviani "Metallurgical Aspects of the Formation of Silicides", Thin Solid Films, 140, 3 (1986)

[14]   L.R. Zheng, L.S. Hung, J.W. Mayer "Silicide Formation in Lateral Diffusion Couples" J. Vac. Sci. Technol. A 1 (2) Apr.-June 1983

[15]   G. Ottaviani and C. Nobili, "Silicide Formation", Thin Solid Films, 163, 111 (1988)

[16]   Lin Zhang and Douglas G. Ivey, "Low temperature reactions of Mn with Si", J. Mater. Res., 6, 1518 (1991)

[17]   R. M. Walser and R. W. Bené, Appl. Phys. Lett., 28, 624 (1976)

[18] G. Majni et. al., Vacuum, 32, 11 (1982)

[19] R. Fastow et al., Appl. Phys. Lett., 46, 1052 (1985)

[20] B. Y. Tsaur et al., Appl. Phys. Lett., 38, 922 (1981)

[21] F.A. Shunk, Constitution of Binary Alloys, Second Supplement, McGraw Hill, New York, 1969

[22] M. Eizenberg and K. N. Tu, "Formation and Schottky behavior of manganese silicides on n-type silicon", J. Appl. Phys. 53, 6885 (1982)

[23] L. Zhang and D. G. Ivey, *to be published*

[24] G. Ottaviani, J. G. Magni, and C. Canali, J. Appl. Phys. 18, 285 (1979)

[25] M. A. Nicolet and S. S. Lau, "Formation and Characterization of Transition-Metal Silicides", in VLSI Electronics: Microstructure Science, Vol 6, ed. N. G. Einspuch and G. B. Larrabee, Academic Press, New York, 1983

[26] K. N. Tu and J. W. Mayer, "Silicide Formation", in Thin Films-Interdiffusion and Reactions, ed. J. M. Poate, K. N. Tu, and T. W. Mayer, Wiley, New York, 1978

[27] S.P. Murarka "Refractory Silicides for Integrated Circuits", J. Vac. Sci. Technology, 17(4) Jul./Aug 1980

[28] M. Bartur and M-A. Nicolet. "Thermal Oxidation of Transition Metal Silicides on Si: Summary" J. Electrochem. Soc., February, 1984.

[29] F. M. D'Heurle "Formation and Oxidation Mechanisms in Two Semiconducting Silicides" Thin Solid Films, 151 (1987)

[30] C.-D. Lien and M-A. Nicolet, "Impurity effects in transition metal silicides", J. Vac. Sci. Technology, B, 2, 738 (1984)

[31] P. B. Ghate, "Metallization for very-large-scale integrated circuits", Thin Solid Films, 93, 359 (1982)

[32] G. Ottaviani, and J. W. Mayer, "Mechanisms and Interfacial Layers in Silicide Formation", in Reliability and Degradation-Semiconductor Devices and Circuits, ed. Howes and Morgan, Wiley, New York, 1981.

[33] M. Wittmer and K. N. Tu, "Low-temperature diffusion of dopant atoms in silicon during interfacial silicide formation", Physical Rev, B, 29, 2010 (1984)

[34] M. Wittmer, C.-Y. Ting, and K. N. Tu, "Redistribution of As during Pd_2Si formation: Electrical measurements", J. Appl. Phys., 54, 699 (1983)

[35] G. Ottaviani "Review of Binary Alloy Formation by Thin Film Interactions" J. Vac. Sci. Technology 16 (5) 1979

[36] D.M. Mattox. "Substrate Preparation for Thin Film Deposition - A Survey." Thin Solid Films, 124 (1985)

[37] David J. Elliott, _Integrated Circuit Fabrication Technology_ 2nd ed, Chapter 5, McGraw Hill, 1989

[38] David J. Elliott, _Integrated Circuit Fabrication Technology_ chapter five, "Surface Preparation", McGraw Hill, 1982

[39] John R. Vig "UV/Ozone Cleaning of Surfaces" Journal of Vacuum Science Technology. A 3 (3), May/Jun 1985

[40] Werner Kern "Cleaning Solutions Based on Hydrogen Peroxide for use in Silicon Semiconductor Technology" RCA review, June 1970

[41] K. Okamoto et al, "Columnar structure and texture of iron films prepared at various evaporation rates", Thin Solid Films, 147, 299 (1987)

[42] T. Urano and T. Kanaji, "Structures of iron films deposited on Si(111) 7x7 surface studied by LEED", Appl. Surf. Sci., 33/34, 68 (1988)

[43] T. Urano, T. Ogawa and T. Kanaji, "Angle resolved ultraviolet photoelectron spectroscopy study of ultrathin iron films on Si(111) surfaces", J. Vac. Sci. Technol. A 5, 2046 (1987)

[44] C. Binns et al., Surf. Sci. 152/153, 237 (1985)

[45] Qi-Gao et al., "Formation of iron silicide thin films", J. Appl. Phys., 60, 2629 (1986)

[46] J.M. Gallego and R. Miranda, "The Fe/Si(100) Interface", J. Appl. Phys, 69, 1377, (1991)

[47] H.C. Cheng, T.R. Yew, and L.J. Chen, "Interfacial reactions of iron thin films on silicon", J. Appl. Phys. 57, 5246 (1985)

[48] SS. Lau et al., Thin Solid Films 25, 415 (1975)

[49] N. Cherief, C. D'Anterroches, R. C. Cinti, T. A. Nguyen Tan, and J. Derrien, "Semiconducting silicide-silicon heterojunction elaboration by solid phase epitaxy", Appl. Phys. Lett., 55 1671 (1989)

[50] Charalabos A. Dimitriadis and Jurgen H. Werner, "Growth mechanism and morphology of semiconducting $FeSi_2$ films", J. Appl. Phys., 68, 94 (1990)

[51] C. A. Dimitriadis, J. H. Werner, S. Logothetidis, M. Stutzmann, J. Weber, and R. Nesper, "Electronic properties of semiconducting FeSi2 films", J. Appl. Phys. 68, 1726, (1990)

[52] J.E. Mahan, K.M. Geib, G.Y. Robinson, R.G. Long, Y. Xinghua, G. Bai, M.A. Nicolet, and M. Nathan, "Epitaxial films of semiconducting $FeSi_2$ on (001) silicon", Appl. Phys. Lett. 56, 2126 (1990)

[53] M.C. Bost and J.E. Mahan. "Optical Properties of Semiconducting Iron Disilicide Thin Films.", J. Appl. Phys. 58, 2696, (1985)

[54]   U. Birkholz and J. Schelm "Electrical Investigation of the Semiconductor to
         Metal Transition in FeSi₂" Physica Status Solidi, 34 K177, 1969

[55]   H.P. Geserich, S.K. Sharma and W.A. Theiner "Some Structural, Electrical,
         and Optical Investigations on a New Amorphous Material : FeSi₂"
         Philosophy Magazine, 27, 1001, 1973

[56]   U. Birkholz and J. Schelm "Mechanism of Electrical Conduction in β-
         FeSi₂", Physica Status Solidi, 27, 413 (1968)

[57]   Toshiyuki Hirano and Masatsugu Kaise, "Electrical resistivities of single-
         crystalline transition-metal disilicides", J. Appl. Phys. 68, 627 (1990)

[58]   Neil Weste, Kamran Eshraghian, Principles of CMOS VLSI Design. A
         Systems Perspective. Addison-Wesley Publishing Company, 1988

[59]   Resistivity from estimates by The Alberta Microelectronic Centre,
         Edmonton, AB

[60]   W. R. Runyan and K. E. Bean, Semiconductor Integrated Circuit Processing
         Technology, Addison-Wesley, New York, 1990, chapter 10

[61]   Dieter K. Schroder, Semiconductor Material and Device Characterization,
         John Wiley & Sons, Toronto, 1990, chapter 3

[62]   M.C. Bost and J.E. Mahan. "Semiconducting Silicides: Potential Materials
         for Electro-Optic VLSI Interconnects"

[63]   S. M. Sze, Physics of Semiconductor Devices, 2nd ed., Wiley, New York
         (1981)

[64]   Makarand Paranjape, Ph.D Thesis Proposal, Vertical Hall Devices for
         Simultaneous Multi-dimensional Magnetic Field Sensing, University
         of Alberta, Department of Electrical Engineering, (1990)

[65]   J. Millman and C. Halkias, Integrated Electronics: Analog and Digital
         Circuits and Systems, McGraw-Hill, New York, (1972)

[66]   Angela Rizzi, Heiko Moritz and Hans Luth, "Electronic and vibrational
         properties of semiconducting crystalline FeSi₂ layers grown on Si(111)",
         J. Vac. Sci. Technol. A, 9, 912, (1991)

[67]   M. C. Bost and John E. Mahan, "A clarification of the index of refraction of
         beta-iron disilicide", J. Appl. Phys. 64, 2034, (1988)

[68]   R.T. Tung, J.M. Poate, J.C. Bean, J.M. Gibson, D.C. Jacobson "Epitaxial
         Silicides"

[69]   A. Zur and T.C. McGill, "Lattice match: An application to heteroepitaxy",
         J. Appl. Phys. 55, 378 (1984)

[70]   A. Zur, T. C. McGill, and M-A Nicolet, "Transition-metal silicides lattice-
         matched to silicon", J. Appl. Phys. 57, 600 (1985)

[71]   Shyam P. Murarka, Martin C. Pecherar Electronic Materials, Science and Technology, Academic Press, Inc, San Diego, 1989

[72]   K. N. Tu, "Surface and interfacial energies of CoSi2 and Si films: Implications regarding formation of three-dimensional silicon-silicide structures", IBM J. Res. Develop. 34, 868 (1990)

[73]   J. W. Cullen, in Heteroepitaxial Semiconductors for Electronic Devices, ed. G. W. Cullen and C. C. Wang, Springer, New York, 1978, p50

[74]   C. W. Pearce, "Epitaxy" VLSI Technology ed. S.M. Sze (New York: McGraw Hill, 1983) pp 51-92

[75]   FL Weichman "Physics 611, Course Notes" University of Alberta, 1990

[76]   L.J. Chen, W.T. Lin, and M.B. Chang, "Epitaxial Growth of $NiSi_2$ on (011)Si", Mat. Res. Soc. Symp Proc. 25, 447 (1984)

[77]   K.C.R. Chiu, J.M Poate, et al, "Interface and surface structure of epitaxial $NiSi_2$ films", Appl. Phys. Lett. 38, 988, (1981)

[78]   J.M. Gallego, R. Miranda, et al., "Growth of cobalt and cobalt disilicide on Si(100)", Surface Science 239, 203, (1990)

[79]   A. E. Dolbak et al., "The initial stages of $NiSi_2$ epitaxy on clean Si(111), Si(100) and Si(110) surfaces", Surface Science, 247, 32 (1991)

[80]   J. Derrien, "Structural and electronic properties of $CoSi_2$ epitaxially grown on Si(111), Surface Science, 168, 171 (1986)

[81]   H. C. Cheng, L. J. Chen, and Y. R. Your, "Epitaxial Growth of $FeSi_2$ on (111) Si", Mater. Res. Soc. Symp. Proc. 25, 441 (1984)

[82]   H. C. Cheng, T. R. Yew and L. J. Chen, "Epitaxial growth of $FeSi_2$ in Fe thin films on Si with a thin interposing Ni layer", Appl. Phys. Lett. 47, 128 (1985)

[83]   S. Kennou, N. Cherief, R .C. Cinti, and T. A. Nguyen Tan, "The Influence of Steps on the Epitaxial Growth of Iron-Silicide on Si(001)", Surf. Sci., 211/212, 685 (1989)

[84]   R.T. Tung, J.C. Bean et al "Growth of single-crystal $CoSi_2$ on Si(111)", Appl. Phys. Lett. 40, 684 (1982)

[85]   S. Saitoh, H. Ishiwara and S. Furukawa, "Double heteroepitaxy in the Si(111)/$CoSi_2$/Si structure", Appl. Phys. Lett. 37, 203 (1980)

[86]   J. C. Bean and J. M. Poate, "Silicon / metal silicide heterostructures grown by molecular beam epitaxy", Appl. Phys. Lett. 37, 643, (1980)

[87]   S. A. Chambers, S. B. Anderson, H. W. Chen and J. H. Weaver, "High-temperature nucleation and silicide formation at the Co/Si(111)-7x7 interface: A structural investigation", Phys. Rev. B 34, 913 (1986)

[88]   Y.-J Chang and J. L. Erskine, "Diffusion-layer microstructure of Ni on
         Si(100)", Phys. Rev. B 26, 4766 (1982)

[89]   Y.-J Chang and J. L. Erskine, "Electronic structure of NiSi₂", Phys. Rev. B
         26, 7031 (1982)

[90]   V. Hinkel, L. Sorva, H Haak, and K. Horn, "Evidence for Si diffusion
         through epitaxial NiSi₂ grown on Si(111)", Appl. Phys. Lett. 50, 1257,
         (1987)

[91]   Gulden Akinci, Timothy Ohno, and Ellen D. Williams, "Summary Abstract:
         Growth of NiSi₂ on stepped Si(111)", J. Vac. Sci. Technol. A 5, 2143,
         (1987)

[92]   JCPDS Powder Diffraction Files

[93]   P.Y. Dusausoy, J. Protas, R. Wandji, and B. Roques "Structure Cristalline du
         Disiliciure de Fer, FeSi₂β", Acta Cryst. B 27, 1209 (1971)

[94]   Soo Young Lee et al., "On the role of indium underlays in the prevention of
         thermal grooving in thin gold films", Thin Solid Films, 149, 29 (1987)

[95]   R. E. Hummel et al., "Thermal grooving, thermotransport and
         electrotransport in doped and undoped thin gold films", Thin Solid
         Films, 78, 1 (1981)

[96]   LJ Ristic, course notes EE 619, University of Alberta, 1991

[97]   D. R. Campbell, S. Mader and W. K. Chu, "Effects of grain boundaries on
         the resistivity of cosputtered WSi₂ films", Thin Solid Films, 93, 341
         (1982)

[98]   M. L. Gimpl et al., "Amorphous Oxide Layers on Gold and Nickel Films
         Observed by Electron Microscopy", J. Appl. Phys., 35, 3572 (1964)

[99]   Walter M. Kane et al., "Effects of Annealing on Thin Gold Films", J. Appl.
         Phys., 37, 2085 (1966)

[100]   S. K. Sharma and J. Spitz, "Hillock Formation , Hole Growth and
         Agglomeration in Thin Silver Films", Thin Solid Films, 65, 339 (1980)

[101]   S. K. Sharma and J. Spitz, "Agglomeration in chemically deposited silver
         films", Thin Solid Films, 66, L51 (1980)

[102]   Nae Lih Wu and Jonathan Phillips, "Reaction-enhanced sintering of
         platinum thin films during ethylene oxidation", J. Appl. Phys. 59, 769
         (1986)

[103]   A. K. Sinha et al., "Thermal stability of thin PtSi films on silicon
         substrates", J. Appl. Phys., 3673 (1972)

[104]   C. M. Kennefick and R. Raj, "Copper on Sapphire: Stability of Thin Films
         at 0.7 T$_m$", Acta metall., 37, 2947 (1989)

[105]   D.J. Srolovitz and S.A. Safran, "Capillary instabilities in thin films. I. Energetics", J. Appl. Phys. 60, 247 (1986)

[106]   E. Jiran and C.V. Thompson, "Capillary Instabilities in Thin Films", Journal of Electronic Materials, Vol. 19, No. 11, 1153 (1990)

[107]   K.T. Miller and F.F. Lange, "The instability of polycrystalline thin films: Experiment and theory", J. Mater. Res., Vol 5, No. 1, 151 (1990)

[108]   D.J. Srolovitz and S.A. Safran, "Capillary instabilities in thin films. II. Kinetics", J. Appl. Phys. 60, 255 (1986)

[109]   Lord Rayleigh, "On the Instability of Jets.", Proc. London Math. Soc. 10, 4 (1878)

[110]   F.A. Nichols and W.W. Mullins, Trans. Metall. Soc. AIME 233, 1840 (1965)

[111]   William W. Mullins, "Flattening of a Nearly Plane Solid Surface due to Capillarity", J. Appl. Phys. 30, 77 (1959)

[112]   W.W. Mullins, "Theory of Thermal Grooving", J. Appl. Phys. 28, 333 (1967)

[113]   G.L. J. Bailey and H.C. Watkins, Proc. Phys. Soc. B 63, 350 (1950)

[114]   Luis Bachmann et al., "Observations on the Morphological Changes in Thin Copper Deposits during Annealing and Oxidation", J. Appl. Phys., 36, 304 (1965)

[115]   B. Chalmers et al., "The thermal etching of silver", Proc. Roy. Soc. A, 193, 465 (1948)

[116]   H.L. Caswell and Y. Budo, "Influence of Oxygen on the Surface Mobility of Tin Atoms in Thin Films", J. Appl. Phys., 35, 644 (1963)

[117]   Fann-Mei Yang and Mao-Chieh Chen, "Formation of cobalt silicide under a passivating film of molybdenum or tungsten", J. Vac. Sci. Technol. B, 9, 3, 1497 (1991)

[118]   C. S. Wu et al., "Surface morphology and electronic properties of $ErSi_2$", Thin Solid Films, 104, 175 (1983)

[119]   Kenneth M. Ralls et al., Introduction to Materials Science and Engineering, John Wiley & Sons, New York, 1976

[120]   T.C. Huang et al., "Effect of ion bombardment during deposition on the x-ray microstructure of thin silver films", J. Vac. Sci. Technol. A 3, 2161 (1985)

[121]   Ken Westra, "Reactive sputtering of Indium Nitride", M.Sc thesis, University of Alberta, 1989

[122]   D. B. Williams, Chap 4 and 6 in Practical Analytical Electron Microscopy in Material Science, Phillips Electronic Instruments, Electron Optics Publishing Group, Mahwah, 1984

[123]   D. G. Ivey and G. R. Piercy, J. Electron Microscopy Technique, 8, 233 (1988)

[124]   J. C. Bravman and R. Sinclair, J. Electron Microscopy Technique, 1, 53 (1984)

[125]   Lin Zhang, M.Sc. Thesis, University of Alberta, 1990

[126]   J. I. Pankove, Optical Processes on Semiconductors, Dover. New York, 1975

[127]   B. E. Sernelius et al., "Band-gap tailoring of ZnO by means of heavy Al doping", Phys. Rev. B 37, 10244 (1988)

[128]   I. Hamburg and C. G. Granquist, "Evaporated Sn-doped In_2O_3: Basic optical properties and applications to energy-efficient windows", J. Appl. Phys. 60, R123, (1986)

[129]   I. Hamberg et al., "Band-gap widening in heavily Sn-doped In_2O_3", Phys. Rev. B, 3240 (1984)

[130]   Private communication with Alan Mitchell, Alberta Microelectronic Center

[131]   M. J. Brett et al., "Nodular Defect Growth in Thin Films", J. Mat. Sci.: Materials in Electronics, To be published

[132]   T. I. Kamins and K. L. Chiang, "Properties of Plasma-Enhanced CVD Silicon Films", J. Electrochem. Soc.: Solid State Science and Technology, 129, 10, 2326 (1982)